On the Use of Expanded Geofoam Inclusion to Reduce Earth Pressure on Retaining Structures under Static and Dynamic Loading

Muhammad Imran Khan
Department of Civil Engineering
McGill University, Montréal, Canada
May 2021

A thesis submitted to McGill University in partial fulfillment of the requirements for the degree of Doctor of Philosophy

This page intentionally left blank

Dedication

This thesis is proudly dedicated to .....

my beloved **Parents**

Abrar & Mohsneen

my amazing **Brothers**

Asad & Saad

my sweet **Sister**

Adia

&

my adored **Wife**

Maryam

Abstract

Expanded polystyrene (EPS) geofoam has been increasingly used in geotechnical engineering applications either as lightweight fill material or as compressible inclusion to reduce earth pressure on earth retaining structure under both static and dynamic loading. These applications involve the installation of geofoam blocks in direct contact with other materials (e.g. steel, soil, concrete etc.) forming a composite structure. In this thesis an attempt has been made to experimentally determine shear strength of monoblock of EPS geofoam and interface strength of geofoam interacting with different materials. Further, numerical studies are carried out to investigate the role of EPS geofoam in reducing lateral earth pressure on rigid non-yielding retaining walls under static and dynamic loading conditions.

First, a series of direct shear tests has been conducted on geofoam samples of three different densities, namely, 15 kg/m^3, 22 kg/m^3 and 39 kg/m^3 under three different normal stresses 18, 36 and 54 kPa. In addition, interface shear tests are also conducted to determine the interface strength parameters as these geofoam blocks interact with selected materials (e.g. PVC, sand, concrete, steel, wood). Test results revealed that geofoam density and applied normal stress have significant effects on the vertical compression and interface strength properties. Next, a 2D plane strain finite element model is developed to investigate the effectiveness of EPS geofoam in reducing static earth pressure on rigid retaining wall. Numerical model is first validated with the results of physical tests. A parametric study is then carried out to investigate the role of EPS geofoam density, relative thickness and backfill frictional properties on reduction of static lateral earth pressure on the wall. Three different geofoam samples having three different thicknesses interacting with four different backfill soils were used in this study.

Finally, a 2D plane strain finite element model is developed to study the role of EPS geofoam in reducing seismic earth pressure. Numerical model is first validated against the results of reduced scale shaking table tests. A numerical parametric study is then conducted to investigate the effectiveness of EPS geofoam density, relative thickness and backfill frictional properties on reduction of seismic earth pressure on the rigid retaining wall. Four different geofoam samples having three different thicknesses interacting with four different backfill materials are used in this study. The results of numerical studies are presented in the form of design charts for practical implication.

Résumé

Le polystyrène expansé (EPS) Geofoam a été de plus en plus utilisé dans les applications d'ingénierie géotechnique soit en tant que matériau de remplissage léger ou comme inclusion compressible pour réduire la pression de la terre sur les structures de soutènement sous les charges statique et dynamique. Ces applications impliquent la mise en place de blocs de Geofoam en contact direct avec d'autres matériaux (par exemple l'acier, du sol, du béton, etc.) formant une structure composite. Dans cette thèse, une tentative a été faite pour déterminer expérimentalement la résistance au cisaillement de monobloc de la EPS Geofoam et la résistance de l'interface de Geofoam en interaction avec différents matériaux. En outre, des études numériques sont effectuées pour étudier le rôle de la EPS Geofoam dans la réduction de la pression latérale de terre sur les murs de soutènement rigides non flexibles dans les conditions de charge statique et dynamique.

Premièrement, une série d'essais de cisaillement direct a été effectuée sur des échantillons de Geofoam de trois densités différentes de 15 kg/m^3, 22 kg/m^3 et 39 kg/m^3 sous les trois contraintes normales différentes de 18, 36 et 54 kPa. De plus, les essaies de cisaillement d'interface sont également faits pour déterminer les paramètres de résistance de l'interface, car ces blocs de Geofoam interagissent avec des matériaux sélectionnés (par exemple PVC, sable, béton, acier et bois). Les résultats des essais ont révélé que la densité de Geofoam et la contrainte normale appliquée ont des effets significatifs sur la compression verticale et les propriétés de la résistance de l'interface. Ensuite, un modèle d'éléments finis de déformation plane 2D est développé pour étudier l'efficacité de la Geofoam EPS dans la réduction de la pression statique de terre sur le mur de soutènement rigide. Le modèle numérique est initialement validé avec les résultats des essais physiques. Une étude paramétrique est ensuite réalisée pour étudier le rôle de la densité de EPS Geofoam, l'épaisseur relative et les propriétés de frottement de remblai sur la réduction de la pression latérale statique de terre sur la paroi. Trois échantillons de Geofoam ayant trois épaisseurs différentes qui interagissent avec quatre différents sols de remblai ont été utilisés dans cette étude. Finalement, un modèle 2D d'éléments finis de déformation plane est développé pour étudier le rôle de la Geofoam EPS dans la réduction de la pression sismique de terre. Le modèle numérique est d'abord validé par rapport aux résultats des essais de la table tremblante à échelle réduite. Une étude paramétrique numérique est ensuite menée pour étudier l'efficacité de la densité de la Geofoam EPS, de l'épaisseur relative et des propriétés de frottement du remblai sur la réduction

de la pression sismique de la terre sur le mur de soutènement rigide. Quatre échantillons différents de Geofoam ayant trois épaisseurs différentes interagissant avec quatre matériaux de remblai différents sont utilisés dans cette étude. Les résultats des études numériques sont présentés sous la forme de tableaux de conception pour implication pratique.

Acknowledgments

Alhamdulillah, I am grateful to Allah, the most Merciful and Beneficent for giving me the strength and courage to complete this thesis.

This research would not have been possible without the help, support and guidance of many people.

I would like to express my sincerest gratitude to my mentor and research supervisor, Prof. Mohamed Meguid, for his continuous support, guidance and invaluable suggestions throughout my PhD. His wisdom and expertise in numerical modeling had a paramount input in completion of this research.

I would like to acknowledge the financial support provided by McGill University and the University of Engineering and Technology, Lahore, Pakistan. I would also like to appreciate and thank Plasti-Fab Inc. for their in-kind support.

I would like to thank Dr. Bill Cook, Mr. John Bartczak and Mr. Jorge Sayat for providing technical assistance during the research.

I would like to thank all my friends and colleagues for all the valuable assistance, encouragement and moral support.

I am highly indebted to my parents and siblings for their unconditional love, support and encouragement throughout the research and during my stay in Montreal.

Finally, I would like to express my gratitude to my wife, for her love, patience and for standing by me throughout these past years.

Muhammad Imran Khan
May 2021

List of Publications

Journal Papers

[J1] Khan, M. I., & Meguid, M. A. (2018). *Experimental investigation of the shear behavior of EPS geofoam*. International Journal of Geosynthetics and Ground Engineering, 4(2), 12. https://link.springer.com/article/10.1007/s40891-018-0129-7

[J2] Meguid, M. A., & **Khan, M. I.** (2019). *On the role of geofoam density on the interface shear behavior of composite geosystems*. International Journal of Geo-Engineering, 10(1), 6. https://link.springer.com/article/10.1186/s40703-019-0103-9

[J3] Khan, M. I., & Meguid, M. A. (2021). *Evaluating the role of geofoam properties in reducing lateral loads on retaining walls*: *A Numerical Study*. Sustainability, 13, 4754. https://www.mdpi.com/1084520

[J4] Khan, M. I., & Meguid, M. A. (2021). *On the Use of EPS Geofoam to Reduce Earth Pressure on Retaining Walls under Dynamic Loading*: *A Numerical Study*. International Journal of Geosynthetics and Ground Engineering, 4(2), 12. (Under review).

Conference Papers

[C1] Khan, M. I., & Meguid, M. A. (2018). *Shear Behavior of EPS Geofoam*. 71st Canadian Geotechnical Conference and the 13th Joint CGS/IAH-CNC Groundwater Conference–GeoEdmonton 2018. https://members.cgs.ca/conferences/GeoEdmonton/papers/geo2018Paper180.pdf

Contribution of Authors

The manuscripts J1, J2, J3, J4 and C1 given in the list of publications are included in this thesis (chapters 2 to 5). All manuscripts are the candidate's original work. All the laboratory experiments, numerical modelling, data analysis and preparation of the manuscripts were completed by the candidate. Prof. Mohamed Meguid supervised the research, provided research direction and guidance, and extensively edited and revised the drafts of the manuscripts as well as the other chapters of this thesis.

Table of Contents

List of Figures

List of Tables

1

Introduction

1.1 General

Expanded polystyrene (EPS) was originally invented in Germany by BASF in 1950 [1]. Expanded polystyrene geofoam refers to a rigid, air filled closed cell, lightweight, plastic foam type material. "Geofoam" is a generic term given to lightweight blocks of EPS by Horvath [2]. It is almost 100 times lighter than soil and 10-30 times lighter than other lightweight fill materials [3]. Besides its lightweight nature, EPS geofoam also posses many other outstanding characteristics e.g. durability, non-biodegradable, water resistant, eco-friendly, easy to install without any specialized equipment, ability to retain its shape, high compressive strength etc. EPS geofoam has been used in many geotechnical engineering applications, some of the important application of EPS geofoam as light weight fill material can be found in: slope stabilization [4-8], sub base fill material [9-11], embankments [12-16], earth retaining structures [4,17], bridge abutments and bridge approaches [18-22] and thermal insulation for roads [23]. High compressibility of EPS geofoam also makes it a suitable for use as compressible material in underground applications [24-26] and as compressible inclusion behind the walls of rigid structures [26-31].

1.2 Motivation of the Study

In most of the geotechnical applications (see Figure 1.1), EPS geofoam is used either in direct contact with other geofoam blocks or with other construction materials to form a composite structure. Successful analysis and design of these structures requires a clear understanding of both; compression and shear behavior of the geofoam material as well as the strength of the interface. Retaining walls are an integral part of many important infrastructure projects, they are mostly provided as preferred countermeasure against soil instability.

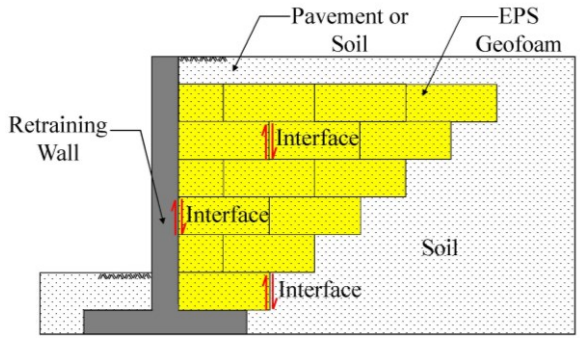

(a) Geofoam as **light weight fill** material

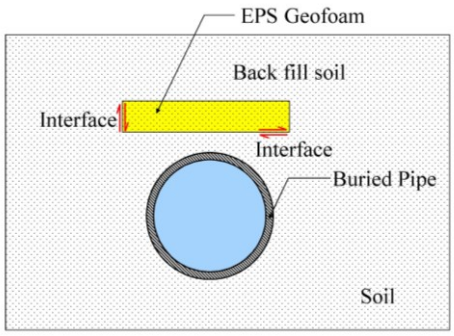

(b) Geofoam as **compressible material** placed above buried pipes

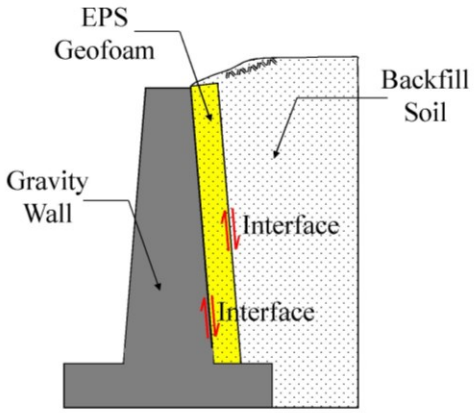

(c) Geofoam as **compressible inclusion**, placed behind the gravity retaining wall

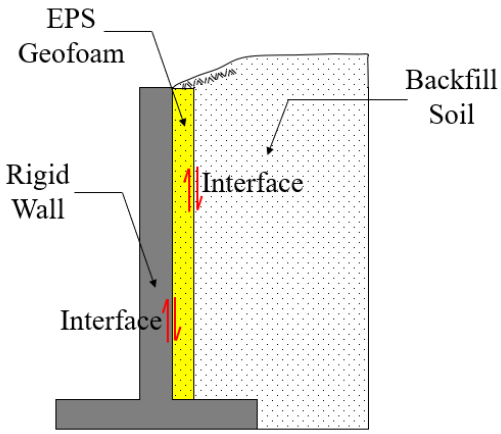

(d) Geofoam as **seismic buffer** placed behind rigid retaining wall

Figure 1.1 Applications of EPS geofoam in geotechnical engineering

Compressible nature of EPS geofoam has shown its potential to be used as inclusion or buffer behind earth retaining structures under static and dynamic loading conditions. Many researchers have demonstrated the use of EPS geofoam inclusion in reducing static earth forces against rigid wall through small-scale laboratory tests [32-35] and monitored field installations [26,36,37]. The concept of reducing seismic earth forces on rigid retaining wall was first reported by Inglis et al. [27] through a field case study. Some researchers also demonstrated the use of EPS geofoam as seismic buffer through reduced-scale shaking table tests [38,39].

It has been observed that very few numerical studies have been done to simulate and expand the results of physical tests conducted on rigid non-yielding retaining walls under static or dynamic conditions. Also, in most of these studies, the numerical results have not been compared with

measured data based on instrumented physical models. Numerical modelling of complex engineering problems involving soil, structure (e.g. footing, walls or buried pipes etc.) and soft or compressible inclusion is a challenging task. The complex behaviour of composite structure is mainly attributed to the different material models and interaction between these materials. Finite Element Method (FEM) has been proven to be effective in calculating stresses and strains within a complex engineering problem.

The present research has two main goals (a) *Experimental*: To evaluate the interface strength parameters of EPS geofoam interacting with different materials. (b) *Numerical*: To use FEM to study the behavior of rigid non-yielding retaining walls with EPS geofoam under static and dynamic conditions.

1.3 Research Objectives and Scope

The major objectives of the present research were:

1. To perform direct shear tests on monoblock geofoam samples to investigate the shear strength parameters of the material.
2. To perform interface direct shear tests on geofoam samples interacting with other materials e.g. PVC, sand, wood, steel, concrete etc. to investigate the interface strength parameters.
3. To develop and validate a numerical model that is able to simulate the response of rigid retaining walls with EPS geofoam under static loading.
4. To carryout a parametric study to investigate the effect of EPS geofoam and backfill properties on the static earth pressure acting on rigid retaining walls.
5. To develop normalized charts that could be used for the selection of EPS geofoam density and thickness to be installed behind rigid retaining walls under static loading.
6. To develop and validate a suitable numerical model to simulate the seismic response of rigid retaining walls with of EPS geofoam inclusion under dynamic loading.
7. To carryout a parametric study to investigate the effect of EPS geofoam and backfill properties on the seismic earth pressure acting on rigid retaining walls.
8. To develop normalized charts that could be used for the selection of EPS geofoam density and thickness to be installed behind rigid retaining walls under dynamic loading.

1.4 Original Contribution

The original contributions of present research are briefly summarized below:

1. Determination of shear strength properties of monoblocks of geofoam and interface shear strength properties of geofoams interacting with different construction materials.
2. Development of a validated numerical model to investigate the effect of EPS geofoam on reduction of static earth pressures on rigid non-yielding retaining walls.
3. Development of a validated numerical model to study the effect of EPS geofoam in reducing seismic earth pressures on rigid non-yielding retaining walls.
4. Development of normalized charts based on the obtained results, which can be helpful in design of composite retaining structures involving EPS geofoam.

1.5 Thesis Organization

This thesis has been organized into six chapters. The chapters follow the order in which the research was carried out and presented. A comprehensive literature review of the past research related to each topic is presented in the corresponding chapters (chapters 2 to 5). A brief breakdown of the thesis is as follows:

Chapter 1: Introduction

This chapter includes the general introduction, problem statement, research objectives and thesis outline.

Chapter 2: Experimental Investigation of the Shear Behavior of EPS Geofoam

This chapter describes the details of direct shear tests conducted on EPS geofoam block and interface direct shear tests conducted on EPS-PVC and EPS-sand interfaces. A series of direct shear tests has been carried out on geofoam samples of three different densities under three different normal stresses.

Chapter 3: On the Role of Geofoam Density on the Interface Shear Behavior of Composite Geosystems

In this chapter the details of interface direct shear tests conducted on EPS-concrete, EPS-wood and EPS-steel interfaces are presented. A series of direct shear tests has been carried out on geofoam samples of three different densities under three different normal stresses.

Chapter 4: On the Use of EPS Geofoam to Reduce Earth Pressure on Retaining Walls under Static Loading: A Numerical Study

This chapter presents the development and validation of numerical model to investigate the effect of EPS geofoam placed behind rigid retaining wall under static loading. A parametric study was then carried out to study the effects of geofoam density, thickness and frictional properties of backfill soil on reduction of static earth pressure acting on rigid retaining wall.

Chapter 5: On the Role of EPS Geofoam to Reduce Earth Pressure on Retaining Walls under Dynamic Loading: A Numerical Study

This chapter presents the development and validation of numerical model to investigate the effect of EPS geofoam placed behind rigid retaining wall under dynamic loading. A parametric study was then carried out to study the effects of geofoam density, thickness and frictional properties of backfill soil on reduction of seismic earth pressure acting on rigid retaining wall.

Chapter 6: Conclusions and Recommendations

This chapter presents the global conclusions of the thesis and claims of originality arising from the present research. Some recommendations are also presented for future research.

1.6 References

[1] BASF Corp. (1997) Styropor Technical Information, BASF Corp., Germany.

[2] Horvath JS (1992) New developments in geosynthetics; 'lite' products come of age. Standardization News 20 (9):50-53.

[3] Stark TD, Arellano D, Horvath JS, Leshchinsky D (2004) Geofoam applications in the design and construction of highway embankments. NCHRP web document 65:24-11.

[4] Elragi AF (2000) Selected engineering properties and applications of EPS geofoam. ProQuest Dissertations and Theses.

[5] Jutkofsky W, Sung J, Negussey D (2000) Stabilization of embankment slope with geofoam. Transportation Research Record: Journal of the Transportation Research Board (1736):94-102.

[6] Sheeley M (2000) Slope stabilization utilizing geofoam. Master's Thesis, Syracuse University, New York.

[7] Srirajan S (2001) Recycled content and creep performance of EPS geofoam in slope stabilization. Doctoral dissertation, Syracuse University, New York.

[8] Negussey D (2002) Slope Stabilization with geofoam. Report to FHWA and the EPS industry. Geofoam research center, Syracuse University, New York.

[9] Duskov M (1991) Use of expanded polystyrene (EPS) in flexible pavements on poor subgrades. In: Proceedings of the International Conference on Geotechnical Engineering for Coastal Development, pp 783-788.

[10] Duskov M (1997) Measurements on a flexible pavement structure with an EPS geofoam sub-base. Geotextiles and Geomembranes 15 (1):pp 5-27. doi:http://dx.doi.org/10.1016/S0266-1144(97)00004-6

[11] Riad HL, Ricci AL, Osborn PW, Horvath JS (2003) Expanded polystyrene (EPS) geofoam for road embankments and other lightweight fills in urban environments. In: Soil and Rock America, 12th Pan-American Conference on Soil Mechanics and Geotechnical Engineering and 39th US Rock Mechanics Symposium.

[12] Refsdal G (1985) Plastic foam in road embankments: future trends for EPS use. Internal Report, Norwegian Road Research Laboratory, Oslo, Norway.

[13] Aaboe R (1987) 13 years of experience with expanded polystyrene as a lightweight fill material in road embankments. Norwegian Road Research Laboratory Publication (61):pp 21-27.

[14] Zou Y, Leo C, Small J (2000) Behaviour of EPS geofoam as flexible pavement subgrade material in model tests. Geosynthetics International 7 (1):pp1-22.

[15] Negussey D, Stuedlein A, Bartlett S, Farnsworth C (2001) Performance of a geofoam embankment at 100 South, I-15 reconstruction project, Salt Lake City, Utah. In: Proceedings on 3rd International Conference on EPS Geofoam.

[16] Farnsworth C, Bartlett SF, Negussey D, Stuedlein A (2008) Rapid construction and settlement behavior of embankment systems on soft foundation soils. Journal of Geotechnical and Geoenvironmental Engineering 134 (3):pp 289-301.

[17] Frydenlund T, Aaboe R (1996) Expended polystyrene-the lightweight solution. In: Proceedings of international symposium on EPS construction method (EPS-Tokyo'96), Tokyo, Japan, pp 31-46.

[18] Williams D, Snowdon R (1990) A 47 Great Yarmouth Western Bypass: performance during the first three years.

[19] Skuggedal H, Aaboe R (1991) Temporary overpass bridge founded on expanded polystyrene. In: Proceedings of the 1st European Conference on Soil Mechanics and Foundation Engineering, pp 559-561.

[20] McDonald P, Brown P(1993) Ultra lightweight polystyrene for bridge approach fill. In: Proceedings of the 11th Southeast Asian Geotechnical Conference, Singapore, pp 664-668.

[21] Bang S (1995) Experimental and analytical study of expanded polystyrene blocks in highway application. In: Proceedings of International Seminar on the Application of EPS for Embankment Construction, Korea Institute of Construction Technology (KICT), Seoul, Korea, pp 105-133.

[22] Abu-Hejleh N, Zornberg JG, Elias V, Watcharamonthein J (2003) Design assessment of the founders/meadows GRS abutment structure. In: Proc., 82nd Annual TRB Meeting.

[23] BASF (1987) Strength characteristics of EPS thermal insulation. Technical Bulletin E-3, Parsippany, NJ, USA.

[24] Meguid M, Hussein M, Ahmed M, Omeman Z, Whalen J (2017) Investigation of soil-geosynthetic-structure interaction associated with induced trench installation. Geotextiles and Geomembranes 45 (4):pp 320-330.

[25] Meguid M, Ahmed M, Hussein M, Omeman Z (2017) Earth pressure distribution on a rigid box covered with u-shaped geofoam wrap. International Journal of Geosynthetics and Ground Engineering 3 (2):p 11.

[26] Partos A, Kazaniwsky P(1987) Geoboard reduces lateral earth pressures. In: Proceedings of Geosynthetics' 87 Conference, New Orleans, USA, pp 628-639.

[27] Inglis D, Macleod G, Naesgaard E, Zergoun M (1996) Basement wall with seismic earth pressures and novel expanded polystyrene foam buffer layer. Paper presented at the 10th Annual Symposium on Earth Retention System, Vancouver, Canada.

[28] Zarnani S, Bathurst R (2007) Experimental investigation of EPS geofoam seismic buffers using shaking table tests. Geosynthetics International 14 (3):pp 165-177.

[29] Horvath JS (1997) The compressible inclusion function of EPS geofoam. Geotextiles and Geomembranes 15 (1):pp 77-120.

[30] Ertugrul OL, Trandafir AC (2013) Lateral earth pressures on flexible cantilever retaining walls with deformable geofoam inclusions. Engineering Geology 158:pp 23-33.

[31] Karpurapu R, Bathurst R (1992) Numerical investigation of controlled yielding of soil-retaining wall structures. Geotextiles and Geomembranes 11 (2):pp 115-131.

[32] McGown A, Murray R, Andrawes K (1987) Influence of wall yielding on lateral stresses in unreinforced and reinforced fills.

[33] McGown A, Andrawes KZ, Murray RT (1988) Controlled yielding of the lateral boundaries of soil retaining structures. In: Symposium on Geosynthetics for Soil Improvement at the ASCE Convention. vol Geotechnical Special.

[34] Reeves J, Filz G (2000) Earth force reduction by a synthetic compressible inclusion. Report of research conducted under the sponsorship of GeoTech Systems Corporation and Virginia's Center for Innovative Technology, Virginia Tech, Department of Civil Engineering, Blacksburg, VA.

[35] Ikizler SB, Aytekin M, Nas E (2008) Laboratory study of Expanded Polystyrene (EPS) Geofoam used with Expansive Soils. Geotextiles and Geomembranes 26 (2):pp. 189-195. doi:http://dx.doi.org/10.1016/j.geotexmem.2007.05.005.

[36] Hoppe EJ (2005) Field study of integral backwall with elastic inclusion. Virginia Transportation Research Council.

[37] Hoppe EJ (2006) Field measurements on skewed semi-integral bridge with elastic inclusion: instrumentation report. Virginia Transportation Research Council.

[38] Hazarika H, Okuzono S, Matsuo Y (2003) Seismic stability enhancement of rigid nonyielding structures. Paper presented at the 13th International Offshore and Polar Engineering Conference, Honolulu, Hawaii, USA.

[39] Bathurst R, Zarnani S, Gaskin A (2007) Shaking table testing of geofoam seismic buffers. Soil Dynamics and Earthquake Engineering 27 (4):pp 324-332. doi:http://dx.doi.org/ 10.1016/ .soildyn.2006.08.003

2

Experimental Investigation of the Shear Behavior of EPS Geofoam*

* A version of this chapter has been published as:
Khan, M. I., & Meguid, M. A. (2018). *Experimental investigation of the shear behavior of EPS geofoam*. International Journal of Geosynthetics and Ground Engineering, 4(2), 12.

2.1 Preface

A brief introduction of EPS geofoam, problem statement, research objectives and thesis outline are presented in chapter 1. In this chapter results of direct shear test (DST) conducted on monoblock of EPS geofoam and interface direct shear test conducted on geofoam-PVC and geofoam-sand interfaces are presented in detail.

2.2 Abstract

Geofoam has been used in a wide range of geotechnical engineering projects since 1960s; either as lightweight fill material (e.g. embankments and bridge approaches) or as compressible inclusion (e.g. retaining walls and culverts). In most of these projects, geofoam is installed either in direct contact with other geofoam blocks or other construction material. Successful design of these composite systems requires a good understanding of both the compression and shear behavior of the geofoam blocks as well as the shear strength of the interface. In this study, an attempt has been made to measure the shear strength parameters of expanded polystyrene (EPS) geofoam blocks of different densities as well as the interface strength parameters as these blocks interact with sand as well as polyvinyl chloride (PVC) material. A series of direct shear tests has been carried out on geofoam samples of three different densities, namely, 15 kg/m^3, 22 kg/m^3 and 39 kg/m^3. Shear test results on geofoam mono-blocks showed that the increase in density results in an increase in the material cohesion, which is associated with a decrease in the internal friction angle. Most interface resistance was found to develop at small displacements. For geofoam-PVC interface, both the adhesion and angle of interface friction slightly increased with the increase in geofoam density.

The measured geofoam-sand interface strength revealed a consistent increase in the angle of interface friction as the density of geofoam material increased. These experimental results can be used to guide engineers in estimating the interface parameters needed for both analytical and numerical analyses involving soil-EPS-structure interaction.
Keywords: EPS geofoam, Direct shear tests, Friction angle, Interface strength, Adhesion.

2.3 Introduction

Expanded polystyrene (EPS) was originally invented in Germany by BASF in 1950 [1]. It is an ultra-lightweight, rigid, closed cell foam which is significantly lighter than conventional backfill material [2]. Geofoam blocks have been successfully incorporated into various geotechnical engineering applications serving as lightweight fill material, vibration barrier, or seismic buffer for rigid structures [3].

Geofoam inclusions placed above buried pipes [4,5] or behind retaining walls [6] are known to reduce earth loads on these structures leading to safer and economical design. Although geofoam blocks in these applications are generally subjected to compressive stresses, interaction with the protected structure and the surrounding ground can lead to the development of shear stresses particularly when geofoam is installed against the sidewalls of the structure. In most of these geotechnical engineering applications, EPS geofoam is installed in direct contact with other materials (e.g. soil, concrete, PVC, and steel). Therefore, understanding the shear behavior of both the geofoam material and interface strength is essential for successful design of these types of structures.

Several studies investigated the strength properties of geofoam monoblocks and the interface properties of geofoam as it interacts with either geofoam or other construction material. A schematic showing typical direct shear tests used in these investigations is shown in Figure 2.1. For monoblocks, shear deformations generally develop along a horizontal shear plane that cuts through the material (Figure 2.1a), whereas interface shear failure develops along the contact surface under a given normal load (Figure 2.1b).

Some of the experimental studies related to the shear behavior of geofoam interface as well as the shear strength of geofoam blocks are summarized below.

2.4 Shear Behavior of Geofoam Interface

The interface shear behavior of EPS geofoam can be classified into three categories: (i) geofoam-geofoam; (ii) geofoam-sand; and (iii) geofoam in contact with other materials (concrete, steel, geotextiles, etc.). The relevant literature for these three categories is given in the following sections.

2.4.1 Geofoam-geofoam interface

Wagner [7] used tilt tests to study the interface strength of two geofoam blocks with density of 22 kg/m^3. The results were compared with those obtained using direct shear tests. The measured geofoam-geofoam friction coefficient using tilt tests was found to be 0.54. Peak and residual interface friction coefficients measured using direct shear tests were found to be 0.63 and 0.52, respectively. The Norwegian Road Research Laboratory [8] recommended an interface coefficeint of 0.7 for geofoam-geofoam whereas the UK Transportation Research Laboratory [9] suggested a a geofoam-geofoam interface coefficeint of 0.5.

Kuroda et al. [10] performed a series of shaking table tests to determine geofoam-geofoam interface strength and evaluate the effectiveness of binder plates installed between block layers under static and dynamic loading. Normal stresses of 7.4 kPa and 14.7 kPa were applied and the measured interface friction coefficients were found to range from 0.2 to 0.4. The effect of water on geofoam-geofoam interface properties was also studied by Sheeley and Negussey [11]. It was found that surface moisture, geofoam density and working stress level have a negligible effect on the characteristics of the geofoam-geofoam interface.

Barrett and Valsangkar [12] conducted direct shear tests on geofoam samples with and without a barbed connector under different normal stresses. Results showed that barbed connector plates did not provide additional interface shearing resistance. Abdelrahman et al. [13] performed direct shear tests on geofoam-geofoam interface and found that the increase in normal stress and the decrease in geofoam density cause an increase in both the peak and residual friction coefficients. AbdelSalam and Azzam [14] showed that the presence of water significantly decreased the shear strength of geofoam-geofoam interface. A summary of some of the available friction coefficient values in this category is given in Table 2.1.

2.4.2 Geofoam-sand interface

Direct shear tests performed by Miki [23] revealed that interface friction coefficients for geofoam-sand interface range from 0.55 to 0.7 depending on the thickness of the sand below the geofoam. Negussey [24] measured geofoam-sand interface friction and found that the friction coefficient is similar to that of the sand material. Xenaki and Athanasopoulos [25] found that geofoam-sand interaction mechanism can be represented by three stages: purely frictional, frictional-adhesional, and purely adhesional depending on the applied normal stress. Direct shear tests were also conducted on geofoam-sand interface by AbdelSalam and Azzam [14]. No significant change in interface friction coefficient was observed under both dry and wet conditions. Some of the available values of coefficient of friction for geofoam-sand interface are summerized in Table 2.2.

2.4.3 Geofoam interface with other material

Direct shear tests were performed by Sheeley and Negussey [11] on geofoam-cast in place concrete and geofoam-geomembrane interfaces. Results showed that geofoam-cast in place concrete provides more interface friction as compared to geofoam-geomembrane interface. Moreover, peak and residual responses were observed in both cases. A study conducted by Chrysikos et al. [19] showed that interface friction coefficient between geofoam and other material (i.e., soils, geotextiles, geomembranes, precast and cast-in-place concrete) ranges between 0.27 to 1.2. Similar study conducted by Padade and Mandal [21] evaluated the interface properties of geofoam in contact with other construction materials (e.g. jute geotextile, geogrid and fly ash). It was found that with the increase in geofoam density, adhesion values slightly increased while interface friction angle remain unchanged. A summary of selected interface coefficients for geofoam interacting with other material is given in Table 2.3.

2.5 Shear Behavior of Geofoam Monoblocks

Direct shear tests performed by Stark et al. [2] on geofoam samples of different densities showed that the cohesive strength is proportionally related to the material density. Similar conclusion was made by Padade and Mandal [26] based on direct shear tests performed on four different geofoam blocks having densities ranging between 15 and 30 kg/m^3. The increase in geofoam density resulted in significant increase in cohesion with slight increase in the angles of internal friction. Özer and Akay [22] conducted direct shear tests on EPS samples under a normal stress range of 10 to 40 kPa and found that the shear strength of the tested geofoam blocks is mainly dependent

on its cohesion while interface shear strength is dependent on both adhesion and friction coefficient. AbdelSalam and Azzam [14] tested both dry and wet geofoam samples and concluded that the presence of water caused approximately 30 % reduction in shear strength of the geofoam blocks under the same contact pressure. A brief summary of some of the available shear strength parameters of geofoam blocks is presented in Table 2.4.

The above studies provided some guidance in estimating the shear parameters of geofoam blocks as well as the interface strength between geofoam and different materials under a given test condition. However, the use of Polyvinyl chloride (PVC) or High-density polyethylene (HDPE) pipes has been growing in geotechnical applications over the past few years and, to date, a little work has been done to evaluate the interface shear parameters for cases where geofoam is installed in contact with PVC material. The objectives of this study are to: (i) carry out experimental investigation to measure the shear behavior of EPS geofoam blocks that span a range of densities from 15 to 39 kg/m^3, and (ii) measure the interface strength parameters for geofoam blocks that is in contact with PVC material as well as sand material.

2.6 Experimental Program

A series of direct shear tests was performed to evaluate the shear strength and interface parameters of three different EPS geofoam materials. A total of 27 tests were conducted- 9 tests on monoblocks and 18 interface shear tests. A brief description of the material properties and test procedure is given below.

2.6.1 Material properties

The material used in this study include EPS geofoam, PVC and sand material. The geofoam samples were cut from three large blocks of different densities, namely, 15 kg/m^3 (EPS15), 22 kg/m^3 (EPS22) and 39 kg/m^3 (EPS39). These densities cover the range of commonly used EPS materials in geotechnical applications [27]. The reported compressive strengths of these materials at 1% strain are 25 kPa, 50 kPa, and 98 kPa, respectively. The PVC samples (density = 1500 kg/m^3) were precisely cut to fit within the lower part of the direct shear box. As shown in Figure 2.2, the tested monoblocks measured 99.5 mm × 99.5 mm × 40 mm whereas the geofoam and PVC samples used in the interface tests measured 99.5 mm × 99.5 mm × 20 mm. Fine-grained silica sand, passing #40 sieve and retaining on #100 sieve was used in this study. The properties of the PVC and sand material used in the experiments are summarized in Table 2.5.

2.6.2 Test procedure

The shear box used throughout this study measures 100 mm ×100 mm × 50 mm and the tests were performed based on ASTM D5321-17 [31] under three different normal stresses, namely, 18 kPa; 36 kPa and 54 kPa. Horizontal displacement was applied at the recommended rate of 0.9 mm/min. Horizontal reaction was measured using a load cell while horizontal and vertical displacements were monitored using Linear Variable Differential Transformers (LVDTs). Tests were terminated when a maximum displacement of 10 mm was reached. This displacement limit was dictated by the horizontal movement allowed by the direct shear apparatus. ASTM D3080-11 [30] specifications suggest that, if no peak is observed, peak shear may be considered at 10% horizontal strain.

A total of 9 tests were performed on monoblocks that measure 99.5 mm × 99.5 mm × 40 mm. This represents three tests for each of the investigated density. Interface shear tests were performed on geofoam in direct contact with the PVC and the sand material. In the PVC interface tests, the geofoam was placed in upper box while the PVC sample was placed in lower box. This arrangement was adopted since the PVC block is considered incompressible compared to the geofoam under the applied loading and, hence, ensuring that the shear surface remains in line with the separation plane between the upper and lower parts of the box. Another advantage of this setup is that it minimizes the tilting that may be experienced if the lower block deforms unevenly during loading. Similar arrangement was used to study the geofoam-sand interface where the sand was placed in the lower part of the box and compacted to the target density (1.60 g/cm^3) before the overlying EPS block is placed. Adjustments were made to the setup before each test and a spirit level was used to ensure that the samples remain horizontal during the experiments.

2.7 Results and Discussion

The applied normal and shear loads as well as the corresponding displacements were measured for each of the performed test. The experimental results are used to develop the failure envelops and determine the shear strength parameters of the investigated conditions. It is noted that actual shear failure or rupture along the shear plan does not usually develop in EPS monoblocks, therefore, apparent failure, or excessive permanent deformation, (see Figure 2.2) is used to define the onset of monoblock shear failure in this study.

2.7.1 Shear strength of geofoam monoblocks

For the three applied normal stress values (18, 36 and 54 kPa), the horizontal displacements and the corresponding shear stresses are presented in Figures 2.3a through 3.3c for EPS15, EPS22, and EPS39, respectively. Shear stresses were found to increase with the increase in displacement and no apparent failure pattern developed up to the maximum applied displacement of 10 mm. The response of the geofoam can be characterized by two phases: (1) for displacement of up to 2 mm, shear stresses increased almost linearly with the increase in shear displacements. The maximum shear stress measured was found to be approximately 25 kPa, 30 kPa, and 40 kPa for EPS15, EPS22, and EPS39, respectively; (2) for displacement of more than 2 mm, shear stresses continued to increase at a slower rate reaching maximum values of 37, 42, and 54 kPa for EPS15, EPS22, and EPS39, respectively.

The measured normal and shear stresses are used to plot the Mohr-Coulomb failure envelops for the three investigated geofoam densities as illustrated in Figure 2.4. The failure envelops are generally parallel with a gentle upward slope. The shear resistance is found to increase with the increase in geofoam density. As far as shear strength parameters, it has been reported [22] that since the horizontal shear plane induced by the shear box passes through the geofoam specimen, the shear resistance is directly related to the cohesion of the geofoam material.

Figure 2.5 shows the changes in cohesion and friction angle for EPS monoblocks of different densities. The cohesive strengths were found to have an increasing trend with the increase in density. The cohesion values ranged from 28 kPa for EPS15 to about 56 kPa for EPS39 as illustrated in Figure 2.5a. Conversely, the friction angles experienced a slight decrease from about 10.5^{o} for EPS15 to 9^{o} for EPS39 as shown in Figure 2.5b. This validates the fact that shear strength of geofoam is mainly dependent on the material cohesion.

The recorded vertical compression of the geofoam blocks for different applied normal stresses is shown in Figure 2.6. In general, EPS15 experienced more vertical compression as compared to EPS39 and the vertical compression increased with the increase in normal stresses. These results are consistent with the fact that the compression of geofoam is directly related to applied normal stress and inversely related to density of geofoam. The trend lines revealed that the rate of compression, reflected by the slope of the lines, was the highest for EPS15 and decreased with the increase in geofoam density.

Another way to evaluate the effect of geofoam density on the shear strength of the tested blocks is to present the results using a normalized shear factor as shown in Figure 2.7. The shear factor is defined as the ratio of shear stress at failure to the corresponding normal stress. Shear factors of greater than 1 indicate that shear resistance is more than the applied normal stress whereas shear factors of less than 1 means that shear resistance is smaller than the normal stress. As illustrated in Figure 2.7, the shear factors decreased from about 1.7 to 0.7 for EPS15 and from 3.3 to 1.2 for EPS39 depending on the applied normal stress. These results confirm that for a given normal stress (e.g. 36 kPa), the shear stress at failure for both EPS15 and EPS22 is slightly higher than the applied normal stress with a difference in shear factor of about 10% between the two materials. EPS39, however, allowed shear stresses to reach up to 1.7 times the applied normal stress.

2.7.2 Interface strength properties

In this section, the results obtained from direct shear tests performed to study the shear resistance of geofoam block interacting with PVC and sand materials are presented.

2.7.2.1 Geofoam-PVC interface

The relationships between shear stresses and horizontal displacements for geofoam-PVC interface are shown in Figure 2.8. The behavior is characterized by rapid linear increase in shear stresses at a very small displacements followed by either a plateau (for EPS15 and EPS22) or slow increase in shear stresses as the displacements increased up to 10 mm. For a given displacement (e.g. 2 mm), the average measured shear resistance was found to be 11 kPa, 14 kPa and 18 kPa for EPS 15, 22 and 39, respectively. No peak or residual stresses were measured for the three investigated geofoam materials.

The failure envelops for the geofoam-PVC interface are shown in Figure 2.9. Shear stresses increased almost linearly with the increase in normal stresses. For all geofoam-PVC interfaces, linear failure envelopes were observed for all the densities of geofoam (Figure 2.10) and adhesion and angle of interface friction were calculated from these envelopes. For a given normal stress, the measured interface shear stress was found to increase with the increase in geofoam density. The slope of each line represents the interface friction angle whereas the intercept with the vertical axis represents the adhesion that develops at the PVC-geofoam interface. The relationships between the interface strength parameters and the geofoam density are shown in Figure 2.10. Adhesion increased from about 2 kPa for EPS15 to 5 kPa for EPS39 (Figure 2.10a). Friction angle did not

change significantly with the increase in density and ranged between 18° to about 21° for the three investigated geofoam materials. This range of interface friction is higher than that measured for the monoblock.

Vertical compression during shear in this case was found to be small as compared to the monoblock with a maximum compression value of 2 mm for EPS15 as shown in Figure 2.11. This is consistent with the thickness of the geofoam blocks used in interface tests, which is half of that of the monoblocks. Vertical compression decreased with the increase in density and the difference was more pronounced at high-applied normal stresses.

2.7.2.2 Geofoam-Sand Interface

The changes in shear stresses with the increase in horizontal displacements are shown in Figure 2.12. Shear stresses increased rapidly with the increase in horizontal displacement up to about 2 mm. The average measured shear resistance at 2 mm displacement was found to be 24 kPa, 28 kPa and 31 kPa for EPS15, EPS22 and EPS39, respectively. Slight reduction in displacements was measured in all cases as the displacement increased from 2 mm to 4 mm followed by a plateau for displacements more than 4 mm. The interface shear stress measured for the geofoam-sand interface was found to be generally higher as compared to that of the geofoam-PVC for the investigated range of normal stress and geofoam density.

Mohr-Coulomb failure envelops developing at the geofoam-sand surface are presented in Figure 2.13. At low normal stress values, the difference between the shear stresses for the three geofoam densities is negligible. With the increase in normal stresses geofoam density started to affect the developing shear stresses that reached values of 32 kPa for EPS15 and 45 kPa for EPS39 at applied normal stress of 54 kPa. This may be attributed to the fact that at low normal stress, little interaction develops at the interface between the geofoam and the underlying sand layer, whereas at higher normal stress, sand particles penetrate into the geofoam surface resulting in much higher shear stress values.

Shear strength parameters for different geofoam densities are shown in Figure 2.14. Adhesion values (Figure 2.14a) were found to decrease from about 12 kPa to 2 kPa as the density increased from 15 kg/m^3 to 39 kg/m^3. This may be attributed to the fact that stiffer geofoam (EPS39) develops less interaction with the sand particles as compared to the soft samples (EPS15), which allows for the sand penetration across the contact surface. Friction angles (Figure 2.14b) increased from 20° for EPS15 to 38° for EPS39. Post-test sample inspection revealed that the upper layer of

the sand particles was pushed into the surface of the soft geofoam blocks (EPS15) during testing creating a rough surface. Less interaction with the sand material was observed for the stiffer geofoam blocks (EPS39).

Vertical compression developing during the geofoam-sand interface tests is shown in Figure 2.15. For the same range of normal stresses, compression values were found to be larger than those measured for the case of geofoam-PVC but smaller than the compression of the monoblock. This is attributed to the compression experienced by the sand material during shear.

The above results suggest that the interface strength at the contact surface between a geofoam block and other material is highly dependent on the level of interaction that could develop at the interface. Stiff geofoam tends to produce small adhesion and friction angle when the geofoam is tested against material that has a smooth surface (e.g. PVC). Geofoam was found to develop more interaction with sand material resulting in higher adhesion and friction angle.

2.8 Conclusions

In this study, a series of direct shear tests was performed to measure the shear strength parameters of EPS monoblocks of different densities. In addition, interface shear tests were also performed to determine the shear parameters at the EPS-sand and EPS-PVC surfaces. Determining shear and interface properties of geofoam is essential for the analysis of geotechnical structures that involves geofoam interacting with other material. The experimental results presented in this study provides the shear parameters required for numerical modeling of similar problems. The following conclusions have been drawn based on this experimental study.

1. Geofoam monoblocks experienced shear deformation with no actual failure under direct shear condition. Shear strength was found to be highly dependent on the material cohesion that increased from 28 kPa to 56 kPa as the density increased from 15 kg/m^3 to 39 kg/m^3. Internal friction angle, however, showed slight decrease from 10.5^o to 9^o with the increase in density.
2. Geofoam-PVC interface showed an increase in adhesion from 2 kPa to 5 kPa with a slight decrease in interface friction angle (from 18^o to about 21^o) as the density of the geofoam increased from 15 kg/m^3 to 39 kg/m^3. For geofoam-sand interface, however, adhesion values decreased from 12 kPa to 2 kPa with the increase in EPS density. This is related to the fact

that low density geofoam interacts better with sand particles under high normal stresses as compared to the high-density geofoam material.

3. The measured compression for both the monoblocks and interface tests showed similar trends, however, the magnitude of compression was found to depend on the thickness of the tested geofoam sample. Monoblocks samples experienced more compression as it has twice the thickness of that used in the interface tests.

Further experiments are needed to study the interface strength properties of geofoam with other construction material, including, concrete, steel and different types of backfill material.

2.9 References

[1] BASF Corp. (1997) Styropor Technical Information, BASF Corp., Germany.

[2] Stark TD, Arellano D, Horvath JS, Leshchinsky D (2004) Geofoam applications in the design and construction of highway embankments. NCHRP web document 65:pp 24-11.

[3] Horvath JS (1997) The compressible inclusion function of EPS geofoam. Geotextiles and Geomembranes 15 (1):pp 77-120.

[4] Meguid M, Ahmed M, Hussein M, Omeman Z (2017) Earth pressure distribution on a rigid box covered with u-shaped geofoam wrap. International Journal of Geosynthetics and Ground Engineering 3 (2):p 11.

[5] Meguid M, Hussein M, Ahmed M, Omeman Z, Whalen J (2017) Investigation of soil-geosynthetic-structure interaction associated with induced trench installation. Geotextiles and Geomembranes 45 (4):pp 320-330.

[6] Bathurst R, Zarnani S, Gaskin A (2007) Shaking table testing of geofoam seismic buffers. Soil Dynamics and Earthquake Engineering 27 (4):pp 324-332.

[7] Wagner G (1986) A senior report on expanded polystyrene as lightweight embankment material. University of New Brunswick, Canada.

[8] NRRL (1992) Expanded polystyrene used in road embankments.Oslo, Norway.

[9] Sanders R, Seedhouse R (1994) The use of polystyrene for embankment construction. TRL Contractor Report (CR 356).

[10] Kuroda S, Hotta H, Yamazaki F (1996) Simulation of shaking table test for eps embankment model by distinct element method. In: Proceedings of International Symposium on EPS (Expanded Poly-Styrol) Construction Method (EPS Tokyo'96).

[11] Sheeley M, Negussey D (2000) An investigation of geofoam interface strength behavior. Geotechnical Special Publication 301:pp 292-303.

[12] Barrett JC, Valsangkar AJ (2009) Effectiveness of connectors in geofoam block construction. Geotextiles and Geomembranes 27 (3):pp 211-216.

[13] Abdelrahman G, Duttine A, Tatsuoka F (2010) Interface friction properties of EPS geofoam blocks from direct shear tests. In: Characterization and Behavior of Interfaces: Proceedings of Research Symposium on Characterization and Behavior of Interfaces, Atlanta, Georgia, USA. IOS Press, p 113.

[14] AbdelSalam S, Azzam S (2016) Reduction of lateral pressures on retaining walls using geofoam inclusion. Geosynthetics International 23 (6):pp 395-407.

[15] McAffee R (1993) Geofoam as lightweight embankment fill. Department of Geological Engineering Senior Report, University of New Brunswick, Fredericton, NB.

[16] Nomaguchi A (1996) Studies on earthquake resisting performance of EPS embankment. In: Proceedings of International Symposium on EPS (Expanded Poly-Styrol) Construction Method (EPS Tokyo'96).

[17] Negussey D, Anasthas N, Srirajan S (2001) Interface friction properties of EPS geofoam. Proc., EPS Geofoam 2001: 3rd Int. Conf., Salt Lake City, UT.

[18] Atmatzidis DK, Missirlis EG, Theodorakopoulos EB (2001) Shear resistance on EPS geofoam block surfaces. In: EPS Geofoam 2001: 3rd Annual Conf., Geotechnical Engineering Laboratory, Univ. of Patras, Greece.

[19] Chrysikos D, Atmatzidis D, Missirlis E (2006) EPS geofoam surface shear resistance. 8thIGS Yokohama, Japan:pp 1651-1654.

[20] Neto JA, Bueno B (2012) Laboratory research on EPS blocks used in geotechnical engineering. Soils and Rock-An International Journal of Geotechnical and Geoenvironmental Engineering 35(2):pp 169-180.

[21] Padade A, Mandal J (2014) Interface strength behavior of expanded polystyrene EPS geofoam. International Journal of Geotechnical Engineering 8 (1):pp 66-71.

[22] Özer AT, Akay O (2015) Interface shear strength characteristics of interlocked EPS-block geofoam. Journal of Materials in Civil Engineering 28 (4):pp 04015156.

[23] Miki G (1996) Ten year history of EPS method in Japan and its future challenges. In: Proceeding of the International Symposium on EPS Construction Method. Tokyo, Japan, pp 394-411.

[24] Negussey D (1997) Properties and applications of geofoam, society of the plastics industry. Inc Foamed Polystyrene Alliance, Washington, DC.

[25] Xenaki V, Athanasopoulos G (2001) Experimental investigation of the interaction mechanism at the EPS geofoam-sand interface by direct shear testing. Geosynthetics International 8 (6):pp 471-499.

[26] Padade A, Mandal J (2012) Direct shear test on expanded polystyrene (EPS) geofoam. In: Proc., 5th European Geosynthetic Congress, International Geosynthetics Society, Jupiter, FL.

[27] Xiao M (2015) Geotechnical engineering design. John Wiley & Sons.

[28] ASTM D421-85(2007) Standard practice for dry preparation of soil samples for particle-size analysis and determination of soil constants. ASTM International, West Conshohocken, PA. http://wwwastmorg.

[29] ASTM D422-63(2007)e2 Standard test method for particle-size analysis of soils. ASTM International, West Conshohocken, PA. http://wwwastmorg.

[30] ASTM D3080 / D3080M-11 Standard Test Method for Direct Shear Test of Soils Under Consolidated Drained Conditions. ASTM International, West Conshohocken, PA. http://wwwastmorg.

[31] ASTM D5321 / D5321M-17 Standard test method for determining the shear strength of soil-geosynthetic and geosynthetic-geosynthetic interfaces by direct shear. ASTM International, West Conshohocken, PA. http://wwwastmorg.

Table 2.1 Selected geofoam-geofoam interface studies

Reference	Test /Sample size (mm x mm)	Sample density (kg/m^3)	Coefficient of friction / friction factor
McAffee [15]	Ring shear test	15	0.90 (peak), 0.62 (residual)
Nomaguchi [16]	Monotonic and cyclic direct shear test	____	0.5
Sheeley, Negussey [11]	Direct shear test 100 × 100 to 500 × 500	18	0.9 (peak), 0.7 (residual) (dry)
	Direct shear test 100 × 100 × 25	20	0.85 (peak), 0.7 (residual) (dry)
			0.80 (peak), 0.65 (residual) (wet)
Negussey et al. [17]	Lower sample: 600 × 600 Upper sample: 175 × 375	18	0.94 (peak), 0.65 (residual)
		20	1.13 (peak), 0.68 (residual)
Atmatzidis et al. [18]	Direct shear test 100 × 300	20	0.83 (peak)
		30	0.93 (peak)
Chrysikos et al. [19]	Direct shear test	15 & 30	0.7-0.84 0.8 (average)
Barrett, Valsangkar [12]	Direct shear test 430 × 280 × 100	30	0.87-1.06 (peak) 0.74-0.86 (residual)
		15	0.60-0.99 (peak) 0.60-0.75 (residual)
Abdelrahman et al. [13]	Direct shear test 120 × 120 × 60	20	0.75-0.90 (peak) 0.55-0.63 (residual)
		30	0.65-0.82 (peak) 0.50-0.59 (residual)
Neto, Bueno [20]	Direct shear test	20	0.65 (peak), 0.51 (residual)
		30	0.75 (peak), 0.48 (residual)
Padade, Mandal [21]	Direct shear test 300 × 300 × 75	22	0.55 (peak), 0.53 (residual)
		30	0.57 (peak), 0.55 (residual)
Özer, Akay [22]	Direct Shear 150 × 100	19	0.79 (peak), 0.72 (residual)
		29	0.98 (peak), 0.63 (residual)
AbdelSalam, Azzam [14]	Direct shear test 100 × 100 × 50	____	0.54 (dry)
			0.71 (wet)

Table 2.2 Selected geofoam-sand interface studies

Reference	**Test /Sample size (mm × mm)**	**Sample density (kg/m^3)**	**Coefficient of friction / friction factor**
Miki [23]	Direct shear test	20	0.70 (sand layer thickness <35mm) 0.55 (sand layer thickness >35mm)
Negussey [24]	Direct shear test	____	same as that of friction angle of sand alone.
Xenaki, Athanasopoulos [25]	Direct shear test 100 × 100	10	0.67 (purely frictional), 0.34 (frictional-adhesional), 0 (purely adhesional.)
		20	0.62 (purely frictional) 0.27 (frictional-adhesional)
AbdelSalam, Azzam [14]	Direct shear test 100 × 100 × 50	____	0.66 (dry) 0.61 (wet)

Table 2.3 Selected geofoam-other material interface studies

Reference	Test /Sample size (mm x mm)	Sample density (kg/m^3)	Interface	Coefficient of friction / friction factor
Sheeley, Negussey [11]	Direct shear test 100 × 100 × 25	____	geofoam-cast in place concrete	2.36 (peak) 1 (residual)
			geofoam- smooth geomembrane	0.7 (peak) 0.4 (residual)
Chrysikos et al. [19]	Direct shear test	____	geofoam-other materials (i.e., soils, geotextiles, geomembranes, precast and cast-in-place concrete).	0.27 to 1.2
Padade, Mandal [21]	Direct shear test 300 × 300 × 75	15	geofoam-geotextile	0.17
			geofoam-geogrid	0.14
			geofoam-fly ash	0.21
		30	geofoam-geotextile	0.19
			geofoam-geogrid	0.12
			geofoam-fly ash	0.23
AbdelSalam, Azzam [14]	Direct shear test 100 × 100 × 50	____	geofoam-concrete smooth (dry)	0.49
			geofoam-concrete smooth (wet)	0.51
		____	geofoam-concrete rough(dry)	0.96
			geofoam- concrete rough (wet)	0.48

Table 2.4 Selected geofoam monoblock studies

Reference	Test /Sample size (mm x mm)	Density (kg/m^3)	Shear strength parameters	
			c_a (kPa)	δ (degrees)
Stark et al. [2]	____	18.4	27.5	____
		28.8	50.0	____
Padade, Mandal [26]	Direct shear test 100 × 100 × 50	15	30.8	3.0
		20	36.0	4.0
		22	40.3	4.5
		30	59.8	6.0
Özer, Akay [22]	Direct shear test 100 × 100	18.5	26.6	10.0
		29.9	49.8	8.9
AbdelSalam, Azzam [14]	Direct shear test 100 × 100 × 50	20	12 (dry)	33 (dry)
		20	16 (wet)	19 (wet)

Table 2.5 Properties of the PVC and sand used in the experiments

PVC material*		
Density	1500 kg/m^3	
Tensile Strength	41368 kN/m^2 (6000 psi)	
Water Absorption	0.13 %	
Coefficient of Thermal Expansion	3.3×10^{-5} 1/ºF	
Silica sand		
Density	1.60 g/cm^3	[28]
Coefficient of uniformity (C_u)	1.9	[29]
Coefficient of curvature (C_c)	1.3	
Peak internal angle of friction (ϕ_{peak})	41º	[30]
Residual internal angle of friction ($\phi_{residual}$)	35º	

* Provided by the manufacturer

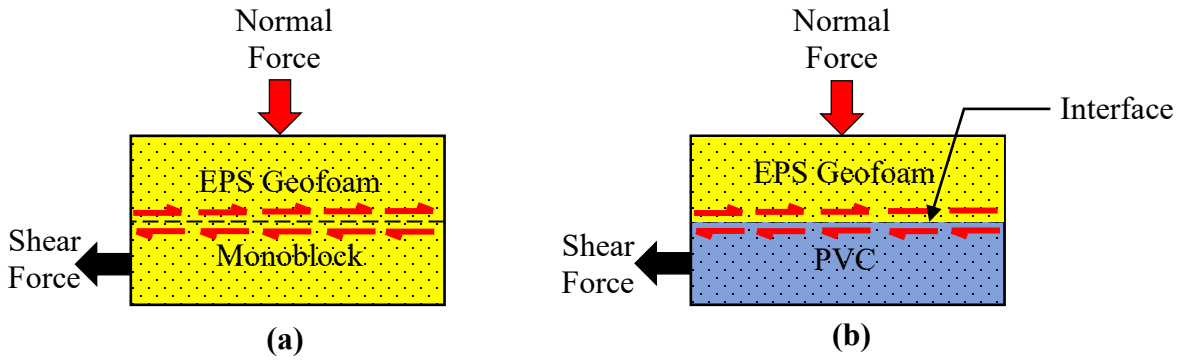

Figure 2.1 Schematics of the direct shear test: (a) geofoam block; (b) geofoam-PVC interface

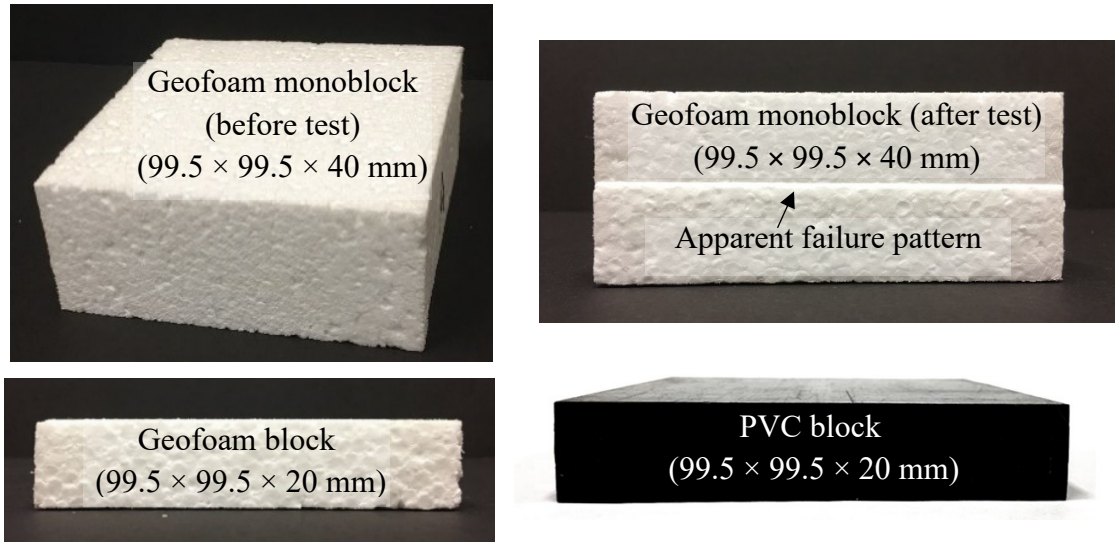

Figure 2.2 Geofoam and PVC samples used in the experiments

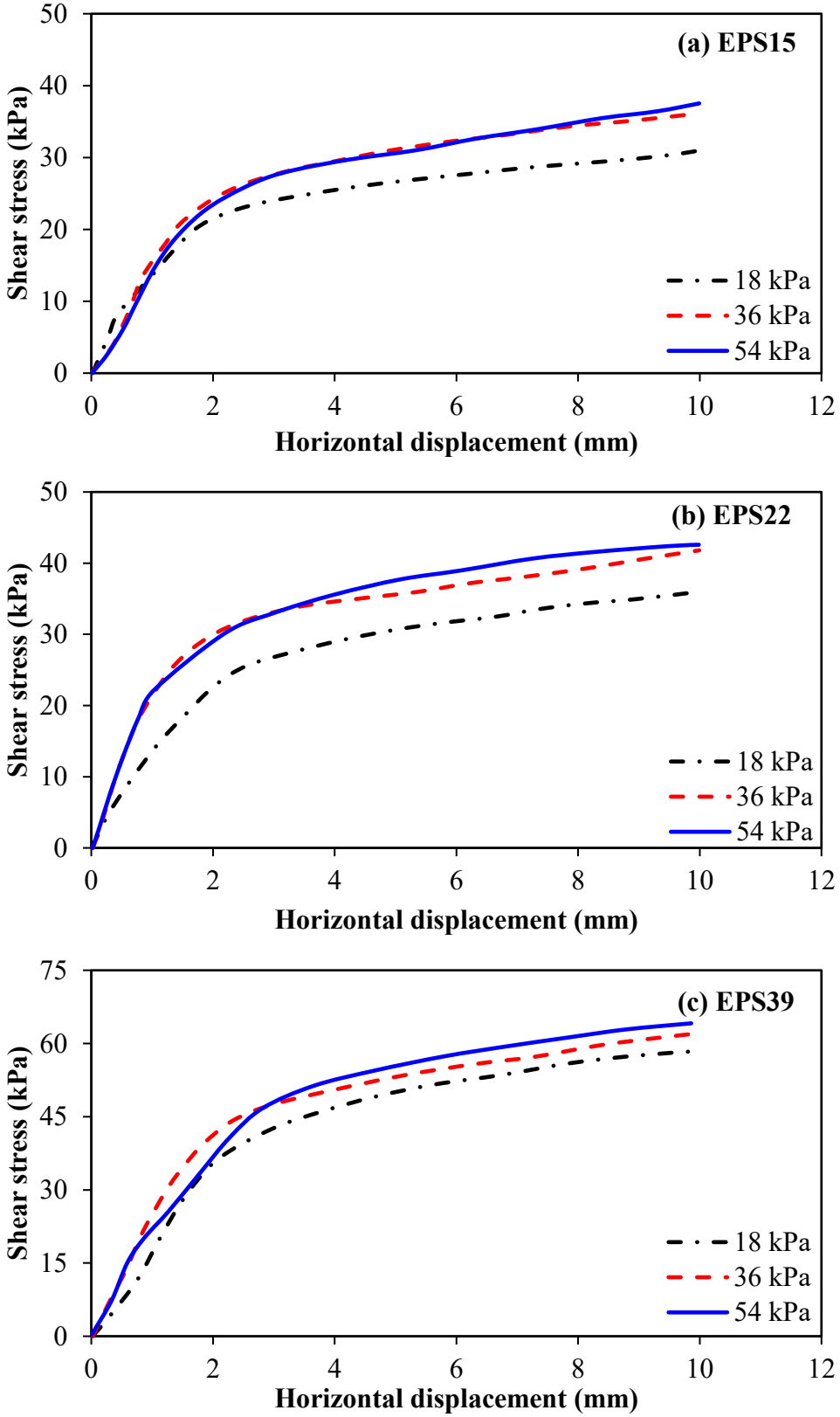

Figure 2.3 Shear stress vs. horizontal displacemnts for monoblocks of different densities: (a) EPS15; (b) EPS22 and (c) EPS39

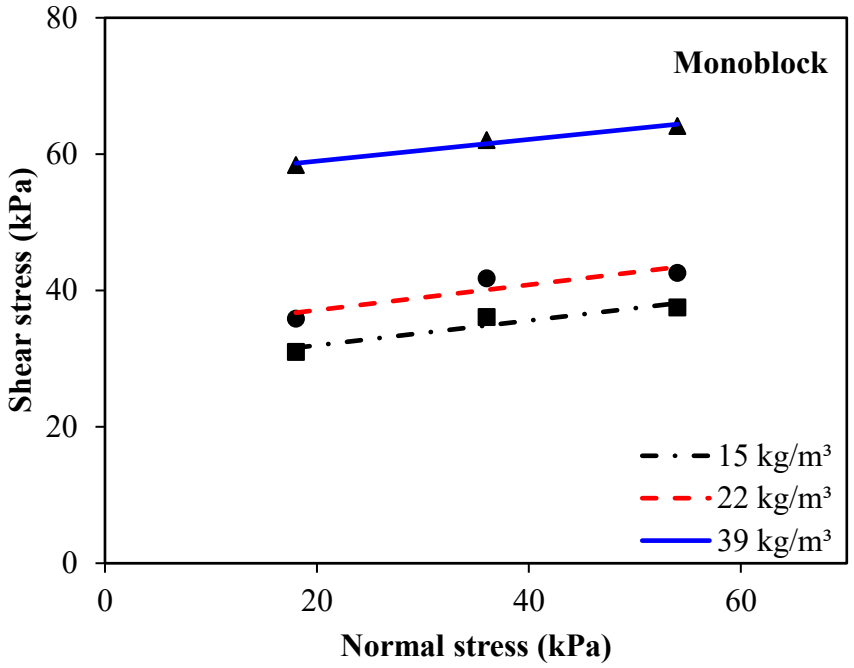

Figure 2.4 Mohr-Coulomb failure envelopes of geofoam monoblocks

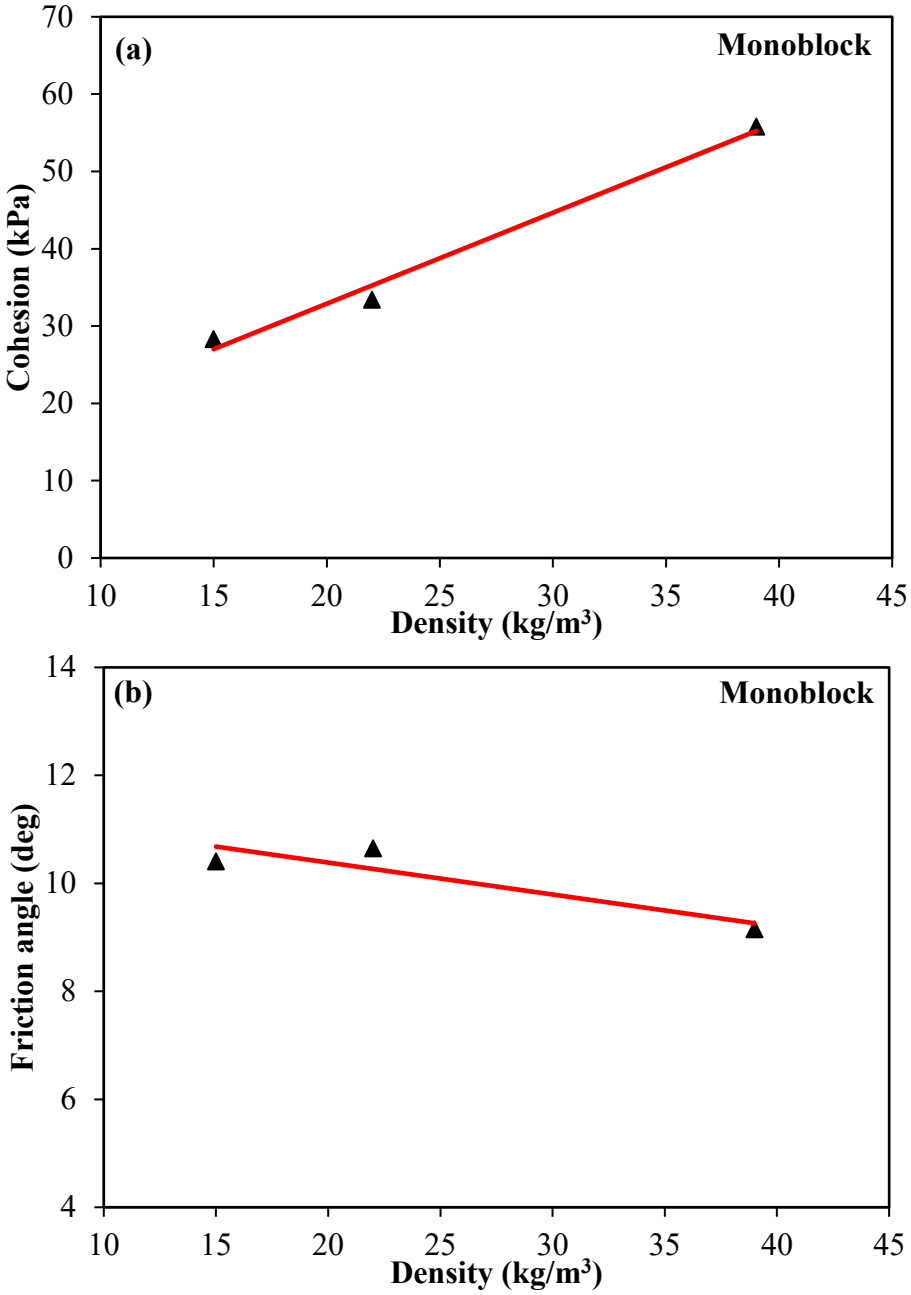

Figure 2.5 Effect of geofoam density on: (a) cohesive strength and (b) friction angle

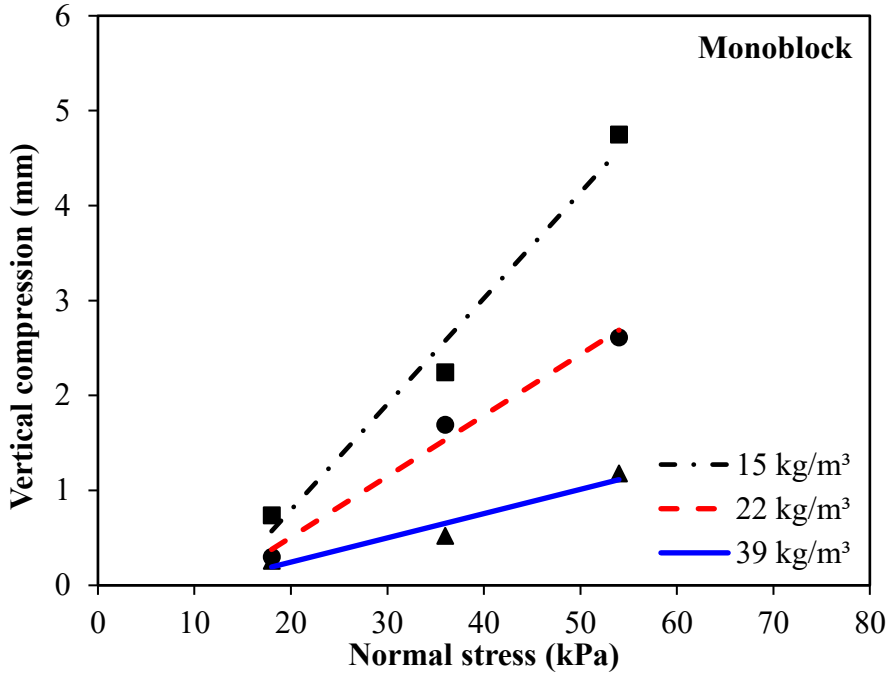

Figure 2.6 Vertical compression measured of geofoam monoblock under different applied normal stresses

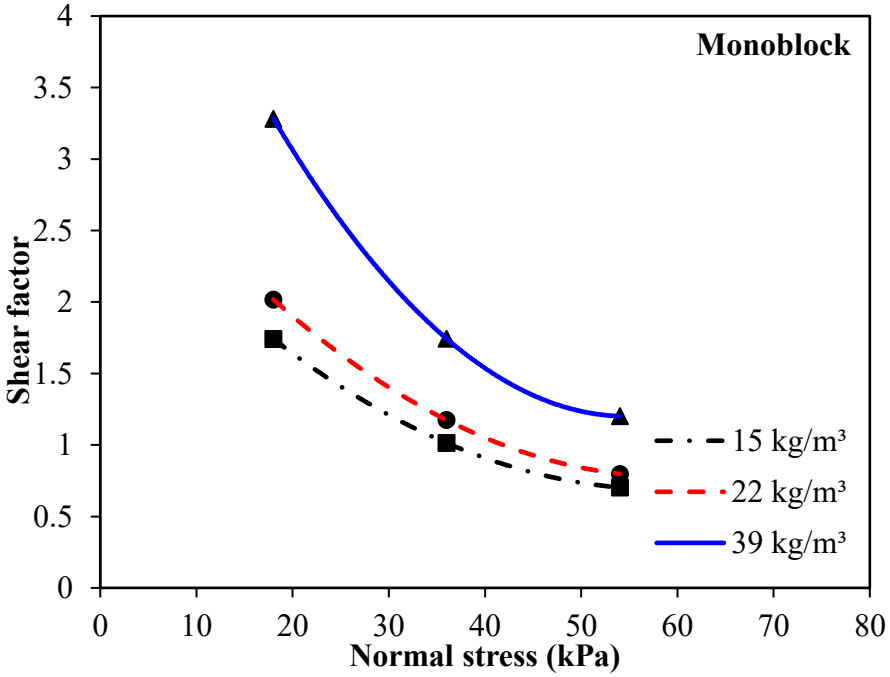

Figure 2.7 Shear factors for different geofoam materials

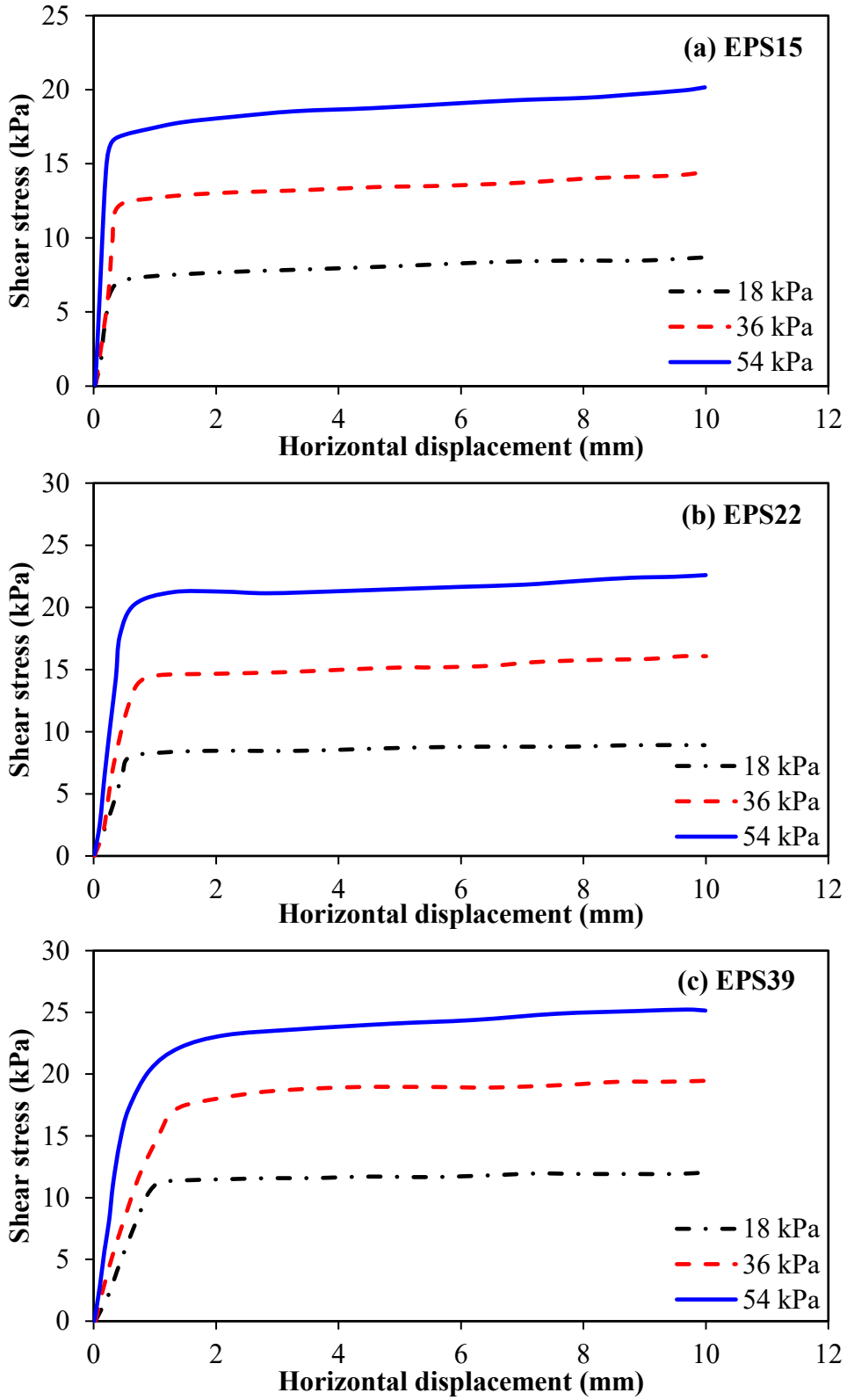

Figure 2.8 Shear stress vs. horizontal displacemnts for geofoam-PVC interface: (a) EPS15; (b) EPS22 and (c) EPS39

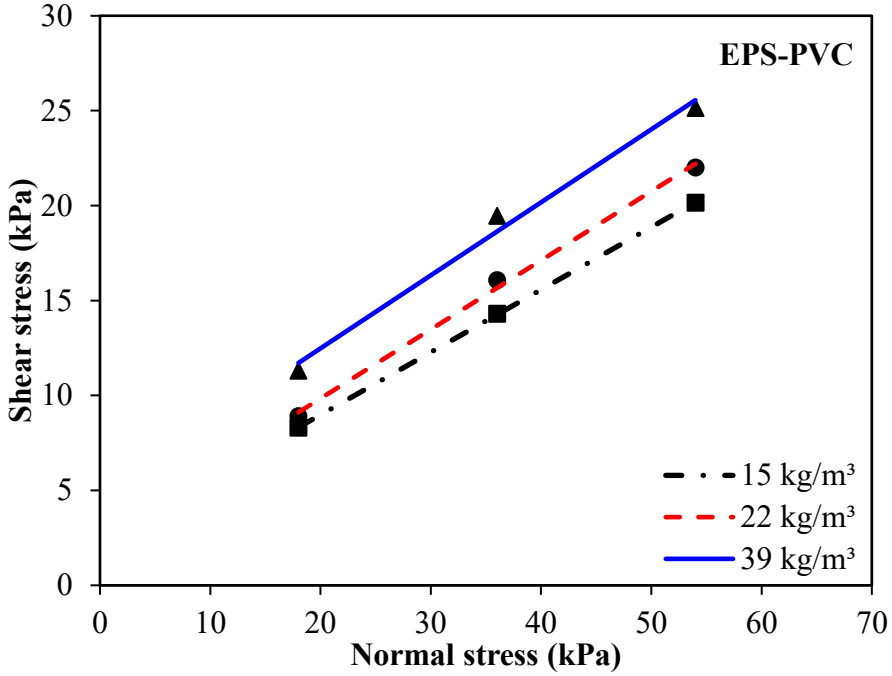

Figure 2.9 Mohr-Coulomb failure envelopes for geofoam-PVC interface

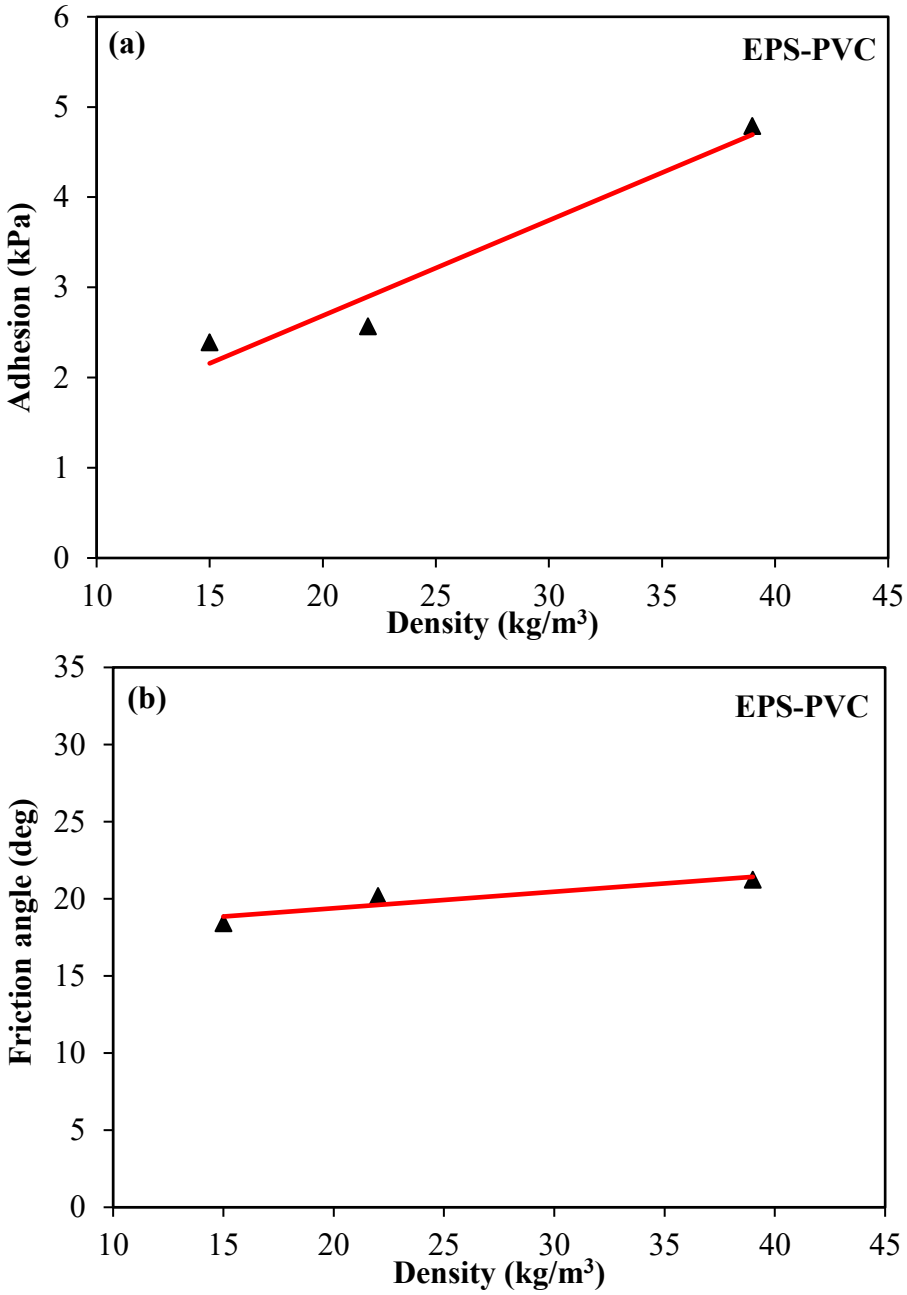

Figure 2.10 Effect of geofoam density on the shear strength of the geofoam-PVC interface: (a) adhesion; and (b) friction angle

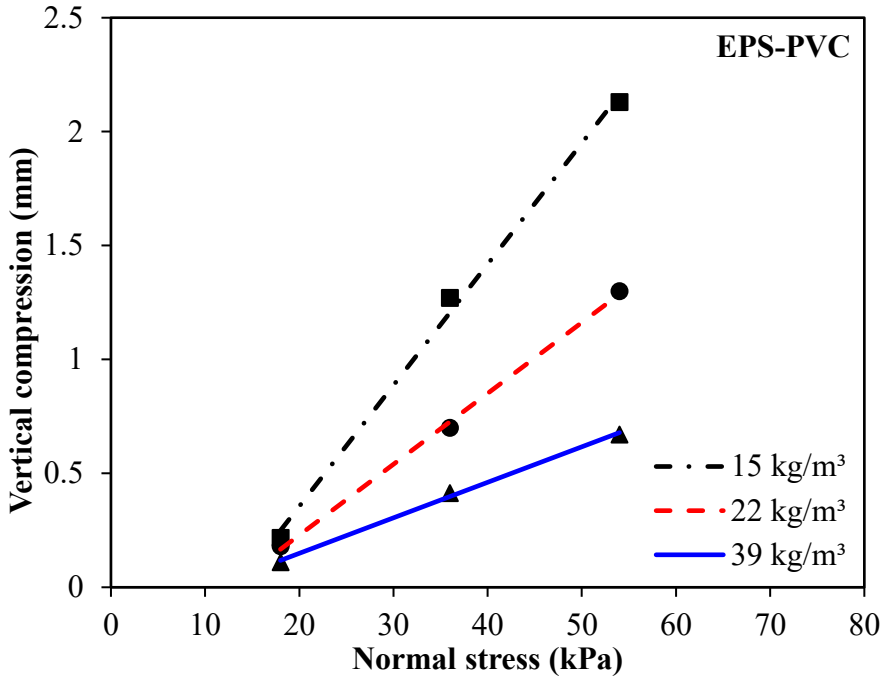

Figure 2.11 Vertical compression measured for the geofoam-PVC interface test under different applied normal stresses

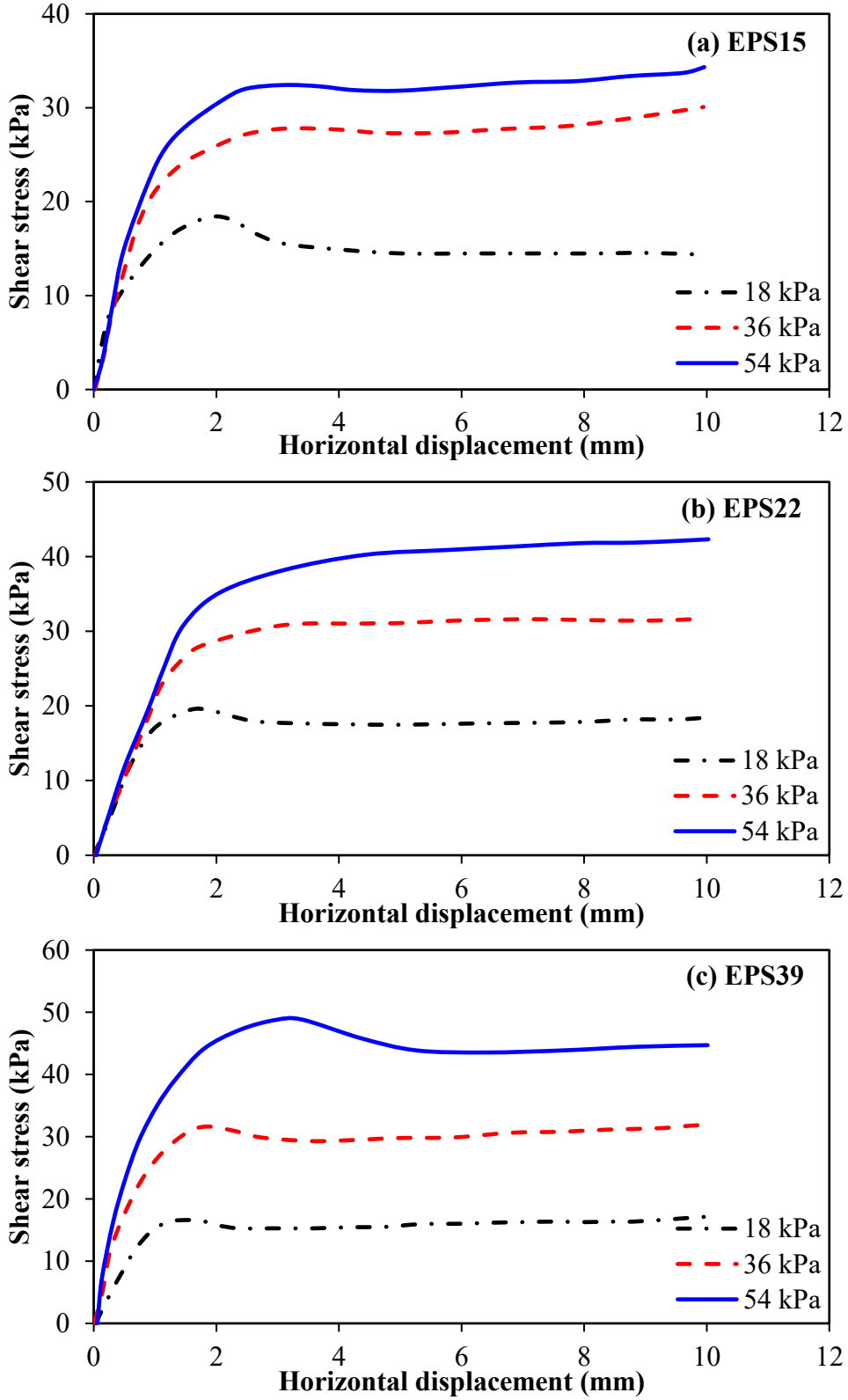

Figure 2.12 Shear stress vs. horizontal displacemnts for geofoam-sand interface: (a) EPS15; (b) EPS22 and (c) EPS39

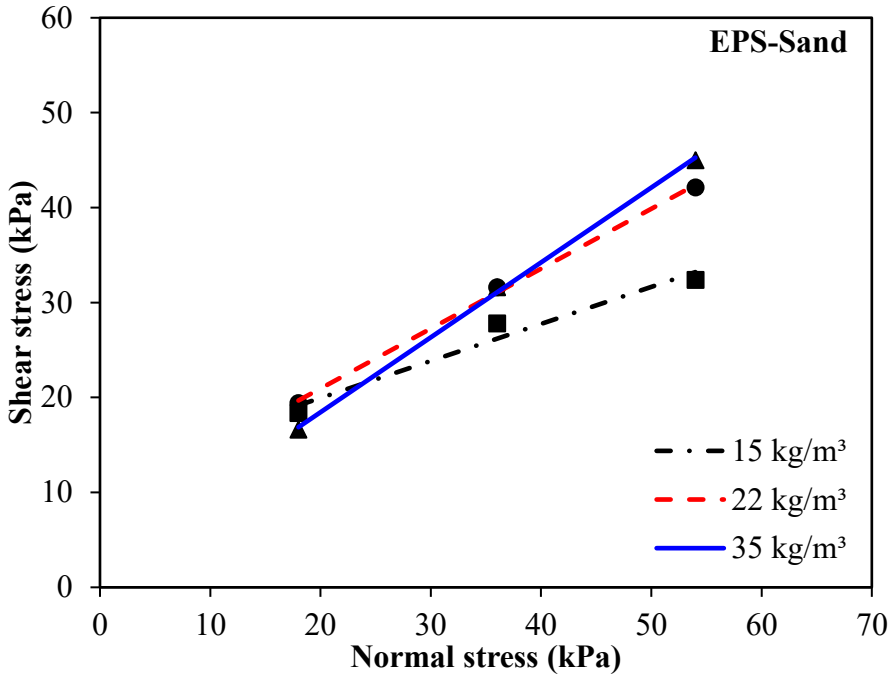

Figure 2.13 Mohr-Coulomb failure envelopes for geofoam-sand interface

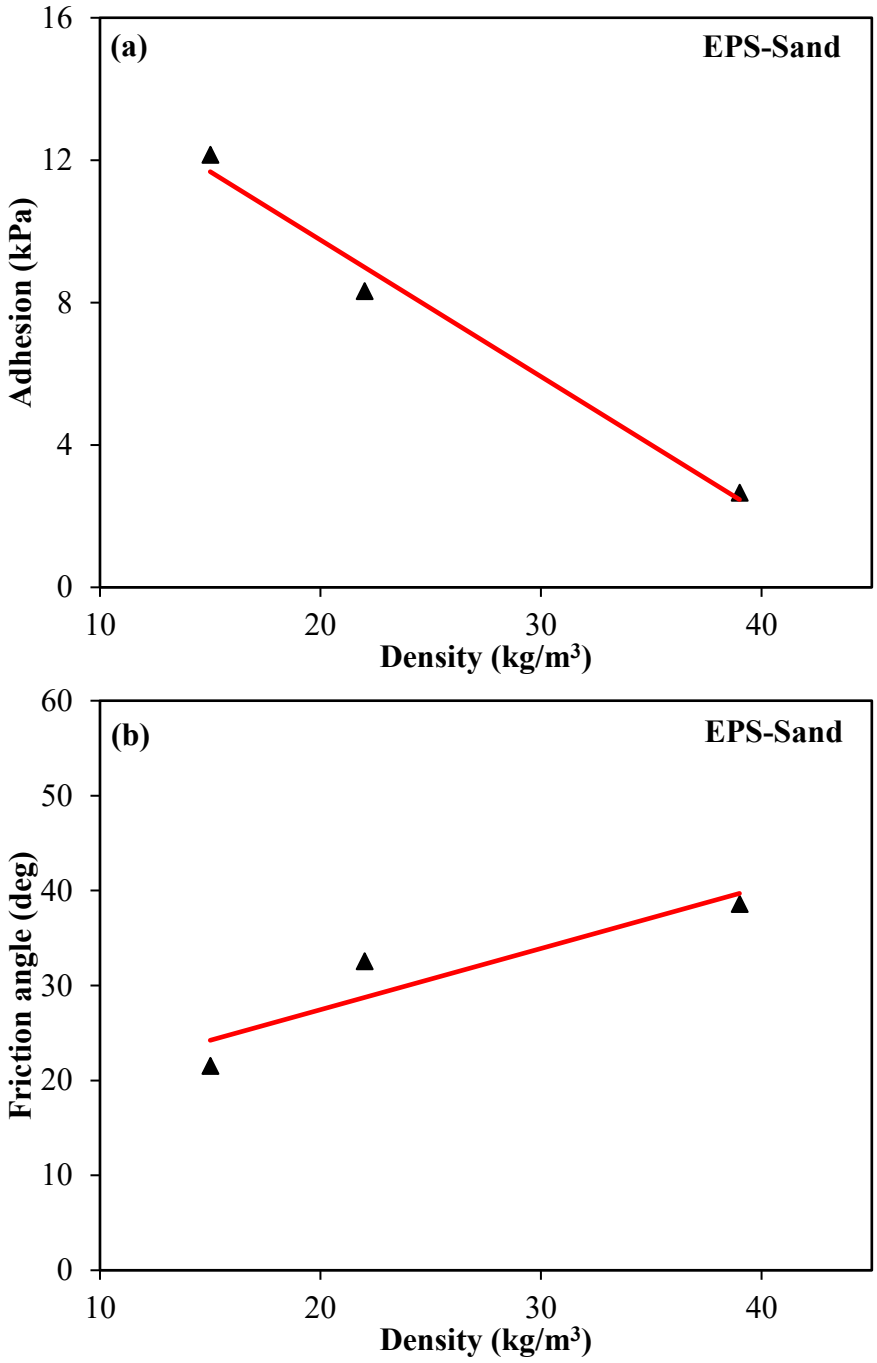

Figure 2.14 Effect of density on the shear strength of the geofoam-sand interface: (a) adhesion; and (b) friction angle

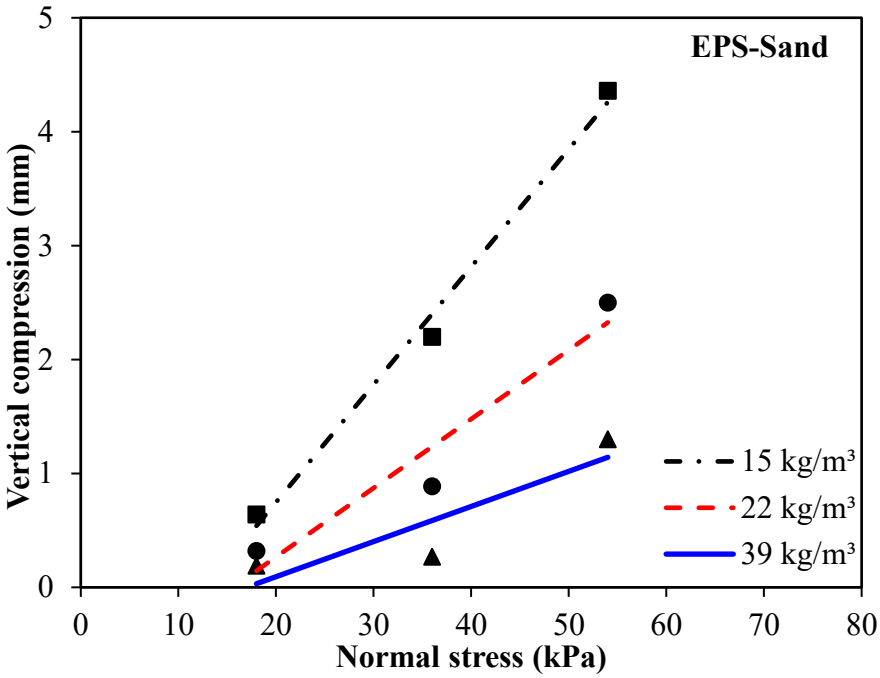

Figure 2.15 Vertical compression measured for the geofoam-sand interface under different normal stresses

3

On the Role of Geofoam Density on the Interface Shear Behavior of Composite Geosystems*

* A version of this chapter has been published as:
Meguid, M. A., & Khan, M. I. (2019). *On the role of geofoam density on the interface shear behavior of composite geosystems*. International Journal of Geo-Engineering, 10(1), 6.

3.1 Preface

Chapter 2 presented the results of direct shear test (DST) conducted on monoblock of EPS geofoam and interface direct shear test conducted on geofoam-PVC and geofoam-sand interfaces. In this chapter interface properties of EPS geofoam have been investigated with some more materials. The results of interface direct shear test conducted on geofoam-concrete, geofoam-steel and geofoam-wood interfaces are presented in detail.

3.2 Abstract

Expanded polystyrene (EPS) geofoam has been increasingly used in geotechnical engineering applications to replace conventional backfill material or to reduce earth pressure on retaining and buried structures. In most of these applications, geofoam blocks are installed in direct contact with different construction material (soil, concrete, steel, wood, etc.). This results in a composite system that is subjected to loading in both the normal and shear directions. Therefore, successful analysis and design of these composite structures require a detailed knowledge of interface strength characteristics of geofoam under a combination of normal and shear stresses. In the current research, an attempt has been made to study the interface shear characteristics of geofoam with selected materials, including concrete, wood and steel. Three different geofoam densities namely, 15, 22 and 39 kg/m^3 were used in this study. A series of direct shear tests (DST) was conducted with a shear box of dimension 100 mm × 100 mm × 50 mm under three different normal stresses 18, 36 and 54 kPa. Test results revealed that geofoam density and applied normal stress have

significant effects on the vertical compression and interface strength properties (i.e. adhesion and friction angle) of the investigated geosystem. Surface roughness was found to play a significant role in the shear resistance at the contact. Geofoam-concrete interface showed maximum strength as compared to wood and steel materials. Care should be exercised when placing geofoam against steel or wood surfaces as the mobilized friction angle is generally small and sliding may develop depending on the applied normal stress level.
Keywords: EPS geofoam, direct shear tests, friction angle, adhesion, interface shear strength.

3.3 Introduction

The use of expanded polystyrene (EPS) geofoam as construction material dates back to the 1960s. Norwegian engineers used EPS geofoam for thermal insulation in road projects constructed in 1965 [1] and large geofoam blocks were used in 1972 as a lightweight fill material in embankments built on soft soils [2]. Since then the use of molded geofoam blocks has been expanded to other geotechnical engineering applications, including slope stabilization [3-7], subbase fill material [8-11], embankments [2,3,9,12-22], earth retaining structures [3,16], bridge approaches [3,15,23-26] and buried pipes [3,27,28]. The high compressibility nature of geofoam material makes it also suitable for applications that require the presence of compressible buffers behind the walls of rigid structures [20,29-31].

In most of the above applications, EPS geofoam is used in conjunction with other construction materials (e.g. soil, concrete, wood, PVC, steel, geogrid) to form a composite system, which is then exposed to static or dynamic loadings. A schematic that illustrates the use of EPS behind a retaining wall is shown in Figure 3.1. Therefore, detailed information of the interface strength is required for successful analysis and design of structures constructed with EPS inclusion. Interface strength is usually determined using the ratio of resisting shear stress to the applied normal stress. Several researchers investigated the interface shear characteristics of geofoam interacting with different construction materials. A summary of these studies is given below.

Sheeley and Negussey [32] performed a series of modified direct shear tests to study the interface properties of geofoam in contact with geomembrane (smooth or textured) and cast-in-place concrete. Tests were conducted on EPS samples of 18 and 29 kg/m^3 densities under constant normal stress that ranges from 14 to 48 kPa. It was found that both smooth and textured geomembranes offered much less interface friction (both peak and residual) as compared to cast-in-place concrete.

Direct shear tests were conducted by Chrysikos et al. [33] to measure the frictional resistance at the interface between geofoam blocks (densities 15 and 30 kg/m^3) and other materials (concrete, soils, geomembranes, and geotextiles). The friction coefficients were found to range from 0.27 to 1.2.

Padade and Mandal [34] performed a series of direct shear tests for various geofoam samples interacting with jute geotextile, fly ash, and geogrid. EPS geofoam samples with densities of 15 and 30 kg/m^3 were tested under normal stress range of 25 to 100 kPa. Results showed that the increase in geofoam density resulted in a slight increase in adhesion with no significant change in interface friction angle. For both geofoam densities, geofoam-geogrid interface showed the least frictional resistance while geofoam-fly ash interface showed the most frictional resistance.

Abdel-Salam and Azzam [35] conducted modified direct shear tests on geofoam-concrete interface under dry and wet conditions. Results indicated that the roughness of the concrete surface has a significant effect on the interface friction coefficient. For dry condition, concrete with rough or textured interface showed much larger frictional resistance over that with a smooth surface. On the contrary, for wet condition, smooth interface developed more frictional resistance.

Khan and Meguid [36] presented experimental results involving geofoam-PVC and geofoam-sand interfaces utilizing EPS samples of 15, 22 and 35 kg/m^3 and a 100 mm × 100 mm direct shear box. To measure the interface coefficient between PVC and geofoam, a PVC block 99.5 × 99.5 × 20 mm was placed in the lower half of the box and then overlain by a geofoam block of the same size. For tests involving geofoam-sand interface, silica sand was compacted in layers in the lower half of the box to reach a density of 1.6 g/cm^3. Tests were performed under a normal stress that ranged from 18 to 54 kPa. Results showed that geofoam-sand interface developed frictional resistance that is much larger that that measured for the geofoam-PVC interface. A summary of some of the available interface friction coefficients is given in Table 3.1.

3.4 Scope and Objectives

Although the above studies covered important aspects related to the interface strength of geofoam interacting with various construction material, there is a need for additional investigations to understand how geofoam density affects the interface strength for a range of materials. The aim of this study is, therefore, to evaluate the role of EPS density on the interface shear strength of three different materials, namely, concrete, wood and steel. Details of the experimental program are given in the subsequent section.

3.5 Experimental Program

A series of direct shear tests were performed to evaluate the interface shear properties of different EPS geofoam blocks placed over a given construction material. A total of nine experiments were performed for each of the three investigated materials (concrete, wood, and steel) such that the test is repeated three times for each geofoam density (15, 22, and 39 kg/m^3). The material properties and test procedure are given below.

3.5.1 Material properties

The materials used in this investigation include EPS geofoam, concrete, wood and steel as depicted in Figure 3.2. Three different sets of geofoam samples with densities of 15 kg/m^3 (EPS15), 22 kg/m^3 (EPS22) and 39 kg/m^3 (EPS39) were examined. These material densities cover a wide range of EPS geofoam used in geotechnical projects [37]. Before commencing the interface tests, uniaxial compressive strength tests were performed on the EPS samples as per ASTM D1621-10 (2010) specifications. The uniaxial compression curves (presented in Figure 3.3) are characterized by a linear increase in response up to about 1% strain (calculated as the ratio of sample compression to the original sample height). This is followed by an increase at a slower rate up to the maximum applied stress. The uniaxial compressive strength properties are summarized in Table 3.2. For EPS15, the uniaxial compressive strength at 1% strain was found to be 50 kPa which increased to 80 kPa at 5% strain and reached 90 kPa at 10% strain. These strength values were almost doubled for EPS22 where the strength values at 1% and 5% strains were found to be 63 kPa and 125 kPa, respectively.

The steel, concrete and wood samples were cut accurately to fit into the lower part of the direct shear box. Plain concrete samples were prepared using fine and coarse granite with a water-cement ratio of 0.65 which has a slump of 228 mm. Visual inspection of samples revealed that the concrete surface was rough while pine wood and steel were characterized by a relatively smooth surface of different texture. Properties of all the three materials as obtained from the manufacturer are given in Table 3.3.

3.5.2 Test procedure

Interface direct shear tests were performed throughout this study following ASTM D5321-17 [39]. A direct shear box of dimensions 100 mm × 100 mm × 50 mm was used throughout this study. For each interface test, a geofoam sample was placed in the upper part of the box while the other

block of interacting material was placed in the lower part of the box as shown in Figure 3.4. This arrangement ensures full contact between the two samples during the test. It also reduces the chances of tilting that may develop if the lower sample compresses non-uniformly. Due to the heavy weight of the steel block, a thin 6-mm steel plate was used with 14 mm dummy wooden block (see Figure 3.2b). This allowed for the weight of the box to be easily managed.

During the test, a horizontal displacement was applied to the lower half of the box at a rate of 0.9 mm/min while the upper half was fixed. Tests were conducted under normal stresses of 18, 36 and 54 kPa. Vertical and horizontal displacements were measured using linear variable differential transformers (LVDTs) and the shear force was measured using a load cell. Tests were terminated when the shear force started to decrease or when the maximum displacement allowed by the direct shear box (i.e. 10 mm) was reached. According to ASTM D3080-11 [40], if no peak behavior is observed during the test, peak shear stress may be considered to develop at 10% horizontal strain. Adhesion and interface friction angles were determined from the results of the direct shear tests for different geofoam densities.

3.6 Results and Discussion

The results of the performed tests are presented in this section for the three investigated materials (concrete, steel and wood). The role of geofoam density in each case is highlighted. Stress-displacement relationships are presented using the normalized stress ratio that represents the ratio between shear and normal stresses as measured in the experiments.

3.6.1 Interface strength properties

3.6.1.1 Geofoam-Concrete interface

The relationship between shear stress ratio and the sample displacements are presented in Figure 3.5 for the three investigated geofoam densities. The applied normal stresses ranged between 18 and 54 kPa. For EPS15 (Figure 3.5a), samples generally showed hardening behavior following an initial linear response. The shear stress ratio was found to decrease with the increase in applied normal stress. Figure 3.5a also shows that the increase in normal stresses is directly related to the increase in the measured vertical displacement of the sample. The maximum vertical displacements at the end of the tests were found to be 3.8 mm, 2.2 mm, and 1 mm for applied normal stress of 18, 36 and 54 kPa, respectively.

For EPS22 and EPS39 (Figure 3.5b and 3.5c), the behavior is characterized by stiffer response as compared to EPS15. This is evident from the small displacement level required to reach the maximum stress ratio. The response reached a plateau at a horizontal displacement of about 2 mm for the investigated range of normal stresses.

The vertical displacements (compression) of the EPS22 and EPS39 samples were found to reach maximum values of 1.8 mm and 0.9 mm, respectively. These values are consistent with the increase in geofoam density under the same level of normal stress.

The failure envelops developing at the geofoam-concrete interface for the three investigated EPS samples are presented in Figure 3.6. Interface friction angles and the corresponding adhesion values along the contact surface are determined using the slopes and intercepts of the failure envelope. It was found that friction angles generally increased with the increase in geofoam density. Adhesion, on the other hand, was found to decrease with the increase in geofoam density. This could be attributed to the fact that under low applied normal stress, less interaction develops between the high-density geofoam (EPS22 and EPS39) and the concrete surface as compared to EPS15. The effect of geofoam density on the interface shear strength parameters is further illustrated in Figure 3.7 by plotting the material density on the horizontal axis and the shear strength parameters on the vertical axes. It is evident that the interface friction angle increases at a slow rate from 37^o to 48^o as the EPS density increased from 15 to 39 kg/m^3, whereas the adhesion along the contact surface rapidly decreased from about 11 kPa to 1 kPa.

Figure 3.8 shows the effect of geofoam density on the maximum vertical compression of the samples as measured in the experiments. The results show that sample compression reached 3.5 mm (about 17% of the sample height) for EPS15 under normal stress of 54 kPa. The compression significantly decreased to 1.6 mm for EPS22 and 0.9 zmm for EPS39. This response is consistent with the increase in material stiffness associated with the increase in density.

3.6.1.2 Geofoam-Wood interface

For geofoam-wood interface tests, stress ratios were plotted against sample displacements as depicted in Figure 3.9. Samples were tested under applied normal stresses that range from 18 to 54 kPa. For EPS15 and EPS22 (Figure 3.9a and 3.9b), initially, stress ratio increased linearly with the increase in sample displacement and then reached the maximum stress ratio at applied displacement that depends on the stress level. For EPS39, the maximum stress ratio reached about 0.75 with a maximum horizontal displacement of around 10 mm. EPS15 and EPS22 were found

to reach maximum vertical displacement of 3.8 mm and 1.8 mm, respectively under normal stress of 54 kPa.

For EPS39, a slightly stiffer response was observed (Figure 3.9c) such that maximum stress ratios corresponded to smaller displacements as compared to the other geofoam cases. Vertical displacements measured showed trends that are consistent with those observed in the previous tests where sample compression decreased with the increase in geofoam density.

Mohr-Coulomb failure envelopes were plotted, and interface strength parameters were calculated for all geofoam-wood interface tests as shown in Figure 3.10. Failure envelops were generally parallel with upward slope. Interface shear strengths values were found to increase with the increase in normal stress and decreases with the increase in geofoam density. This may be attributed to the fact that low density geofoam (EPS15) develops more interaction with the wood grains as compared to higher density geofoam (EPS39) under the same applied normal stress. As the geofoam density increased from 15 kg/m^3 to 39 kg/m^3, adhesion values decreased from 7.6 kPa to 2.33 kPa whereas the angles of interface friction remained almost unchanged as shown in Figure 3.11.

Figure 3.12. shows the relationship between the maximum vertical displacements and the applied normal stress for the three investigated geofoam densities. Results show that vertical compression of geofoam is directly related to applied normal stress and inversely related to geofoam density. EPS15 showed maximum compression of 3.6 mm (18% of the sample height) while EPS39 showed maximum compression of 1.6 mm (8% of the sample height). The rate of increase in sample compression was more rapid for EPS15 as compared to the two other densities.

3.6.1.3 Geofoam-Steel interface

The relationships between the stress ratio and measured horizontal displacements for the case of geofoam-steel interaction are shown in Figures 3.13a through 3.13c for EPS15, EPS22 and EPS39, respectively. EPS15 showed insignificant hardening behavior (Figure 3.13a) with soft response at small strains compared to EPS22 and EPS39 (Figure 3.13b & 3.13c). The maximum stress ratios reached 0.8, 0.65, 0.56 at displacements of 1 mm, 0.45 mm, and 0.4 mm for EPS15, EPS22 and EPS39, respectively. In addition, vertical displacements measured during the shear tests showed trends that are consistent with the geofoam density. EPS15, EPS22 and EPS39 experienced maximum compression values of 3.2 mm, 1.1 mm and 0.7 mm, respectively, under an applied normal stress of 54 kPa.

For all geofoam-steel interface tests, linear Mohr Coulomb failure envelopes were plotted in Figure 3.14. It was found that for a particular value of normal stress, higher density geofoam samples showed lower interface strength as compared to lower density geofoam. This is attributed to the fact that low density geofoam interacts better with the contacting material as compared to high density geofoam. This observation is also confirmed by the decrease in adhesion from 7.6 kPa to 3.9 kPa and decrease in angle of interface friction from 21.6^{o} to 20.3^{o} as shown in Figure 3.15. Maximum compression is plotted in Figure 3.16 for the range of applied normal stress. Trends are found to be consistent with previous test results where the rate of compression was rapid for EPS15 compared to the rest of the samples.

3.7 Practical Significance

For comparison purpose, the results of this study are combined with those reported by Khan and Meguid [36] for cases involving geofoam-sand and geofoam-PVC interaction as summarized in Figure 3.17. It should be noted that the density of EPS39 used in this study is slightly different from EPS35 used previously by Khan and Meguid [36]. This is attributed to the changes made during the manufacturing process and therefore, the results presented for EPS39 for sand and PVC materials are considered approximate.

For all investigated materials, adhesion at the interface generally decrease with the increase in geofoam density (Figure 3.17a) except for PVC where the adhesion was relatively small due to the low surface roughness. EP15 and EPS22 seem to interact better with construction material of rough surfaces particularly sand and concrete. Under the same normal load, EPS39 did not allow enough surface interaction resulting in smaller adhesion for all studies materials. As far as the friction angle component of the interface strength, concrete, wood, and sand presented higher surface friction that increased with the increase in EPS density. This was not the case for steel and PVC as the friction angle did not significantly change and was about half of that of the concrete material. A summary of the measured test results and the average friction coefficient values for each material is provided in Table 3.4.

The practical significance of these results is that EPS density plays a role in the interface shear strength properties of a composite system. The reported values in this study may be used to estimate the expected shear resistance when designing a geotechnical structure with EPS geofoam inclusion that may experience movement along the interface.

3.8 Conclusions

In this study, 27 direct shear tests were performed to investigate the behavior of geofoam in contact with different construction materials. Tests were conducted using three geofoam densities interacting with three different construction materials, namely, concrete, wood and steel. The following conclusions have been drawn from this experimental study.

1. When EPS geofoam blocks are subjected to a combination of normal and shear stresses, geofoam density and applied normal stress play an important role on the shear resistance at the interface.
2. Geofoam blocks in contact with concrete, wood and steel showed a decreasing trend in adhesion as the geofoam density increased from 15 to 39 kg/m3. However, the interface friction angle was found to increase for the case of concrete compared to other materials.
3. Vertical compression of EPS geofoam showed trends consistent with the geofoam density for all investigated materials. Compression values are directly related to applied normal stress and inversely related to geofoam density.
4. Using rough surface concrete is recommended for projects involving EPS gefoam blocks in direct contact with the concrete and backfilled with sand material as the increase in interface friction coefficient on both sides of the geofoam blocks will result in an increase in the shear resistance of the composite system.

3.9 References

[1] Aaboe R (2000) Evidence of EPS long term performance and durability as a light weight fill. Vegteknisk avdeling.

[2] Frydenlund T (1991) Expanded polystyrene: A lighter way across soft ground. vol 1502. ICON Group International.

[3] Elragi AF (2000) Selected engineering properties and applications of EPS geofoam. ProQuest Disssertations and Theses.

[4] Jutkofsky W, Sung J, Negussey D (2000) Stabilization of embankment slope with geofoam. Transportation Research Record: Journal of the Transportation Research Board (1736):94-102.

[5] Sheeley M (2000) Slope stabilization utilizing geofoam. Master's Thesis, Syracuse University, New York.

[6] Srirajan S (2001) Recycled content and creep performance of EPS geofoam in slope stabilization. Doctoral dissertation, Syracuse University, New York.

[7] Negussey D (2002) Slope Stabilization with geofoam. Report to FHWA and the EPS industry. Geofoam research center, Syracuse University, New York.

[8] Stark TD, Arellano D, Horvath JS, Leshchinsky D (2004) Geofoam applications in the design and construction of highway embankments. NCHRP web document 65:pp 24-11.

[9] Duskov M (1991) Use of expanded polystyrene (EPS) in flexible pavements on poor subgrades. In: Proceedings of the International Conference on Geotechnical Engineering for Coastal Development, pp 783-788.

[10] Duskov M (1997) Measurements on a flexible pavement structure with an EPS geofoam sub-base. Geotextiles and Geomembranes 15 (1):pp 5-27.

[11] Riad HL, Ricci AL, Osborn PW, Horvath JS (2003) Expanded polystyrene (EPS) geofoam for road embankments and other lightweight fills in urban environments. In: Soil and Rock America, 12th Pan-American Conference on Soil Mechanics and Geotechnical Engineering and 39th US Rock Mechanics Symposium.

[12] Refsdal G (1985) Plastic foam in road embankments: future trends for EPS use. Internal Report, Norwegian Road Research Laboratory, Oslo, Norway.

[13] Aaboe R (1987) 13 years of experience with expanded polystyrene as a lightweight fill material in road embankments. Norwegian Road Research Laboratory Publication (61):pp 21-27.

[14] Magnan J, Serratrice J (1989) Mechanical properties of expanded polystyrene for applications in road embankment. Bull Liaison LCPC 164:pp 25-31.

[15] Williams D, Snowdon R (1990) A 47 Great Yarmouth Western Bypass: performance during the first three years.

[16] Frydenlund T, Aaboe R (1996) Expended polystyrene-the lightweight solution. In: Proceedings of international symposium on EPS construction method (EPS-Tokyo'96), Tokyo, Japan, pp 31-46.

[17] Van Dorp T (1996) Building on EPS geofoam in the 'low-lands'. Experiences in the Netherlands. In: Proceedings of International Symposium on EPS (Expanded Poly-Styrol) Construction Method (EPS Tokyo'96)), Tokyo, Japan.

[18] Zou Y, Leo C, Small J (2000) Behaviour of EPS geofoam as flexible pavement subgrade material in model tests. Geosynthetics International 7 (1):pp1-22.

[19] Negussey D, Stuedlein A, Bartlett S, Farnsworth C (2001) Performance of a geofoam embankment at 100 South, I-15 reconstruction project, Salt Lake City, Utah. In: Proceedings on 3rd International Conference on EPS Geofoam.

[20] Zarnani S, Bathurst R (2007) Experimental investigation of EPS geofoam seismic buffers using shaking table tests. Geosynthetics International 14 (3):pp 165-177.

[21] Farnsworth C, Bartlett SF, Negussey D, Stuedlein A (2008) Rapid construction and settlement behavior of embankment systems on soft foundation soils. Journal of Geotechnical and Geoenvironmental Engineering 134 (3):pp 289-301.

[22] Newman MP, Bartlett S, Lawton E (2009) Numerical modeling of geofoam embankments. Journal of Geotechnical and Geoenvironmental Engineering 136 (2):pp 290-298.

[23] Skuggedal H, Aaboe R (1991) Temporary overpass bridge founded on expanded polystyrene. In: Proceedings of the 1st European Conference on Soil Mechanics and Foundation Engineering, pp 559-561.

[24] McDonald P, Brown P (1993) Ultra lightweight polystyrene for bridge approach fill. In: Proceedings of the 11th Southeast Asian Geotechnical Conference, Singapore, pp 664-668.

[25] Bang S (1995) Experimental and analytical study of expanded polystyrene blocks in highway application. In: Proceedings of International Seminar on the Application of EPS for Embankment Construction, Korea Institute of Construction Technology (KICT), Seoul, Korea, pp 105-133.

[26] Abu-Hejleh N, Zornberg JG, Elias V, Watcharamonthein J (2003) Design assessment of the founders/meadows GRS abutment structure. In: Proc., 82nd Annual TRB Meeting.

[27] Meguid M, Hussein M, Ahmed M, Omeman Z, Whalen J (2017) Investigation of soil-geosynthetic-structure interaction associated with induced trench installation. Geotextiles and Geomembranes 45 (4):pp 320-330.

[28] Meguid M, Ahmed M, Hussein M, Omeman Z (2017) Earth pressure distribution on a rigid box covered with u-shaped geofoam wrap. International Journal of Geosynthetics and Ground Engineering 3 (2):p 11.

[29] Horvath JS (1997) The compressible inclusion function of EPS geofoam. Geotextiles and Geomembranes 15 (1):pp 77-120.

[30] Bathurst RJ, Keshavarz A, Zarnani S, Take WA (2007) A simple displacement model for response analysis of EPS geofoam seismic buffers. Soil Dynamics and Earthquake Engineering 27 (4):pp 344-353.

[31] Ossa A, Romo M (2011) Dynamic characterization of EPS geofoam. Geotextiles and Geomembranes 29 (1):pp 40-50.

[32] Sheeley M, Negussey D (2000) An investigation of geofoam interface strength behavior. Geotechnical Special Publication 301:pp 292-303.

[33] Chrysikos D, Atmatzidis D, Missirlis E (2006) EPS geofoam surface shear resistance. 8thIGS Yokohama, Japan:pp 1651-1654.

[34] Padade A, Mandal J (2014) Interface strength behavior of expanded polystyrene EPS geofoam. International Journal of Geotechnical Engineering 8 (1):pp 66-71.

[35] AbdelSalam S, Azzam S (2016) Reduction of lateral pressures on retaining walls using geofoam inclusion. Geosynthetics International 23 (6):pp 395-407.

[36] Khan MI, Meguid M (2018) Experimental investigation of the shear behavior of EPS geofoam. International Journal of Geosynthetics and Ground Engineering 4:p 12.

[37] Xiao M (2015) Geotechnical engineering design. John Wiley & Sons.

[38] ASTM D6817 / D6817M-17 Standard Specification for Rigid Cellular Polystyrene Geofoam. ASTM International, West Conshohocken, PA. http://wwwastmorg.

[39] ASTM D5321 / D5321M-17 Standard Test Method for Determining the Shear Strength of Soil-Geosynthetic and Geosynthetic-Geosynthetic Interfaces by Direct Shear. ASTM International, West Conshohocken, PA. http://wwwastmorg.

[40] ASTM D3080 / D3080M-11 Standard Test Method for Direct Shear Test of Soils Under Consolidated Drained Conditions. ASTM International, West Conshohocken, PA. http://wwwastmorg.

Table 3.1 Selected geofoam interface studies

Reference	Test /Sample Size (mm x mm)	Sample density (kg/m^3)	Interface	Friction Coefficient
Sheeley and Negussey [32]	Direct shear test 100 x 100 x 25	____	geofoam-cast in place concrete	2.36 (peak) 1 (residual)
			geofoam- smooth geomembrane (PVC)	0.7 (peak) 0.4 (residual)
Chrysikos et al. [33]	Direct shear test	____	geofoam-other materials (i.e., soils, geotextiles, geomembranes, precast and cast-in-place concrete)	0.27 - 1.2
Padade and Mandal [34]	Direct shear test 300 x 300 x 75	15	geofoam-geotextile	0.17
			geofoam-geogrid	0.14
			geofoam-fly ash	0.21
		30	geofoam-geotextile	0.19
			geofoam-geogrid	0.12
			geofoam-fly ash	0.23
AbdelSalam and Azzam [35]	Direct shear test 100 x 100 x 50	____	geofoam-concrete smooth (dry)	0.49
			geofoam-concrete smooth (wet)	0.51
		____	geofoam-concrete rough (dry)	0.96
			geofoam- concrete rough (wet)	0.48
Khan and Meguid [36]	Direct shear test 100 x 100 x 50	15	geofoam-PVC block	0.7 - 1.7
		22	geofoam-PVC block	0.78 - 2.0
		35	geofoam-PVC block	1.2 - 3.2

Table 3.2 Physical property requirements of EPS geofoam [38]

Type	**EPS15**	**EPS22**	**EPS39**
Density, min., (kg/m^3)	14.4	21.6	38.4
Compressive Resistance, min., (kPa) at 1 %	50	63	190
Compressive Resistance, min., (kPa) at 5 %	80	125	350
Compressive Resistance, min., (kPa) at 10 %	90	140	385

Table 3.3 Properties of material used

Properties of Concrete	
w/c ratio	0.65
Cement (c)	335 kg/m^3
Water (w)	218 kg/m^3
Coarse granite	1060 kg/m^3
Fine granite	680 kg/m^3
Concrete Density	2293 kg/m^3
Slump	228 mm
Properties of Steel*	
Density	8142 kg/m^3
Yield Strength	60000 psi (413.685 MPa)
Tensile Strength	95000 psi (655 MPa)
Elastic modulus	27557-30458 ksi (190-210 GPa)
Poisson's ratio	0.27-0.30
Hardness (Rockwell)	B 90 (Medium)
Properties of Pine wood*	
Density	375 kg/m^3
Tensile Strength, Ultimate	305 psi (2103Pa)
Modulus of Rupture	8.56 ksi (59 MPa)
Flexural Yield Strength	6000 psi (413.69 MPa)
Flexural Modulus	1200 - 1240 ksi (8274-8550 MPa)
Compressive Yield Strength	508 psi (3503 kPa)
Shear Strength	899 psi (6198 kPa)

* Provided by the manufacturer

Table 3.4 Summary of experimental results

Test /Sample Size (mm x mm)	Sample density (kg/m^3)	Interface	Coefficient of friction	
			Measured	Average
Direct shear test 100 x 100 x 50	15	geofoam-concrete	0.96 - 1.39	1.2
	22		1.04 – 1.33	1.1
	35		1.17- 1.28	1.2
Direct shear test 100 x 100 x 50	15	geofoam- wood	0.84 - 1.04	0.95
	22		0.81 – 1.02	0.92
	35		0.76 – 0.83	0.80
Direct shear test 100 x 100 x 50	15	geofoam-steel	0.54 – 0.79	0.67
	22		0.47 – 0.66	0.56
	35		0.44 – 0.58	0.50

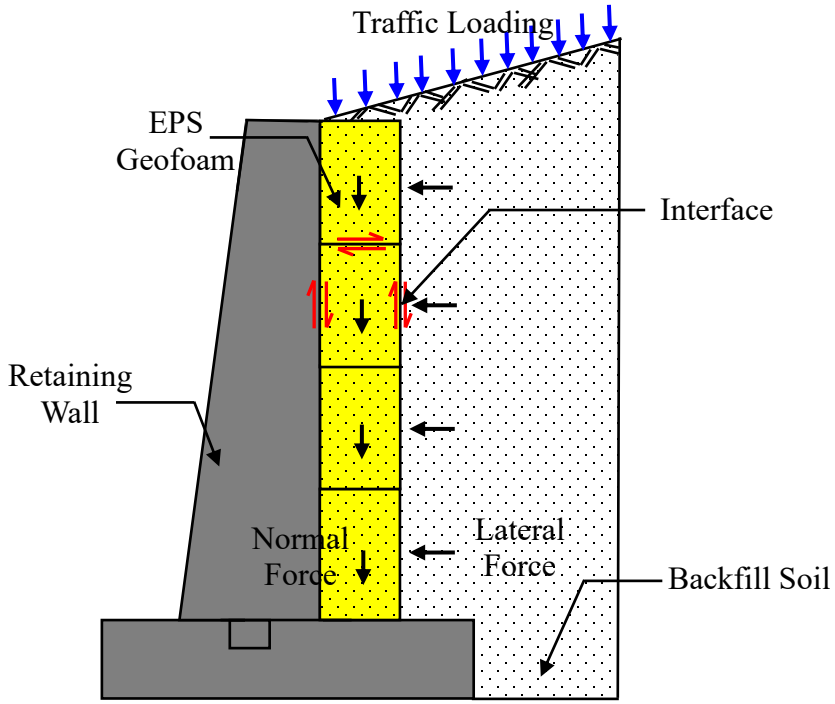

Figure 3.1 Application of geofoam behind Retaining Wall

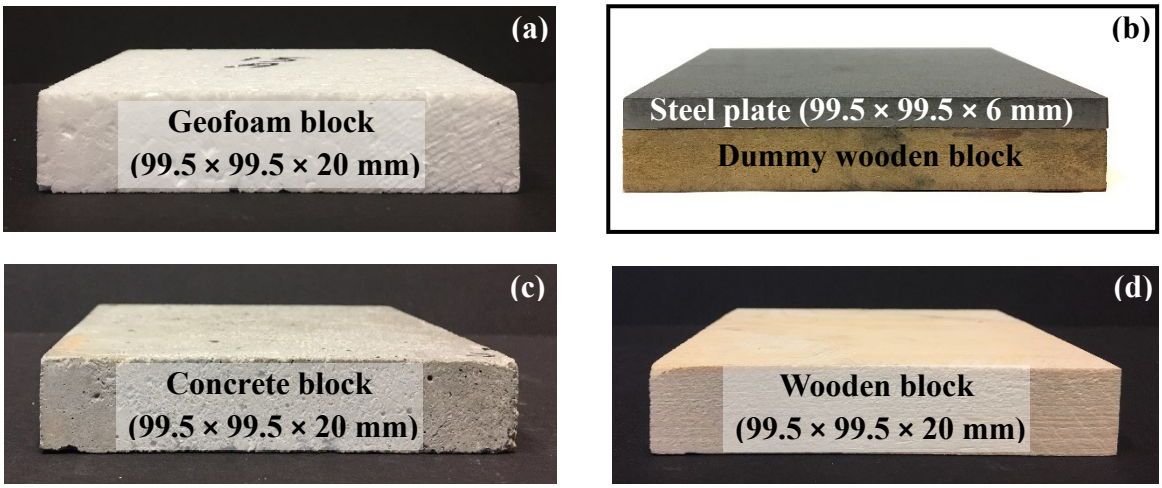

Figure 3.2 Tested materials: (a) EPS geofoam; (b) steel; (c) concrete; (d) wood

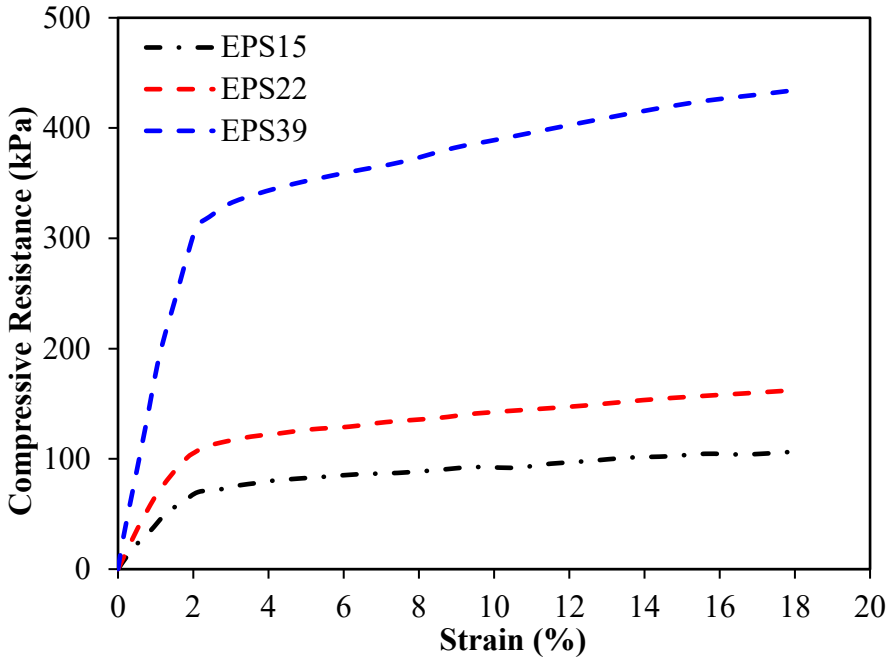

Figure 3.3 Stress strain curve of EPS material

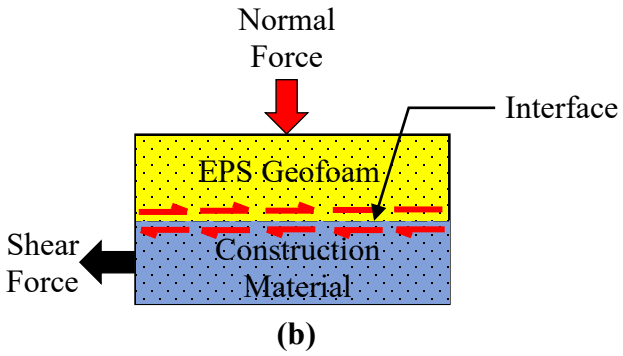

Figure 3.4 Schematic of a typical interface shear test

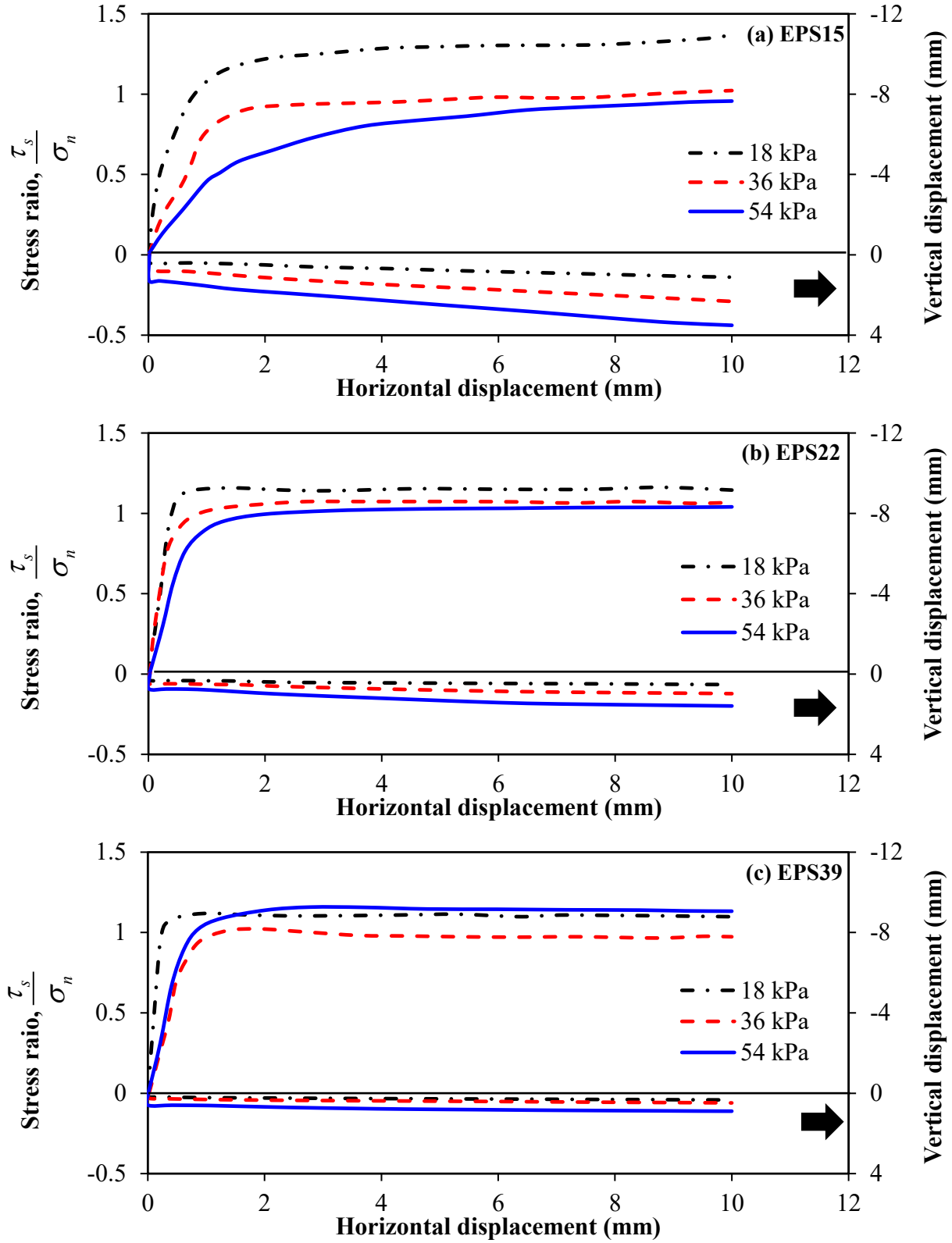

Figure 3.5 Relationships between sample displacements and stress ratio for geofoam-concrete interface: (a) EPS15; (b) EPS22; (c) EPS39

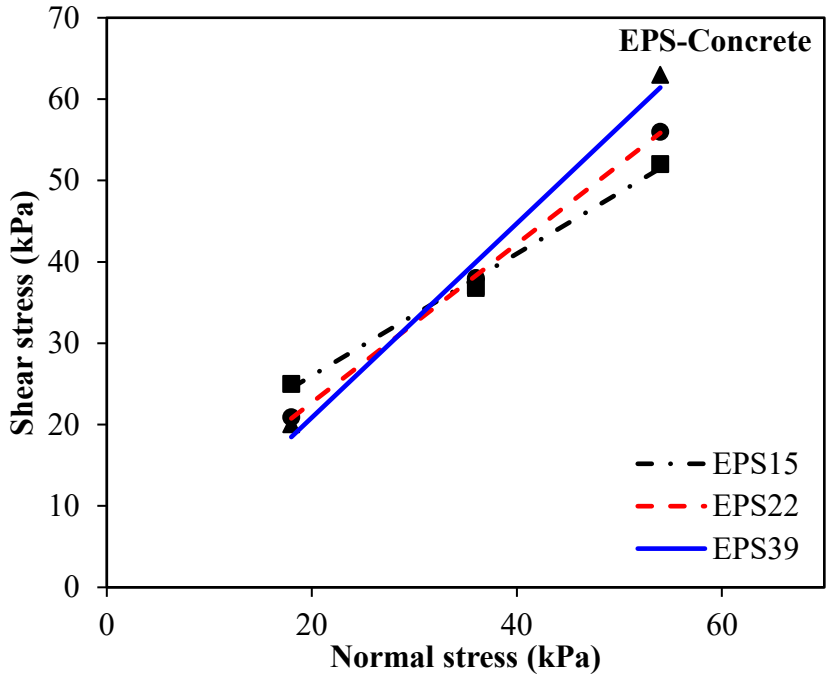

Figure 3.6 Mohr-Coulomb failure envelopes at the geofoam-concrete interface

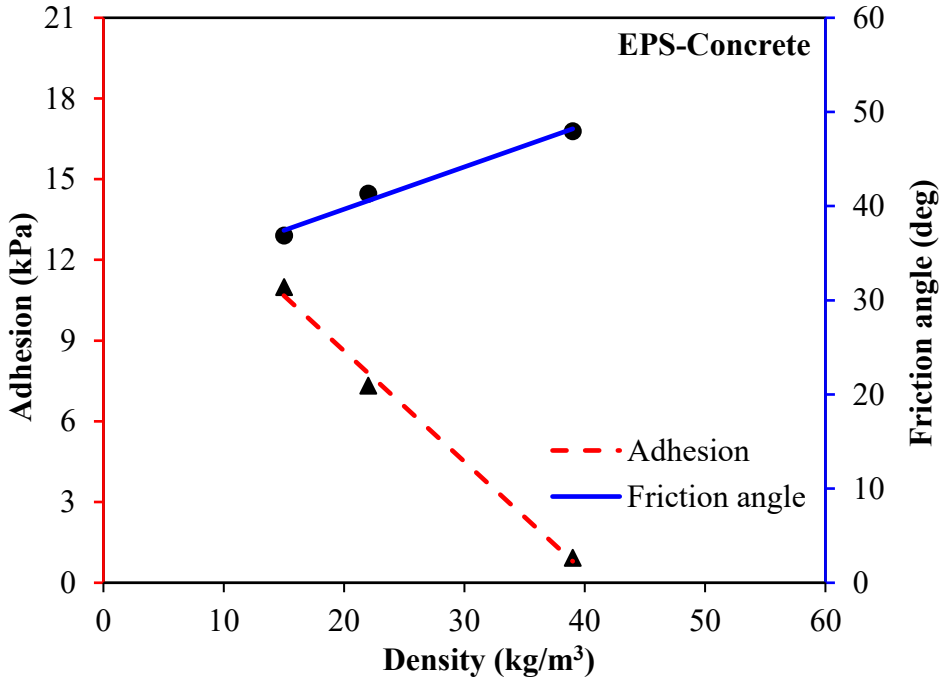

Figure 3.7 Effects of EPS density on the shear strength parameters developing at the geofoam-concrete interface

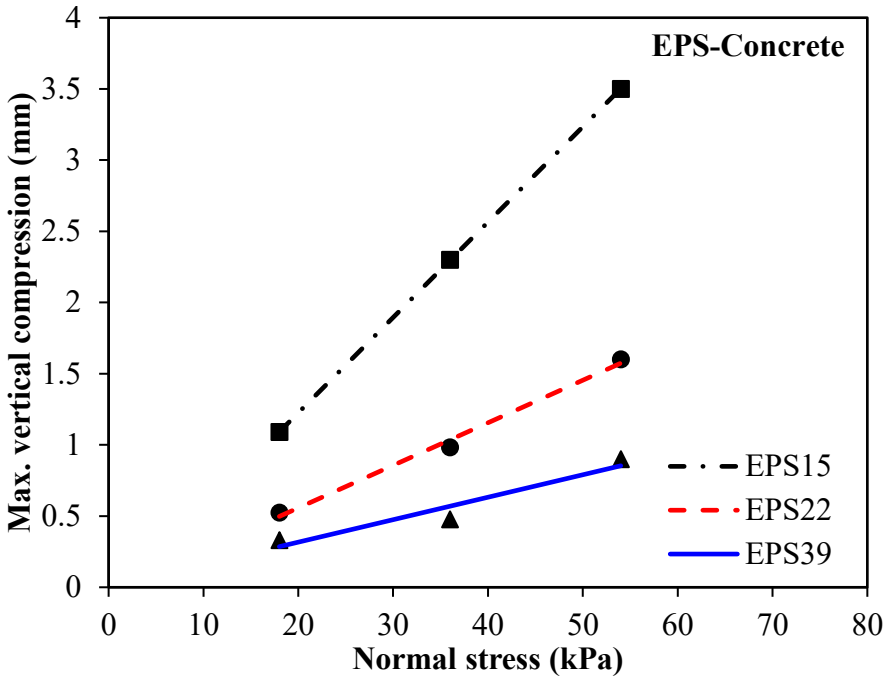

Figure 3.8 Changes in vertical compression with the increase in normal load for the geofoam-concrete tests

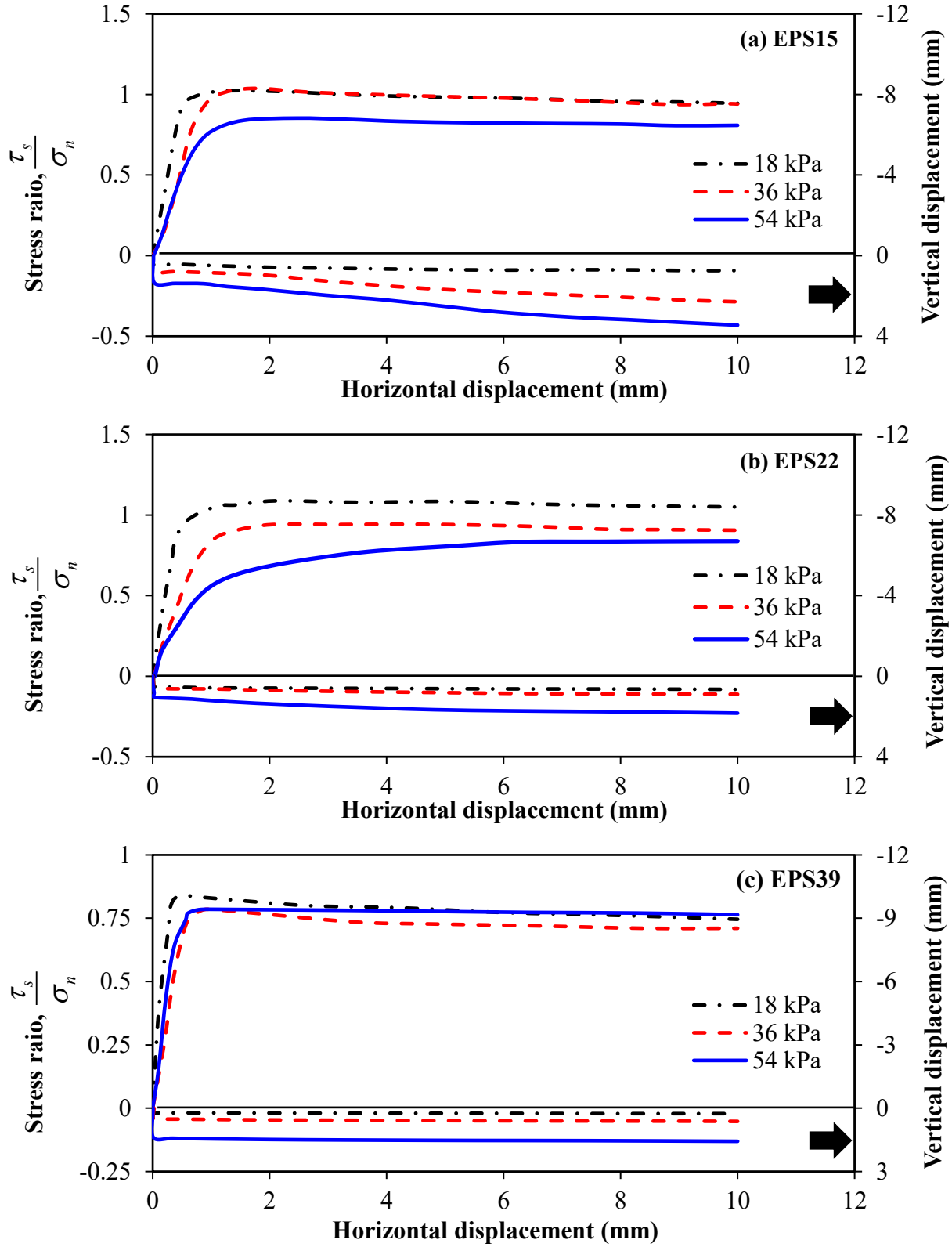

Figure 3.9 Relationships between sample displacements and stress ratio for geofoam-wood interface: (a) EPS15; (b) EPS22; (c) EPS39

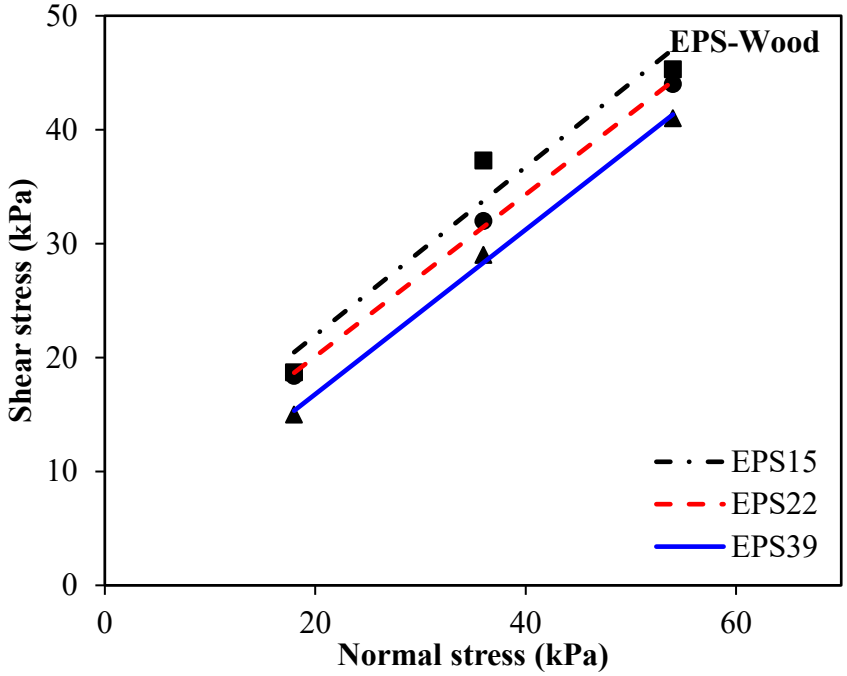

Figure 3.10 Mohr-Coulomb failure envelopes at the geofoam-wood interface

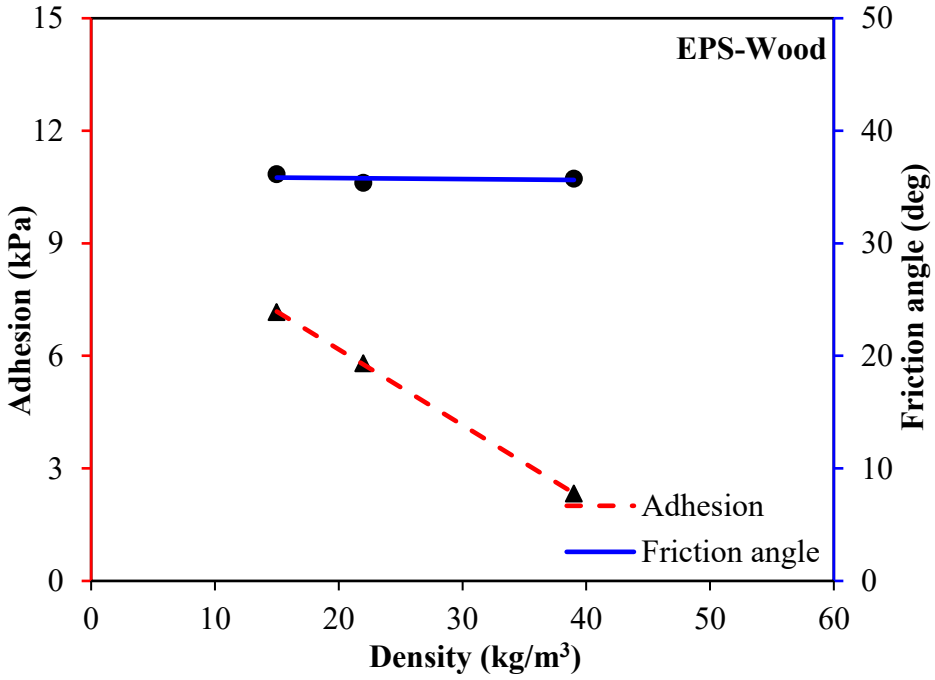

Figure 3.11 Effects of EPS density on the shear strength parameters developing at the geofoam-wood interface

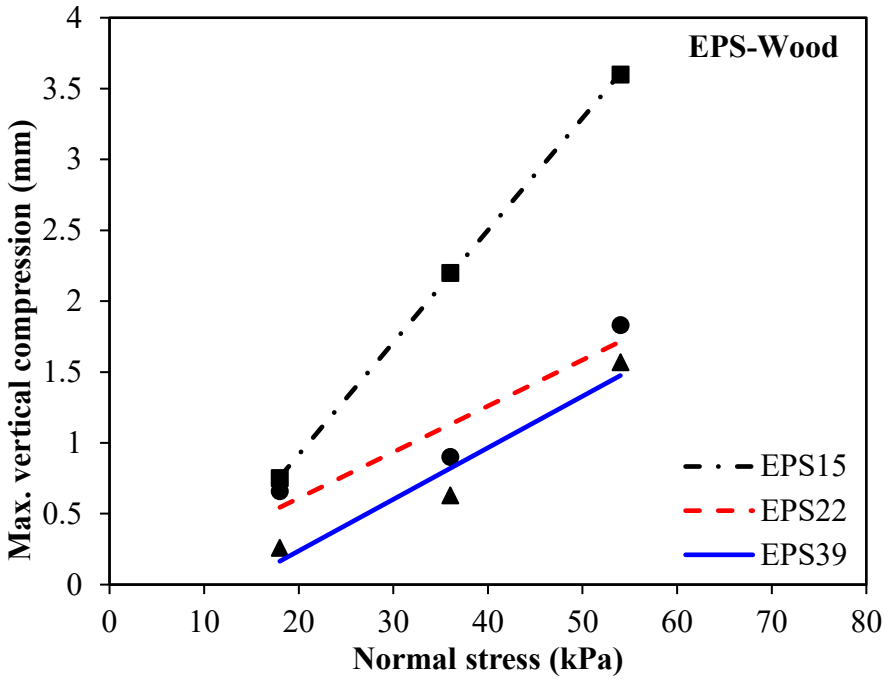

Figure 3.12 Changes in vertical compression with the increase in normal load for the geofoam-wood tests

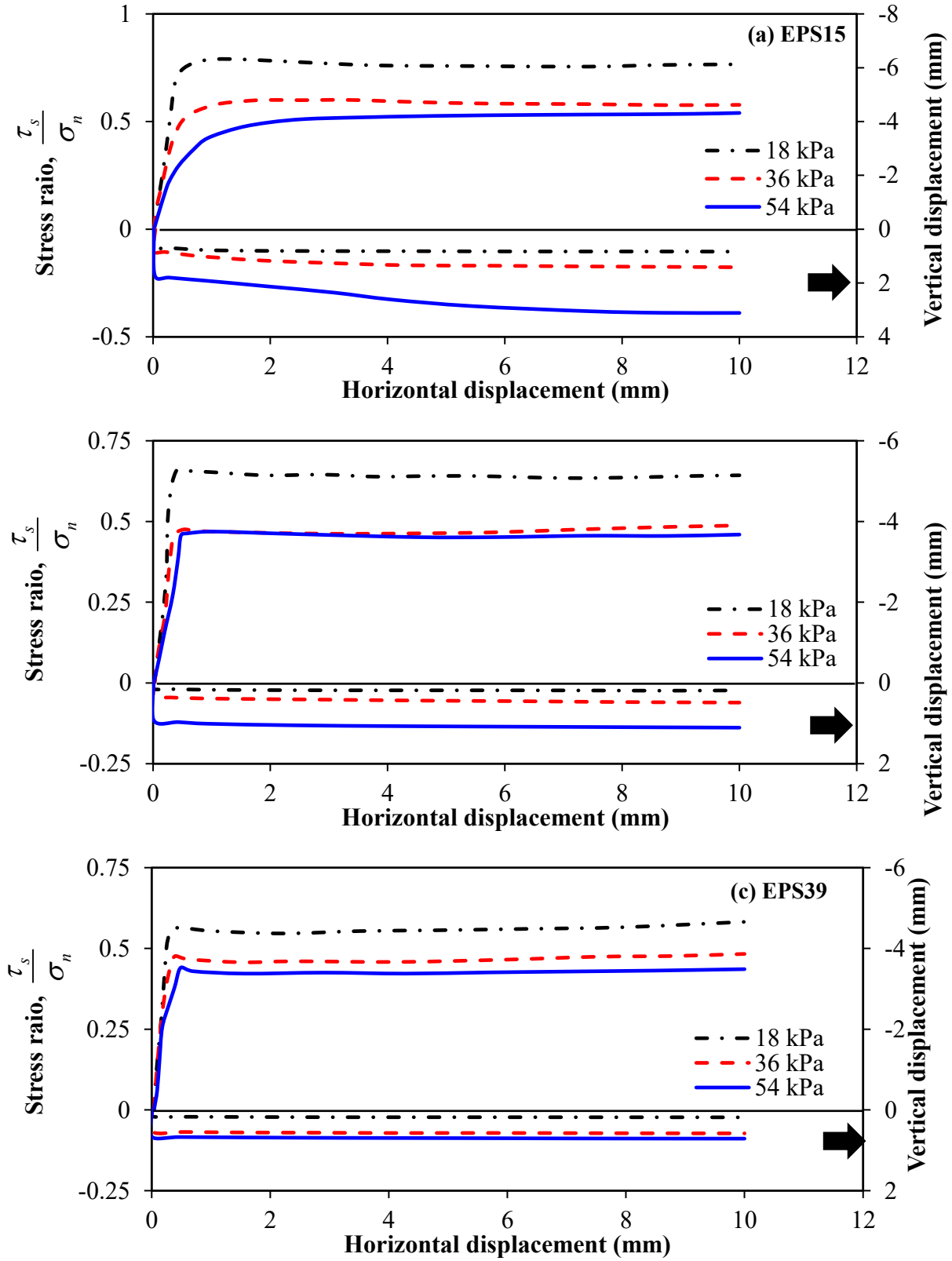

Figure 3.13 Relationships between sample displacements and stress ratio for geofoam-steel interface: (a) EPS15; (b) EPS22; (c) EPS39

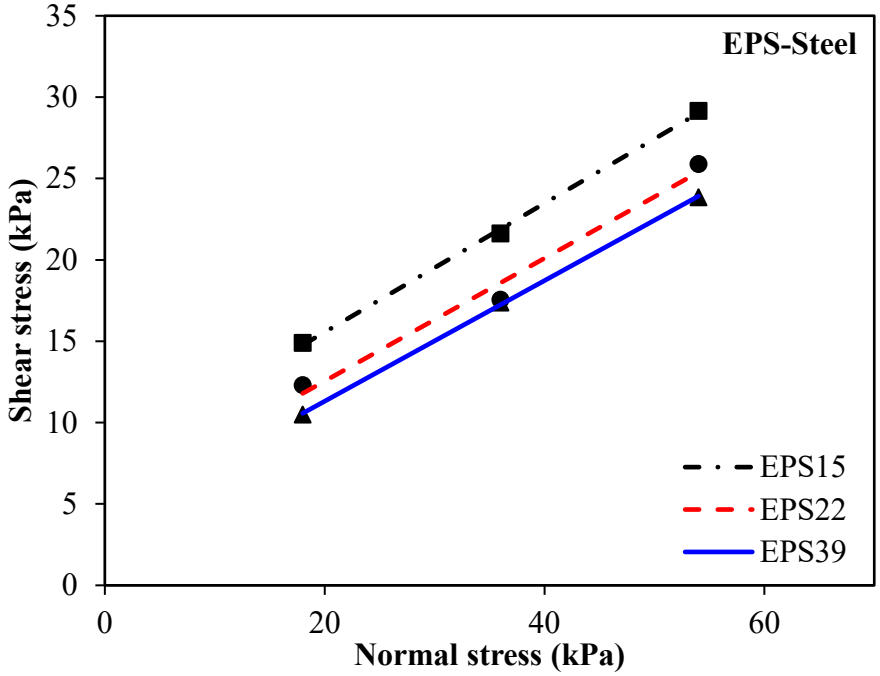

Figure 3.14 Mohr-Coulomb failure envelopes at the geofoam-steel interface

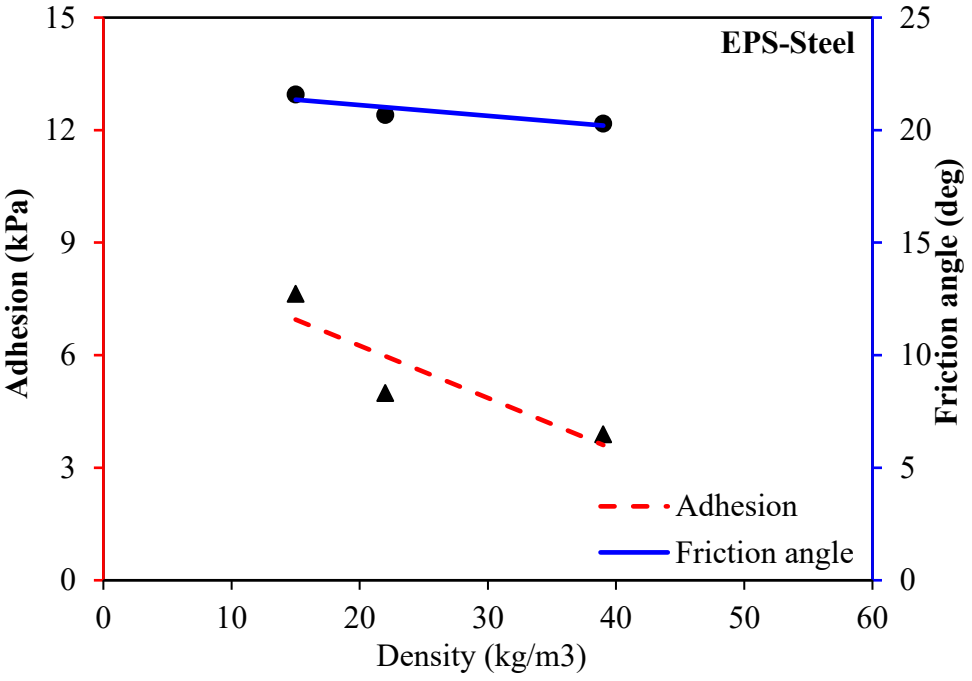

Figure 3.15 Effects of EPS density on the shear strength parameters developing at the geofoam-steel interface

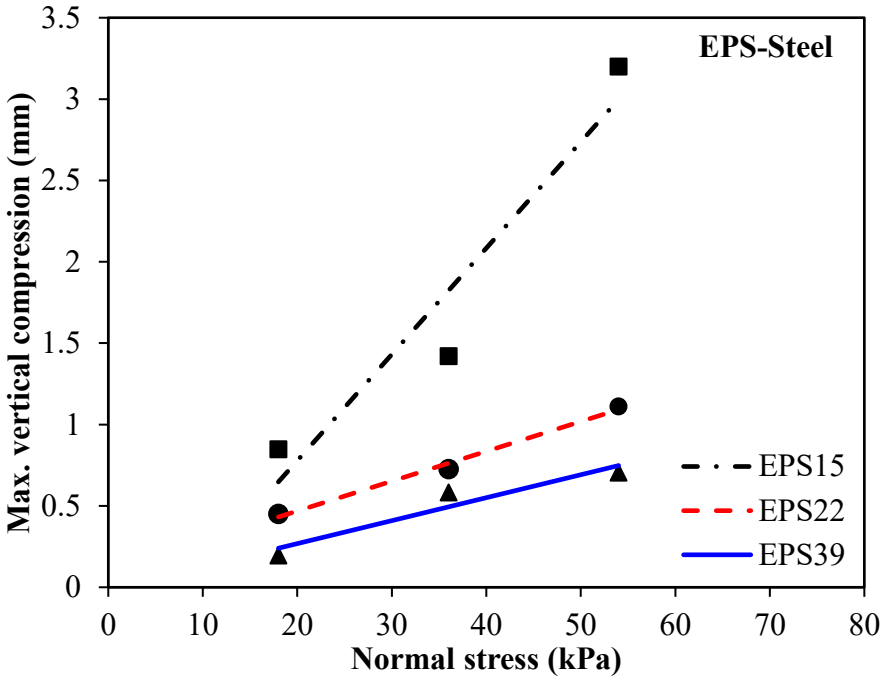

Figure 3.16 Changes in vertical compression with the increase in normal load for the geofoam-wood tests

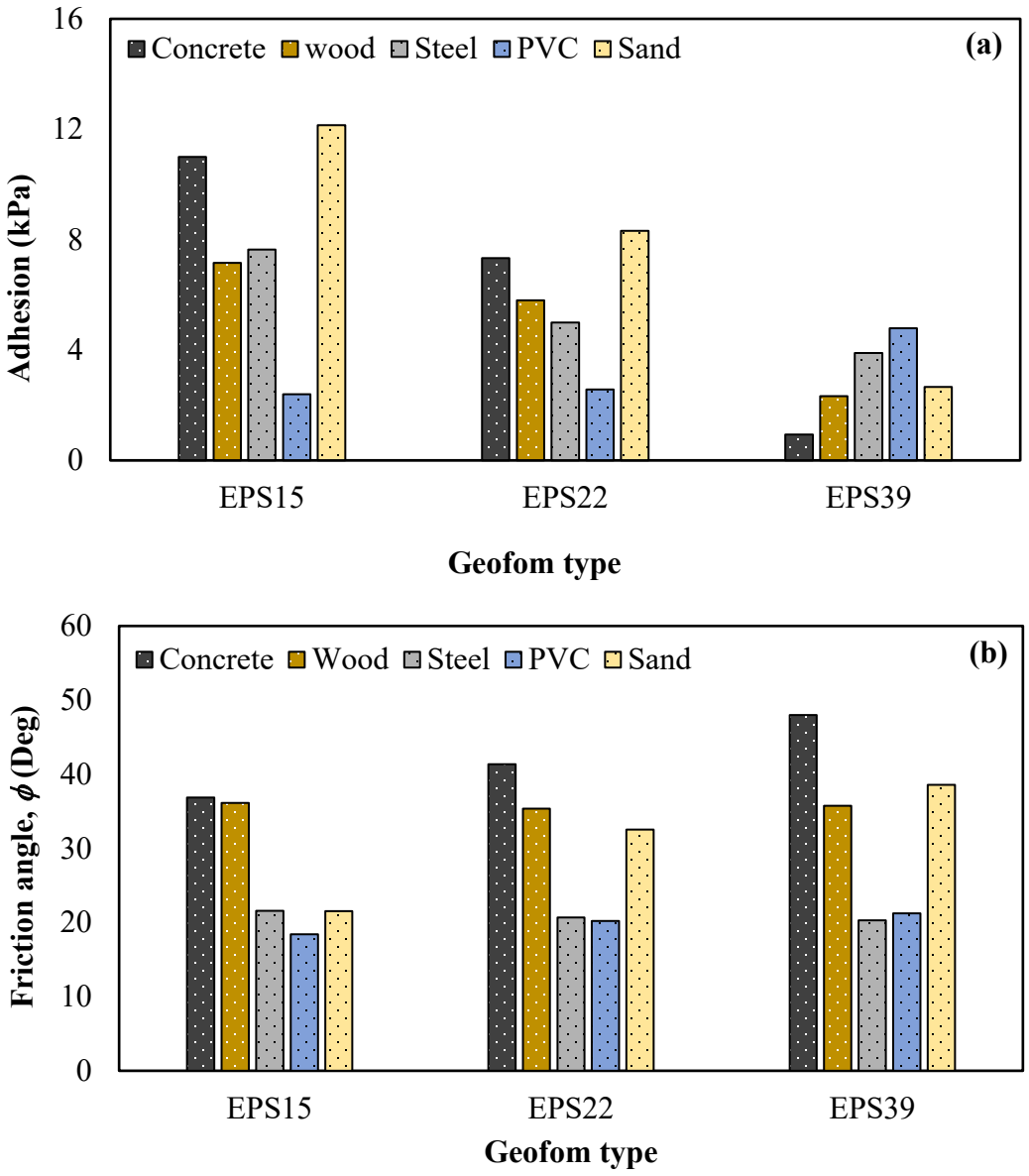

Figure 3.17. Comparison of interface shear strength properties of EPS geofoam: (a) Adhesion; (b) Friction angle

4

Evaluating the Role of Geofoam Properties in Reducing Lateral Loads on Retaining Walls: A Numerical Study*

* A version of this chapter has been published as:
Khan, M. I., & Meguid, M. A. (2021). *Evaluating the role of geofoam properties in reducing lateral loads on retaining walls: A Numerical Study.* Sustainability, 13, 4754.

4.1 Preface

In previous two chapters (chapter 2 and chapter 3), focus was to experimentally determine the shear strength of monoblock of EPS geofoam and interface strength properties of EPS geofoam with different interacting materials e.g. PVC, sand, concrete, steel and wood. In this chapter, a 2D finite element model has been developed and validated to investigate the role of EPS geofoam in reducing lateral earth pressure on rigid wall under static loading. A parametric study was also conducted, and results were presented in the form of design charts for practical use.

4.2 Abstract

Expanded polystyrene (EPS) geofoam is a lightweight compressible material that has been widely used in various civil engineering projects. One interesting application of EPS in geotechnical engineering is to reduce the lateral earth pressure on rigid non-yielding retaining walls. The compressible nature of the EPS geofoam allows for the shear strength of the backfill soil to be mobilized, which leads to a reduction in lateral earth pressure acting on the wall. In this study, a finite element model is developed and used to investigate the role of geofoam inclusion between a rigid retaining wall and the backfill material on the earth pressure transferred to the wall structure. The developed model was first calibrated using experimental data. A parametric study was then conducted to investigate the effect of EPS geofoam density, relative thickness with respect to the wall height and frictional angle of backfill soil on the effectiveness of this technique in reducing lateral earth pressure. Results showed that low-density EPS geofoam inclusion provided the best

performance, particularly when coupled with backfill of low friction angle. The proposed modeling approach has shown to be efficient in solving this class of problems and can be used to model similar soil-geofoam-structure interaction problems.

Keywords: EPS geofoam, Inclusion; Rigid retaining wall; Isolation efficiency; Finite element modelling; Lateral earth pressure.

4.3 Introduction

Expanded polystyrene (EPS) is a lightweight, closed cell, rigid foam material that is almost 100 times lighter than soil and 10-30 times lighter than other construction fill materials [1]. Horvath [2] first used the term "geofoam" for expanded polystyrene and recommended its addition to the geosynthetic category. Early application of EPS geofoam as engineering fill material started in the 1960s. The Norwegian geotechnical engineers in 1965 used EPS geofoam in a road project for thermal insulation [3]. In 1972, EPS geofoam was used to construct embankments on soft soils [4]. Over the past 40 years, EPS geofoam has been successfully used in a variety of engineering projects, most of which involve the use of molded blocks of EPS geofoam as light weight construction material for slope stabilization [5-9], subbase fill material [1,10-12], embankments on soft ground [10,13-17], earth retaining structures [5,18], bridge approaches and abutments [5,19-23] and buried pipes [5,24,25]. The compressible nature of the EPS geofoam also encourages its use as a compressible inclusion [26-29].

Retaining structures are integral components of many important structures including bridges, ports, highways, railway and underground structures. These retaining structures are typically designed to resist lateral earth pressure exerted by the surrounding soil mass. The design of a retaining wall is strongly related to the magnitude and distribution of earth pressure acting on the wall. The higher the earth pressure, the more the cost of the wall structure. Various methods are suggested to reduce the magnitude of lateral earth pressure on retaining walls. Pressure reduction can be achieved by allowing controlled yield of the backfill soil by introducing compressible material between the wall and backfill soil. Partosand and Kazaniwsky [30] introduced EPS geofoam of low stiffness between a relatively higher stiffness retaining structure and the retained soil mass (see Figure 4.1). The least stiff material (EPS geofoam) generally compresses more than the other two materials, which causes reduction in the lateral earth pressure due to the mobilization of the shear strength within the adjacent soil [27].

Depending on the response of the earth retaining structures under the applied lateral loading, retaining walls can be broadly classified as: **(i) Non-yielding:** when the structure is not allowed to displace or deform horizontally under the applied loads. These structures are typically designed based on at-rest earth pressure condition; **(ii) Yielding:** when the structure is allowed to displace or deform horizontally under the applied load. Mostly, these structures are designed for active earth pressure condition. Compressible geofoam inclusion is generally more beneficial for non-yielding (rigid) retaining walls.

Researchers [30-35] showed that the magnitude of the lateral loads on retaining walls could be reduced by installing a material of lower stiffness between the backfill soil and the wall structure, without increasing the wall stiffness. Partos and Kazaniwsky [30] reported reduction in lateral earth pressure on a non-yielding basement wall by placing a prefabricated expanded polystyrene beaded drainage board between the wall and the granular backfill. Karpurapu and Bathurst [35] used numerical modeling to demonstrate that installing a geofoam layer with thickness that is equal to 1% of the wall height can bring the lateral earth pressure to a minimum level. Hatami and Witthoeft [36] extended the geofoam application to geosynthetic reinforced soil walls. Numerical results confirmed that the total forces that cause external sliding and overturning decreased by about 30% and 25%, respectively. Trandafir et al. [37] concluded that the presence of EPS geofoam within the upper half of the wall can help with the load reduction.

Ertugrul and Trandafir [34] studied the behavior of geofoam inclusion behind flexible walls. Results indicated that geofoam inclusion behind a retaining wall can cause significant decrease in lateral thrust. This was attributed to the relative stiffness between the wall and the backfill material. Azzam and AbdelSalam [38] carried out numerical analysis to investigate the performance of rigid yielding retaining walls with geofoam inclusion. Results showed that use of EPS significantly reduced the lateral pressure depending on the ratio between the EPS thickness and wall height. Chauhan and Dasaka [33] showed that geofoam inclusion can provide 8-42 % reduction in lateral pressure for a surcharge of 10-50 kPa.

4.4 Scope and Objective

This study focuses on the use of EPS geofoam in reducing the lateral earth pressure behind rigid non-yielding retaining walls. A two-dimensional finite element model is developed and validated using experimental data reported by Ertugrul and Trandafir [39]. A parametric study is then performed to examine the role of relative thickness, stiffness of the EPS geofoam and strength

parameters of the backfill soil on the lateral earth pressure acting on rigid retaining wall. The results of this study are presented in the form of design charts for a wide range of wall configuration and material properties.

4.5 Description of the Physical Model

Ertugrul and Trandafir [39] performed a series of experiments on a rigid non-yielding retaining wall with vertical EPS geofoam inclusion. A steel wall with dimensions 700 mm × 980 mm × 8 mm was firmly welded to a steel base 980 mm × 500 mm × 8 mm and hosted in a rigid container 2m × 1m × 1m. A schematic of the test setup and the locations of the pressure transducers (P1 to P4) are shown in Figure 4.2. Dry, clean sand was used as backfill material. Triaxial compression tests conducted on sand samples of relative density, D_r, of 70% indicated friction and dilatancy angles of 43.5° and 22.5°, respectively. Blocks of EPS15 geofoam (15 kg/m^3) were installed between the wall and backfill. The properties of the sand and the EPS geofoam materials are summarized in Table 4.1.

Experiments were conducted on four different wall configurations. In the first set of tests, lateral earth pressures were measured against the rigid wall with no geofoam inclusion, whereas the other sets of tests involved three different geofoam thicknesses that correspond to t/H ratios of 0.07, 0.14 and 0.28, where t is the geofoam thickness and H is the wall height. The geofoam was placed behind the rigid retaining wall and the earth pressures were measured using four pressure transducers installed vertically along the wall height at 20 cm spacing as shown in Figure 4.2.

4.6 Numerical Analysis and Model Validation

A two-dimensional finite element model was developed based on the experimental setup reported by Ertugrul, Trandafir [39]. The analysis was performed using the commercial software PLAXIS 2D 2015 [40]. The retaining wall and the backfill material are modeled using 15-node triangular elements as shown in Figure 4.3. Smooth rigid boundary conditions are specified along the vertical boundaries whereas rough rigid boundary condition is specified along the base of the model. Both the backfill and foundation soil were modeled as Mohr-Coulomb elastoplastic materials whereas, EPS geofoam was modelled as linear elastic material. Given that the EPS15 geofoam used in the experiments was subjected to a maximum horizontal pressure of about 3.6 kPa, which is much smaller than the yield stress (σ_y = 38 kPa), the use of elastic material model for the geofoam is considered acceptable. Table 4.1 summarizes the material properties of both the soil and the EPS

geofoam used in validating the numerical model. The retaining wall and its base were modelled as plate elements. Material properties of wall and the base are given in Table 4.2. The soil-wall, geofoam-wall and soil-geofoam interfaces were modelled using Mohr-Coulomb elastoplastic interface elements. The interface friction angles were back-calculated to match the experimental data. For geofoam-wall, soil-geofoam and soil-wall interfaces, the interface friction angles were found to be 16°, 8° and 5°, respectively. EPS15 blocks of similar dimensions and material properties to those used in the experiments was adopted in the model with three different geofoam thicknesses that correspond to *t/H* ratios of 0.07, 0.14 & 0.28.

The steps taken in modeling the retaining wall can be summarized as follows: (1) the foundation bed is first generated; (2) the wall and the base are activated; (3) the EPS blocks are introduced against the wall; (4) the backfill material is added in layers to reach the target height.

Four cases were numerically investigated starting with the reference model where no geofoam blocks are installed (*t/H* = 0).

The model validation results are presented in Figure 4.4, where the lateral earth pressure values, σ_h, are normalized with respect to the vertical pressure at the wall base $(\sigma_{v-base} = \gamma H = 11.55\ kPa)$, and are plotted against the wall depth. For the four investigated cases, the calculated lateral pressures are compared with the experimental data. The results show that the numerical model is generally able to capture the pressure distribution with depth. This is particularly true for the case where no geofoam is installed, as represented by the solid line in Figure 4.4. For the cases where geofoam is placed behind the wall, the numerically computed results slightly underestimated the lateral pressure near the base of the wall. This could be attributed to the frictional forces mobilized at the soil-base and the geofoam-base interfaces.

It is observed that for all investigated wall models, EPS geofoam experienced maximum horizontal stress values σ_{hmax} of 2.5, 2.0 and 1.3 kPa for *t/H* of 0.07, 0.14 and 0.28, respectively. This is found to be within the elastic limit of the used EPS15 geofoam, which has a compressive resistance of about 19 kPa at 1% strain [39]. This also confirms the assumption of linear elastic response for the EPS geofoam under the applied loading. It is also found that the presence of geofoam inclusion behind the non-yielding retaining wall resulted in arching effect within the lower half of the wall, which helped in absorbing the majority of the lateral earth pressure acting on the wall.

The difference between the experimental data and the numerically calculated total lateral thrust was found to range between 5% and 9% for the four investigated cases.

4.7 The Effect of Geofoam and Backfill Properties on the Lateral Earth Pressure Acting on the Wall

A parametric study was conducted using a full-scale model to investigate the effect of geofoam density, thickness and backfill friction angle (ϕ) on the lateral earth pressure acting on the wall. A 2.80 m high retaining wall model was developed using 15-nodded plane strain triangular elements. A wall (2800 mm × 3920 mm × 32 mm) with rigid base (3920 mm × 2000 mm × 32 mm) was modelled using plate elements. The numerical parameters used to model the wall and the base are summarized in Table 4.2. The foundation and backfill soils were modelled using Mohr-Coulomb elastoplastic material model. In addition, Mohr-Coulomb elastoplastic interface elements were used at the wall-soil, wall-geofoam and soil-geofoam interfaces. For the wall-geofoam, geofoam-soil and wall-soil interfaces, a range of friction angles between 8^o and 22° was used in the analysis to cover wide possibilities of contact properties.

Three different geofoam materials, namely EPS22, EPS29 and EPS39, of different relative thicknesses with respect to the wall height (t/H = 0, 0.05, 0.1, 0.15, 0.2, 0.25 & 0.3) were considered. The results of the uniaxial compressive strength tests performed on the three geofoam materials are depicted in Figure 4.5. For the three geofoam materials, with densities of 22, 29, and 39 kg/m^3, the reported compressive strength results at 1% strain are found to be 70, 94 and 192 kPa, respectively. Given the expected range of lateral pressure (3 to 23 kPa), the geofoam materials are subjected to pressure levels that are within the linear elastic range. Material properties of both the soil and geofoam used in this parametric study are summarized in Table 4.3. It is worth noting that the material properties, aspect ratio, and boundary conditions used in the numerical model of the large-scale wall are similar to those used in the model calibration shown in Figure 4.3. The results of the parametric study are provided in the following section.

4.8 Results and Discussion

The results of the numerical analysis are presented in this section by comparing the changes in horizontal pressure with depth for the benchmark case (no geofoam) with those obtained when geofoam blocks of different thicknesses and densities are installed. The calculated lateral earth pressure distributions with depth are presented using four sets of charts grouped in Figure 4.6(a) through 4.6(c) for backfill material with friction angle of 30^o; Figure 4.6d through 4.6(f) for backfill material with friction angle of 35^o; Figure 4.6(g) through 4.6(i) for backfill material with

friction angle of 40°; and Figure 4.6(j) through 4.6(l) for backfill material with friction angle of 45°. Three EPS densities are examined, namely, 22, 29 and 39 kg/m^3. The relative thicknesses of the geofoam panels *t/H* were chosen to cover a wide range of possibilities starting from *t/H* ratio of 0 (no geofoam) and increasing incrementally to 0.3. Rankine's active earth pressure (R. AEP) and Jáky's [41] at rest earth pressure (J. AREP) lines are also added to compare the theoretical value with those calculated using the numerical analysis. The effects of different parameters on the lateral pressure distribution on the wall for each case are presented under separate headings below.

4.8.1 Benchmark case (no geofoam)

By inspecting the results in Figure 4.6(a) through 4.6(f), it is evident that for backfill materials with lower friction angle values, 30° and 35°, the calculated earth pressure distributions were generally found to linearly increase with depth consistent with that of the theoretical at-rest earth pressure (J. AREP) line. However, for backfill with higher friction angles of 40° and 45° (Figure 4.6(g) through 4.6(l) the lateral pressure distributions change from linear to nonlinear near the middle of the wall.

As the friction angle increased from 30° to 45°, the at rest earth pressure coefficient decreased resulting in a decrease in lateral pressure from 22.4 to 13.4 kPa. This can be attributed to the frictional forces developing at the interface between the backfill and the base plate supporting the wall, which differs from the theoretical solution obtained for semi-infinite soil medium.

4.8.2 Effect of geofoam density

By inspecting Figure 4.6(a) through 4.6(l), it is evident that for a given geofoam thickness and backfill properties, density of EPS geofoam has significant effect on the lateral pressure acting on the retaining wall. It was found that, for a given type of backfill material, geofoam of lower density absorbs more lateral pressure and can bring the soil into active or near active state as compared to higher density geofoam that has the same thickness. For example, for $t/H = 0.1$ and $\phi_{soil} = 30°$, the maximum pressure decreased from 12.4 kPa to 10.8 kPa as the geofoam density decreased from 39 kN/m^3 to 22 kN/m^3. This is consistent with the fact that geofoam of lower density compresses more under the same applied lateral pressure resulting in more movement and consequently less pressure on the wall. This shows that low density geofoams are considered to be effective in absorbing static lateral pressure acting on rigid retaining walls.

4.8.3 Effect of geofoam thickness

For a given geofoam density and backfill material, the relative thickness of the geofoam (*t/H*) can significantly affect the magnitude of lateral earth pressure as depicted in Figure 4.6(a) through 4.6(l). EPS geofoam with smaller *t/H* value absorbed less pressure as compared to geofoam of higher thickness ratio for the same geofoam density and soil type. For example, for a geofoam density 22 kg/m^3 (EPS22) and $\phi_{soil} = 30^o$, the maximum earth pressure decreased from 10.82 kPa to 8.38 kPa as the geofoam relative thickness (*t/H*) increased from 0.1 to 0.3. This is attributed to the fact that thicker geofoam can compress more under the same applied lateral pressure, which in turn produces more movement and less pressure on the wall. However, as increasing the thickness of the geofoam can result in adding more costs to the project, a balance needs to be struck between the additional cost of the geofoam material and the design benefits associated with the reduction in lateral earth pressure on the wall.

4.8.4 Effect of friction angle of backfill soil

The magnitude of lateral earth pressure is found to be also influenced by the friction angle of backfill soil, ϕ_{soil}. Soils with higher friction angles exert less pressure on the retaining wall due to smaller coefficient of active earth pressure. As shown in Figure 4.6(a) through 4.6(l), soils with smaller friction angle induced less lateral pressure as compared to those with higher friction angle for the same geofoam density and thickness. For example, for geofoam with density of 22 kg/m^3 (EPS22) and *t/H* = 0.1, soil with $\phi_{soil} = 30^o$ corresponded to 38% reduction in pressure while soil with $\phi_{soil} = 45^o$ corresponded to 28% reduction in lateral earth pressure. This indicates that the use of EPS geofoam inclusion is effective in soils that have lower friction angle values.

It is important to mention that although the presence of geofoam inclusion behind rigid retaining walls caused reduction in lateral earth pressure, there exist a limiting combination of geofoam density and relative thickness of the geofoam (*t/H*) to achieve active state, which depends on the frictional properties of backfill material as depicted in Figure 4.6(a) through 4.6(l). For example, for backfill with $\phi_{soil} = 40^o$, active condition can be achieved using *t/H* = 0.1 for EPS22, *t/H* = 0.2 for EPS29 or *t/H* = 0.3 for EPS39. Therefore, depending on the frictional properties of the backfill material and the magnitude of tolerable stresses on the retaining wall, a suitable geofoam density along with required *t/H* value may be selected to achieve active or near active conditions in the backfill.

4.8.5 Isolation Efficiency (I_E)

Another way to evaluate the performance of EPS inclusion is by expressing the results in terms of isolation efficiency. Isolation efficiency (I_E) is defined as "the ratio of the difference between the total lateral thrust on the wall before and after the geofoam in installed (T_o - T_{EPS}) divided by T_o".

$$I_E = \frac{T_o - T_{EPS}}{T_o} \times 100$$

The total thrust lateral acting on the wall can be computed using the following equation:

$$T = \int_0^H \sigma_x dz$$

where, T is the total lateral thrust acting on the wall, σ_x is the lateral earth pressure and H is the wall height. Figure 4.7 shows the effects of density and relative thickness of the geofoam and the frictional properties of the soil on the isolation efficiency. The results show that for the investigated four soil types, the isolation efficiency increases with the increase in the relative geofoam thickness. It was also found that the isolation efficiency increased with the reduction in the friction angle of the backfill material. For example, for geofoam density of 22 kg/m^3 (EPS22) and t/H of 0.1, the isolation efficiency decreased from 38% to 28% as the friction angle of the backfill soil increased from 30^o to 45 ^{o}. This is due to the fact that higher friction angles (ϕ_{soil}) correspond to smaller at-rest earth pressure coefficient, which induces smaller lateral pressures on the geofoam and the wall. The maximum isolation efficiency is achieved with EPS22 for backfill soil with ϕ_{soil} = 30^o, whereas the minimum value of isolation efficiency is obtained with EPS39 for backfill soil having ϕ_{soil} = 45^o. This response is consistent with the increase in the material stiffness associated with the increase in the geofoam density [42-44].

4.8.6 Lateral earth pressure coefficient ratio

The lateral earth pressures obtained from the numerical models were used to back-calculate the coefficient of lateral earth pressure K_{FEM} based on following equation:

$$K_{FEM} = \frac{2}{\gamma H^2} \int_0^H \sigma_x dz$$

where, γ is the unit weight of soil, σ_x is lateral earth pressure and H is the wall height. The K_{FEM} values were then normalized using Rankine active earth pressure coefficient, K_a, and presented in Figure 4.8, where,

$$K_a = \frac{1-\sin\phi}{1+\sin\phi}$$

Figure 4.8(a) through 4.8(d) show the change in lateral earth pressure coefficient ratio (K_{FEM}/K_a) with the change in the relative thickness of the geofoam (t/H) for the three investigated densities of geofoam, 22, 29 & 39 kg/m^3 and the four different backfill soils (ϕ_{soil} =30^o, 35^o, 40^o, 45^o). A K_{FEM}/K_a ratio of less than 1 means that the lateral earth pressure values are less than the corresponding Rankine's active earth pressure. Also, for a given soil friction angle, a decreasing trend in K_{FEM}/K_a ratio with the increase in t/H indicates a better geofoam performance. For example, for ϕ_{soil} = 30^o, maximum performance is achieved with EPS22 at t/H = 0.3 where K_{FEM}/K_a ratio is minimum.

It is important to note that an increasing trend in K_{FEM}/K_a ratio with the increase in friction angle should not be interpreted as "K_{FEM} increases with the increase in friction angle (ϕ_{soil})". This is due to the fact that K_a is not constant for the four investigated backfill soils (ϕ_{soil} =30^o, 35^o, 40^o, 45^o) as K_a decreases with the increase in friction angle.

4.8.7 Horizontal displacement in backfill soil

Figure 4.9(a) through 4.9(d) present the effect of geofoam density, relative thickness and backfill properties on the horizontal displacement obtained in the backfill soil. It is found that for a given backfill soil, the horizontal displacement increases with the increase in t/H ratio and decreases with the increase in geofoam density. Moreover, for backfill with different frictional properties, horizontal displacement decreases with the increase in friction angle. For example, for a soil with ϕ_{soil} =30^o, geofoam density of 22 kg/m^3, the horizontal displacement decreased from 1.34 mm to 0.23 mm as t/H decreased from 0.3 to 0.05. This is due to the fact that thicker geofoam inclusion allows for more mobilization of the soil strength as compared to geofoam of reduced thickness. The maximum horizontal displacement (1.34 mm) is achieved for the case of EPS22 and ϕ_{soil} of 30^o, whereas the minimum horizontal displacement (0.24 mm) is achieved for the case of EPS39 and ϕ_{soil} of 45^o.

4.9 Practical Implication

The results of this parametric study suggest that the isolation efficiency, I_E, associated with a case of geofoam inclusion behind a rigid wall depends on the used geofoam density and thickness and the frictional properties of the backfill material. Therefore, the normalized charts presented in this

study can help for the preliminary assessment of the various design options that could guide engineers in their design. The charts presented in Figure 4.7 can be easily adapted and used to select a suitable geofoam density and thickness to achieve a specific isolation efficiency. To illustrate this procedure, a design example is given below:

Given Data:

H = 4.0 m

ϕ_{soil} = 35°

I_E = 40 %

Find geofoam EPS22 thickness = t =?

Solution:

For I_E = 40 %

Using Figure 5.10(c):

t/H = 0.118

$t = 0.118 \times H$

$t = 0.118 \times 4 = 0.472$ m = 47.2 cm

The nominal required EPS thickness (t) that satisfies a 40% reduction in pressure is 47 cm.

4.10 Conclusions

In the present study, the effect of EPS geofoam inclusion on rigid non-yielding retaining wall is numerically investigated using plane strain finite element modeling. Experimental data obtained using controlled laboratory tests was used to validate the numerical model. A parametric study is then performed to examine the effects of EPS geofoam density and relative thickness and the properties of the backfill soil on reducing the lateral earth pressure acting on a non-yielding retaining wall. The investigated parameters included three different geofoam densities and thickness interacting with four different backfill soils. The following conclusions can be drawn from this study:

1. Geofoam inclusion placed vertically behind rigid non-yielding retaining walls can allow the backfill soil to move towards the wall. This deformation helps in mobilization the soil shear strength leading to reduction in lateral earth pressure acting on the wall.

2. The response of the granular backfill soil in these applications can be reasonably predicted using Mohr-Coulomb elastoplastic material model, whereas linear elastic model is found to be suitable for the geofoam material.
3. Relative thickness and density of the EPS geofoam and the frictional properties of the backfill material are found to play major roles in the magnitude of the isolation efficiency. It is also found that low density geofoam can provide better performance compared to higher density material. For a same geofoam density, the thickness of the geofoam inclusion is found to have an effect on the geofoam compression. It is also found that EPS geofoam inclusions are more effective in soils with relatively low friction angles.

Notation

The following symbols are used in this paper:

D_r = Relative density of soil

t = Thickness of geofoam

H = Wall height

σ_h = Horizontal pressure

σ_{yield} = Yield stress

σ_{v-base} = Vertical pressure at the wall base

σ_E = Elastic limit

ϕ, ϕ_{soil} = Friction angle of soil

I_E = Isolation efficiency

T_o = Total lateral thrust for without geofoam case

T_{EPS} = Total lateral thrust for with geofoam case

T = Total thrust lateral acting on the wall

K_{FEM} = Back-calculated coefficient of lateral earth pressure from FE analysis

γ = Unit weight of soil

K_a = Rankine active earth pressure coefficient

4.11 References

[1] Stark TD, Arellano D, Horvath JS, Leshchinsky D (2004) Geofoam applications in the design and construction of highway embankments. NCHRP web document 65:pp 24-11.

[2] Horvath JS (1992) New developments in geosynthetics;'lite'products come of age. Standardization News 20 (9):pp 50-53.

[3] Aaboe R (2000) Evidence of EPS long term performance and durability as a light weight fill. Vegteknisk avdeling.

[4] Frydenlund T (1991) Expanded polystyrene: A lighter way across soft ground. vol 1502. ICON Group International.

[5] Elragi AF (2000) Selected engineering properties and applications of EPS geofoam. ProQuest Disssertations and Theses.

[6] Jutkofsky W, Sung J, Negussey D (2000) Stabilization of embankment slope with geofoam. Transportation Research Record: Journal of the Transportation Research Board (1736):pp 94-102.

[7] Sheeley M (2000) Slope stabilization utilizing geofoam. Master's Thesis, Syracuse University, New York.

[8] Srirajan S (2001) Recycled content and creep performance of EPS geofoam in slope stabilization. Doctoral dissertation. Syracuse University, New York.

[9] Negussey D (2002) Slope stabilization with geofoam. Report to FHWA and the EPS Industry. Geofoam Research Center, Syracuse University, New York.

[10] Duskov M (1991) Use of expanded polystyrene (EPS) in flexible pavements on poor subgrades. In: Proceedings of the International Conference on Geotechnical Engineering for Coastal Development, pp 783-788.

[11] Duskov M (1997) Measurements on a flexible pavement structure with an EPS geofoam sub-base. Geotextiles and Geomembranes 15 (1):pp 5-27.

[12] Riad HL, Ricci AL, Osborn PW, Horvath JS(2003) Expanded polystyrene (EPS) geofoam for road embankments and other lightweight fills in urban environments. In: Soil and Rock America, 12th Pan-American Conference on Soil Mechanics and Geotechnical Engineering and 39th US Rock Mechanics Symposium.

[13] Refsdal G (1985) Plastic foam in road embankments: future trends for EPS use. Internal Report, Norwegian Road Research Laboratory, Oslo, Norway.

[14] Aaboe R (1987) 13 years of experience with expanded polystyrene as a lightweight fill material in road embankments. Norwegian Road Research Laboratory Publication (61):pp 21-27.

[15] Zou Y, Leo C, Small J (2000) Behaviour of EPS geofoam as flexible pavement subgrade material in model tests. Geosynthetics International 7 (1):pp 1-22.

[16] Negussey D, Stuedlein A, Bartlett S, Farnsworth C (2001) Performance of a geofoam embankment at 100 South, I-15 reconstruction project, Salt Lake City, Utah. In: Proceedings on 3rd International Conference on EPS Geofoam.

[17] Farnsworth C, Bartlett SF, Negussey D, Stuedlein A (2008) Rapid construction and settlement behavior of embankment systems on soft foundation soils. Journal of Geotechnical and Geoenvironmental Engineering 134 (3):pp 289-301.

[18] Frydenlund T, Aaboe R (1996) Expanded polystyrene-the light solution. In: Proceedings of Proceedings of International Symposium on EPS Construction Method (EPS-Tokyo'96), Tokyo, Japan, pp 31-46.

[19] Williams D, Snowdon R (1990) A 47 Great Yarmouth Western Bypass: performance during the first three years.

[20] Skuggedal H, Aaboe R (1991) Temporary overpass bridge founded on expanded polystyrene. In: Proceedings of the 1st European Conference on Soil Mechanics and Foundation Engineering, pp 559-561.

[21] McDonald P, Brown P(1993) Ultra lightweight polystyrene for bridge approach fill. In: Proceedings of the 11th Southeast Asian Geotechnical Conference, Singapore, pp 664-668.

[22] Bang S (1995) Experimental and analytical study of expanded polystyrene blocks in highway application. In: Proceedings of International Seminar on the Application of EPS for Embankment Construction, Korea Institute of Construction Technology (KICT), Seoul, Korea, pp 105-133.

[23] Abu-Hejleh N, Zornberg JG, Elias V, Watcharamonthein J (2003) Design assessment of the founders/meadows GRS abutment structure. In: Proc., 82nd Annual TRB Meeting.

[24] Meguid M, Hussein M, Ahmed M, Omeman Z, Whalen J (2017) Investigation of soil-geosynthetic-structure interaction associated with induced trench installation. Geotextiles and Geomembranes 45 (4):pp 320-330.

[25] Meguid M, Ahmed M, Hussein M, Omeman Z (2017) Earth pressure distribution on a rigid box covered with u-shaped geofoam wrap. International Journal of Geosynthetics and Ground Engineering 3 (2):p 11.

[26] Zarnani S, Bathurst R (2007) Experimental investigation of EPS geofoam seismic buffers using shaking table tests. Geosynthetics International 14 (3):pp 165-177.

[27] Horvath JS (1997) The compressible inclusion function of EPS geofoam. Geotextiles and Geomembranes 15 (1):pp 77-120.

[28] Bathurst RJ, Keshavarz A, Zarnani S, Take WA (2007) A simple displacement model for response analysis of EPS geofoam seismic buffers. Soil Dynamics and Earthquake Engineering 27 (4):pp 344-353.

[29] Ossa A, Romo M (2011) Dynamic characterization of EPS geofoam. Geotextiles and Geomembranes 29 (1):pp 40-50.

[30] Partos A, Kazaniwsky P(1987) Geoboard reduces lateral earth pressures. In: Proceedings of Geosynthetics' 87 Conference, New Orleans, USA, pp 628-639.

[31] AbdelSalam S, Azzam S (2016) Reduction of lateral pressures on retaining walls using geofoam inclusion. Geosynthetics International 23 (6):pp 395-407.

[32] Azzam SA, Shokry BM, AbdelSalam SS (2017) 3D Modeling of EPS geofoam buffers behind diaphragm walls. In: International Congress and Exhibition “Sustainable Civil Infrastructures: Innovative Infrastructure Geotechnology”. Springer, pp 46-53.

[33] Chauhan V, Dasaka S (2017) Assessment of lateral earth pressure reduction using EPS geofoam-A numerical study. Paper presented at the CoNMiG-2017, Conference on Numerical Modeling in Geomechanics.

[34] Ertugrul OL, Trandafir AC (2013) Lateral earth pressures on flexible cantilever retaining walls with deformable geofoam inclusions. Engineering Geology 158:pp 23-33.

[35] Karpurapu R, Bathurst R (1992) Numerical investigation of controlled yielding of soil-retaining wall structures. Geotextiles and Geomembranes 11 (2):pp 115-131.

[36] Hatami K, Witthoeft A (2008) A numerical study on the use of geofoam to increase the external stability of reinforced soil walls. Geosynthetics International 15 (6):pp 452-470.

[37] Trandafir AC, Moyles JF, Erickson BA (2010) Finite-element analysis of lateral pressures on rigid non-yielding retaining walls with EPS geofoam inclusion. In: Earth Retention Conference, pp 756-763.

[38] Azzam SA, AbdelSalam SS (2015) EPS Geofoam to reduce lateral earth pressure on rigid walls. In: International Conference on Advances in Structural and Geotechnical Engineering, Hurghada, Egypt.

[39] Ertugrul O, Trandafir A (2011) Reduction of lateral earth forces acting on rigid nonyielding retaining walls by EPS geofoam inclusions. Journal of Materials in Civil Engineering 23 (12):pp 1711-1718.

[40] Brinkgreve R, Broere W (2015) PLAXIS 2D Reference Manual 2015. Delft, Netherlands.

[41] Khan MI, Meguid M (2018) Experimental investigation of the shear behavior of EPS geofoam. International Journal of Geosynthetics and Ground Engineering 4:p 12.

[42] Khan MI, Meguid M (2018) Investigation of the shear behavior of EPS geofoam. Paper presented at the GeoEdmonton 2018- The 71st Canadian Geotechnical Conference, Edmonton, Alberta, Canada.

[43] Meguid MA, Khan MI (2019) On the role of geofoam density on the interface shear behavior of composite geosystems. International Journal of Geo-Engineering 10 (1):p 6.

Table 4.1 Material properties of soil & EPS geofoam (Validated model [39])

Property	**Backfill Soil**	**Foundation soil**	**EPS Geofoam**
Material model	Mohr-Coulomb	Mohr-Coulomb	Linear Elastic
Unit weight, γ (kN/m^3)	16.5	17.5	0.15
Young's Modulus, E (kN/m^2)	5200	5500	1500
Poisson's ratio, υ	0.33	0.33	0.01
Cohesion c' (kN/m^2)	0.01	0.01	-
Friction angle ϕ' (degrees)	43.5	45	-
Dilatancy angle Ψ' (degrees)	22.5	22.5	-
K_o determination	0.3116 (automatic)	0.2929 (automatic)	-
Maximum void ratio	0.745	-	-
Minimum void ratio	0.436	-	-
Specific gravity	2.66	-	-
c_c (coefficient of curvature)	0.80	-	-
c_u (coefficient of uniformity)	3.31	-	-
Percent finer than #200 sieve	1.14	-	-

Table 4.2 Material properties of wall and wall base

Property	Validated Model [39]		Parametric study	
	Wall	**Wall Base**	**Wall**	**Wall Base**
Material type	Elastic; Isotropic	Elastic; Isotropic	Elastic; Isotropic	Elastic; Isotropic
Normal stiffness, *EA* (kN/m)	9.02E+05	6.44E+05	1.44E+07	1.03E+07
Flexural rigidity, *EI* (kN m^2/m)	6.87	6.87	4.40E+02	4.40E+02
Weight, *w* (kN/m/m)	0.624	0.624	2.496	2.496
Poisson's ratio, υ	0.25	0.25	0.25	0.25

Table 4.3 Material properties of soil and EPS geofoam (Parametric study)

Property	**Backfill Soil**	**Foundation soil**	**EPS22**	**EPS29**	**EPS39**
Material model	Mohr-Coulomb	Mohr-Coulomb	Linear Elastic	Linear Elastic	Linear Elastic
Unit weight, γ(kN/m^3)	16	17	0.22	0.29	0.39
Young's Modulus, E (kN/m^2)	25,000	30,000	6,910	10,000	178,000
Poisson's ratio, υ	0.33	0.33	0.12	0.13	0.15
Cohesion c' (kN/m^2)	0.01	0.01	-	-	-
Friction angle ϕ' (degrees)	30^o - 45^o	45	-	-	-
Dilatancy angle Ψ' (degrees)	0	0	-	-	-
K_o determination	0.292 – 0.50	0.2929	-	-	-

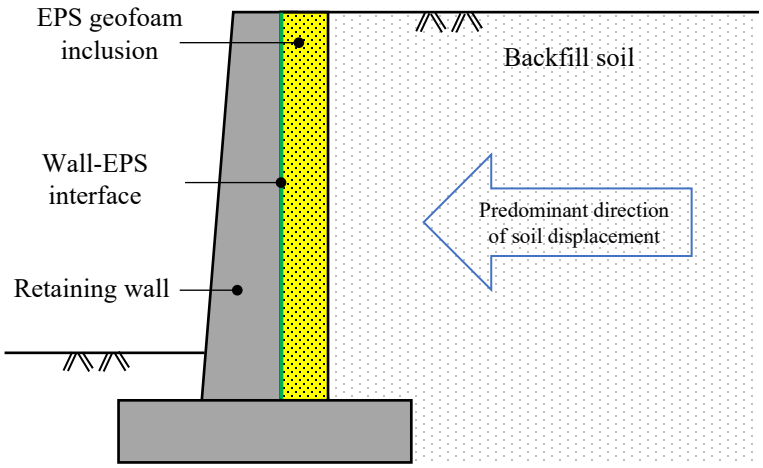

Figure 4.1 Use of EPS behind retaining walls

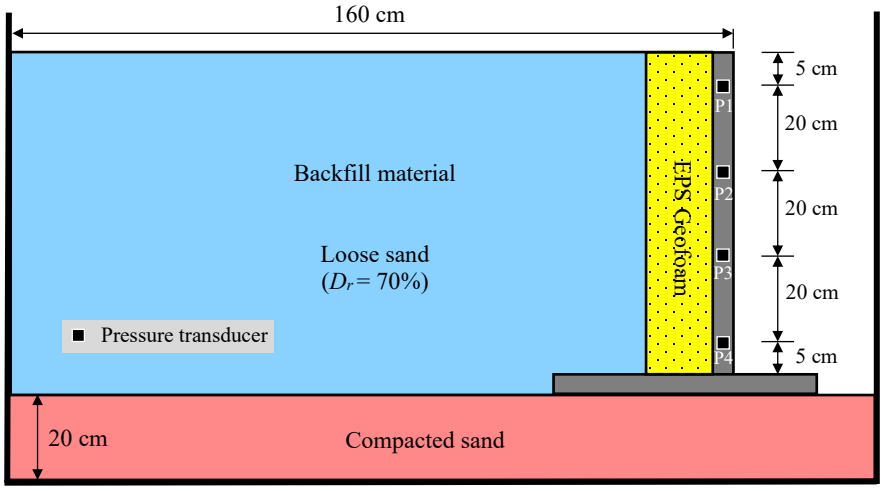

Figure 4.2 Geometry and configurations of the physical model [39]

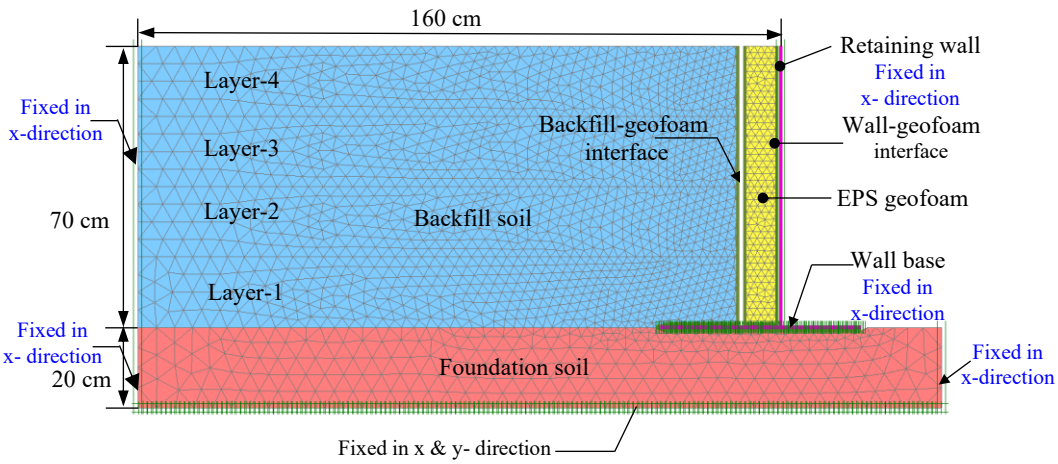

Figure 4.3 Finite element mesh of the rigid non-yielding retaining wall with geofoam inclusion

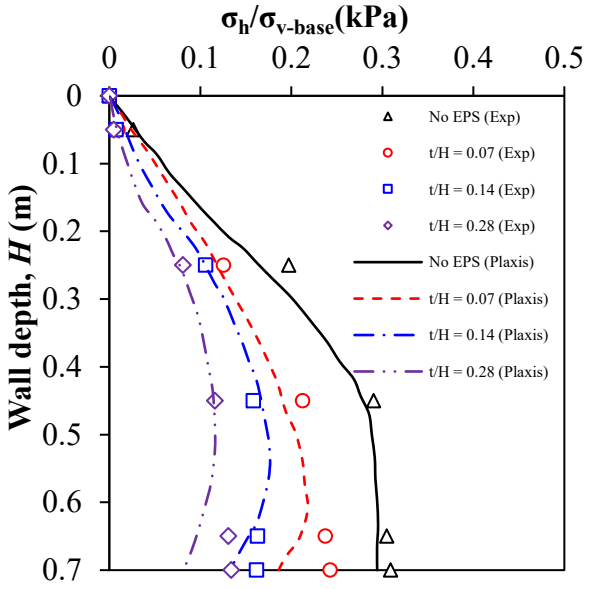

Figure 4.4 Normalized lateral earth pressures vs wall depth

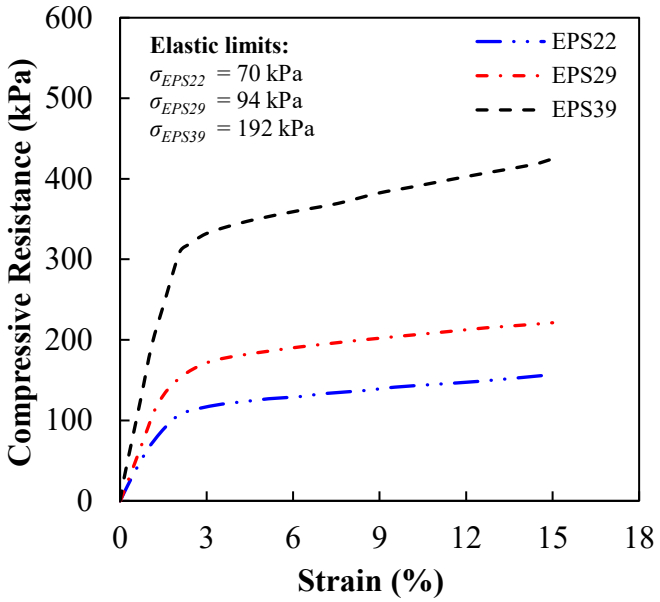

Figure 4.5 Stress-strain relationships of EPS22, EPS29 & EPS39

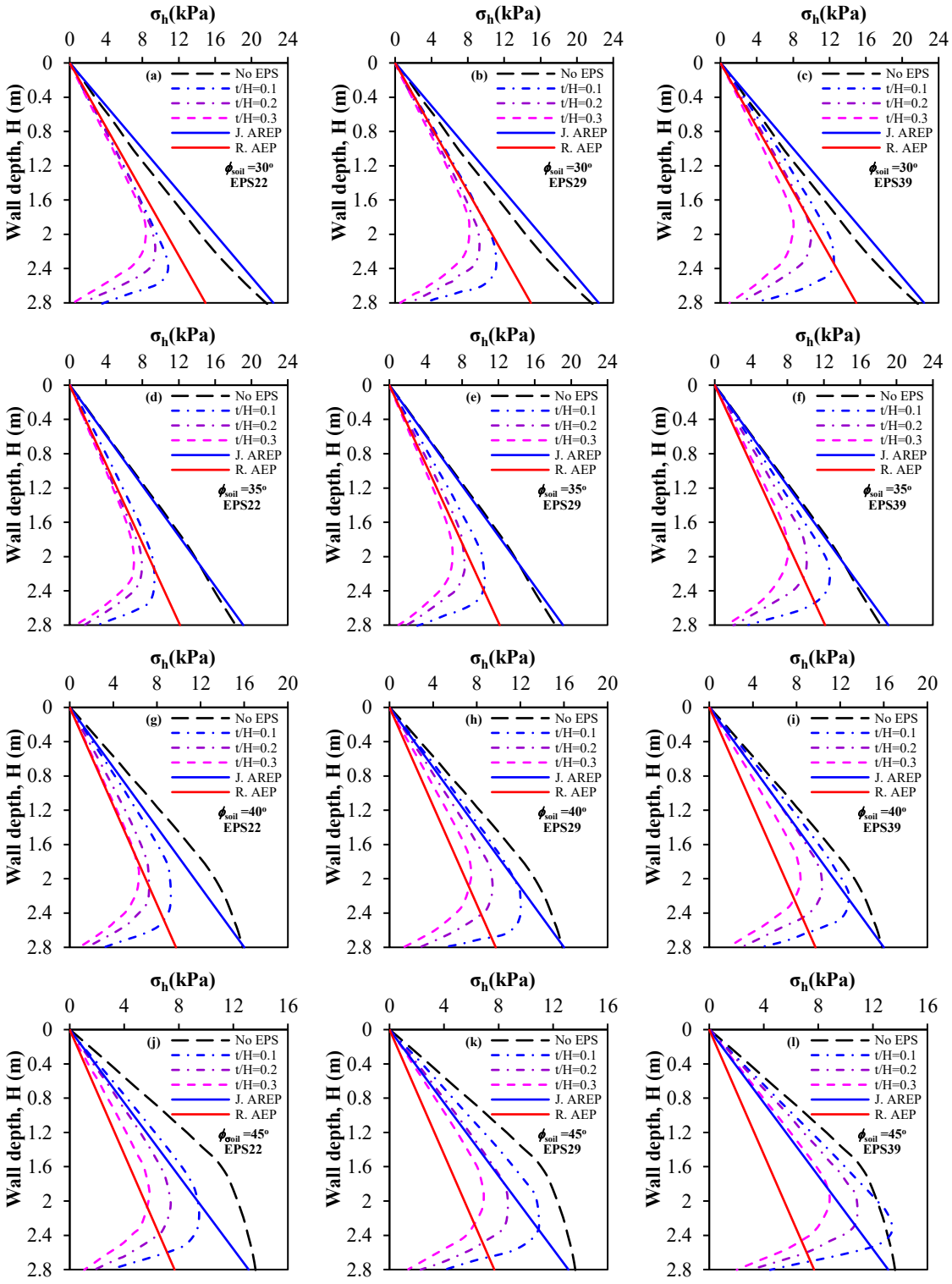

Figure 4.6 Lateral earth pressure distributions on walls for different geofoam densities, thicknesses, and backfill material

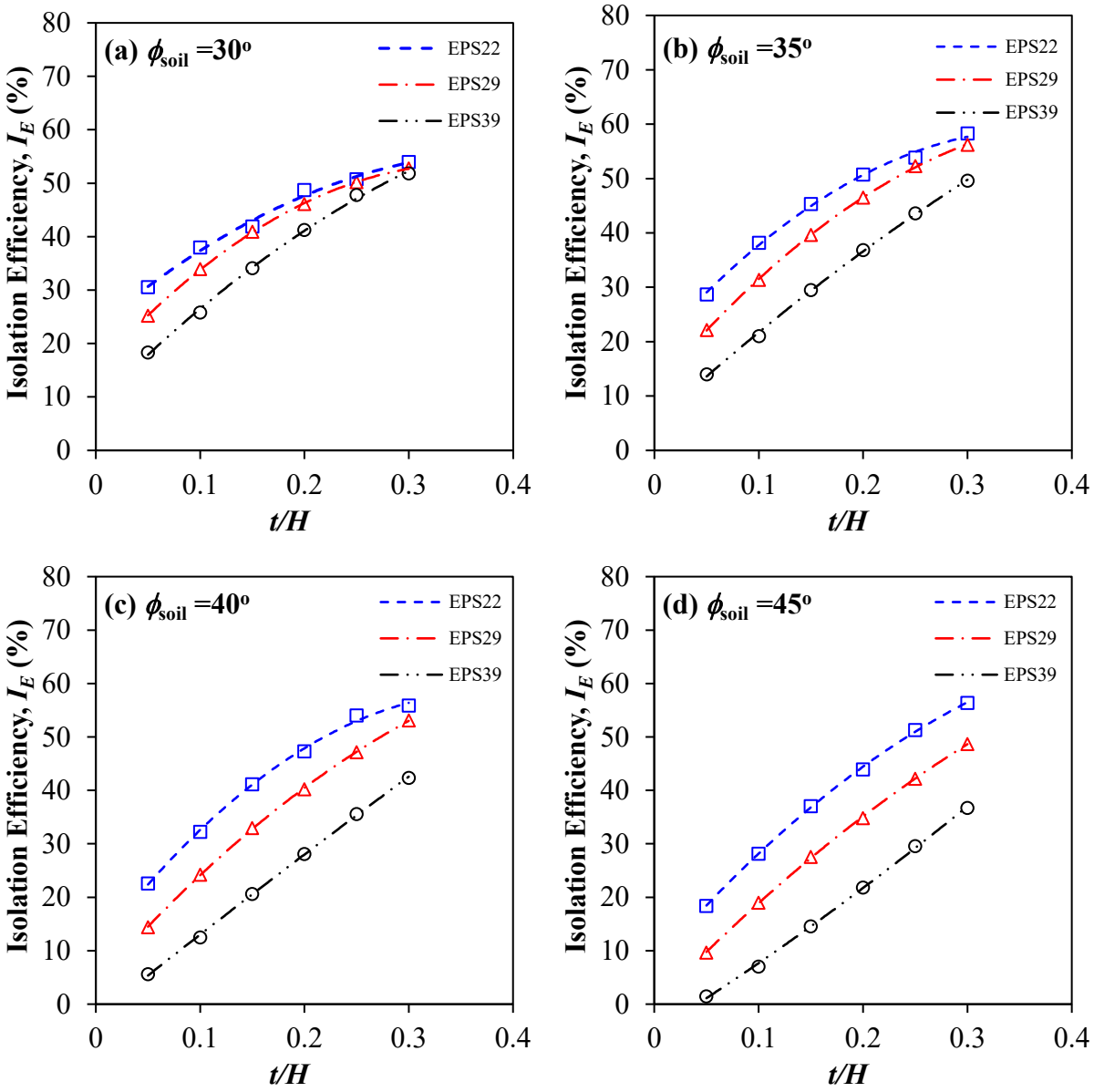

Figure 4.7 Isolation efficiency vs *t/H* for EPS22, EPS29 & EPS39: (a) ϕ=30°, (b) ϕ=35°, (c) ϕ =40°, (d) ϕ=45°

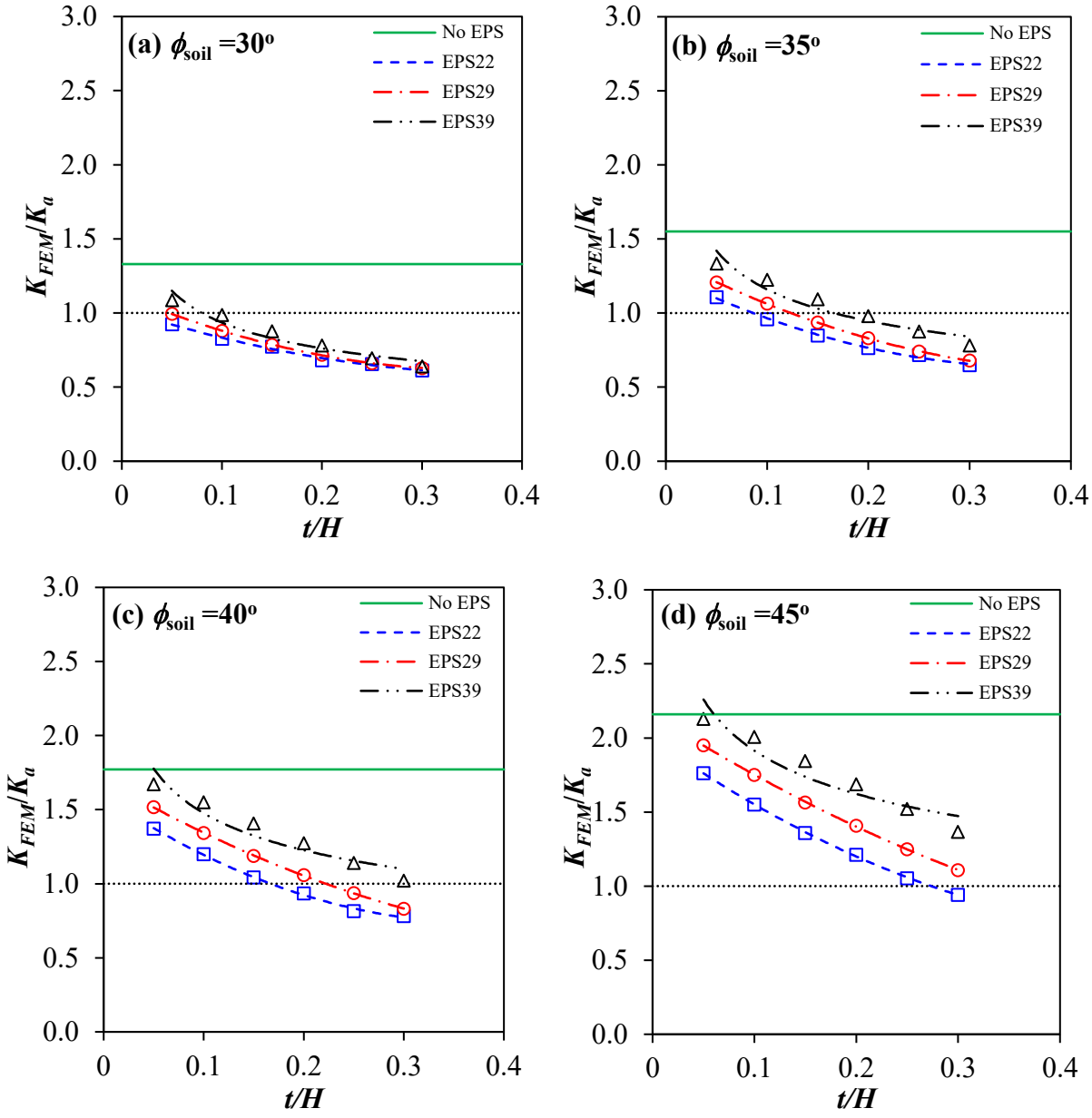

Figure 4.8 Variation of lateral earth pressure coefficient ratio K_{FEM}/K_a ratio for various t/H , EPS & backfill ϕ *values*: (a) ϕ =30°, (b) ϕ =35°, (c) ϕ =40°, (d) ϕ =45°

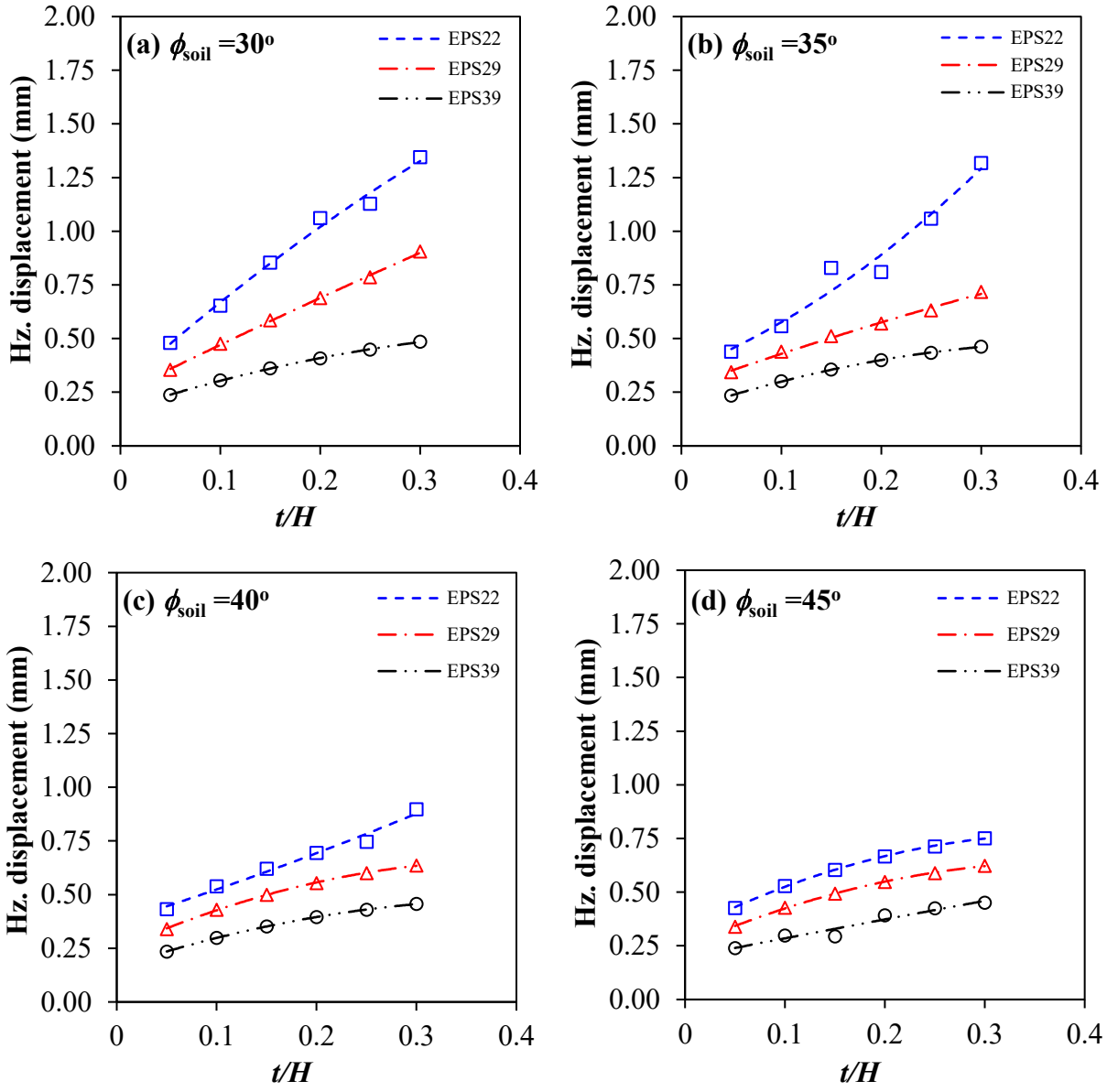

Figure 4.9 Horizontal displacement of backfill soil vs *t/H* for EPS22, EPS29 & EPS39: (a) ϕ=30°, (b) ϕ=35°, (c) ϕ=40°, (d) ϕ=45°

5

On the Use of EPS Geofoam to Reduce Earth Pressure on Retaining Walls under Dynamic Loading: A Numerical Study*

* A version of this chapter has been submitted as:
Khan, M. I., & Meguid, M. A. (2021). *On the use of EPS geofoam to reduce earth pressure on retaining walls under dynamic loading: A numerical study*. International Journal of Geosynthetics and Ground Engineering.

5.1 Preface

In the previous chapter (chapter 4), role of EPS geofoam on reducing lateral earth pressure on rigid retaining wall was studied using a numerical parametric study and results were presented in the form of design charts. In this chapter, a 2D finite element model has been developed and validated to investigate the role of EPS geofoam in reducing seismic earth pressure on rigid wall. A parametric study was then conducted, and results were presented in the form of design charts for practical implication.

5.2 Abstract

The magnitude of lateral earth pressure plays an important role in the analysis and design of earth retaining structures. Expanded polystyrene (EPS) geofoam panels have been successfully used in reducing lateral thrust on walls under static loading condition. The presence of geofoam panels between a rigid wall and the backfill soil allows for controlled deformation to develop, which leads to the mobilization of soil shear strength. When subjected to dynamic loading, the magnitude of earth pressure acting on a rigid wall can become significantly larger. In this study, a finite element model is developed to investigate the effectiveness of installing geofoam buffer behind a rigid retaining wall on the seismic lateral thrust induced by the backfill material. A parametric study was then conducted to investigate the effect of geofoam density, relative thickness of the geofoam with respect to the wall height and the friction angle of the backfill soil on the effectiveness of this technique to reduce the impact of seismic events on the stability of the wall. Results showed that

provision of EPS geofoam behind rigid non-yielding retaining wall can provide 10-40% reduction in seismic thrust depending on the geofoam density, relative thickness and frictional properties of the backfill soil.

Keywords: EPS geofoam, Seismic buffer; Rigid retaining wall; Isolation efficiency; Finite element modelling; Lateral earth pressure; Plaxis.

5.3 Introduction

Expanded polystyrene (EPS) geofoam has a long history with successful applications in the field of transportation and geotechnical engineering. The generic term "geofoam" was first introduced by Horvath [1] for rigid plastic foam type materials used in geotechnical applications. Later, the term "geofoam" was expanded to include any cellular material manufactured by an expansion process [2]. These synthetic materials are now part of the geosynthetic family as proposed by Horvath [3].

The early use of EPS geofoam in geotechnical engineering started in 1960s. The Norwegian geotechnical engineers used EPS geofoam for thermal insulation in roads [4] and in lightweight road embankments constructed over soft soils [5]. Due to its extreme lightweight nature (ρ = 12 to 39 kg/m^3), high compressibility and high strength, EPS geofoam has been used in several geotechnical applications, for example: slope stabilization [6-10], subbase fill material [11-14], embankments [15-19], earth retaining structures [20], bridge approaches and abutments [21-25], buried pipes [26-28] and compressible inclusion or seismic buffer [29-33].

Retaining walls (e.g. cantilever walls, basement walls or bridge abutments) are an integral part of many important infrastructure projects, they are mostly provided as preferred countermeasure against soil instability. Retaining wall could be "non-yielding" or "yielding" depending on whether horizontal displacement and wall deformation are permitted [34].

Past experience showed that retaining walls may be vulnerable to severe damage under excess dynamic forces induced during an earthquake. Several post-earthquake studies revealed that large displacements can lead to excessive deformation and possibly failure of the retaining walls [35]. Therefore, in seismically active areas, a retaining structure must be designed to resist both static and dynamic earth pressures. The current USA and Canadian design codes emphasises the use of an increased earthquake return period in the design of civil engineering structures in seismically active regions [36,37], which results in higher design loads on earth retaining structures. Therefore, both geotechnical and structural engineers are interested in developing new methodologies to

attenuate larger seismic loads on earth retaining structures which in turn leads to an economical and safe design.

EPS geofoam has proved its potential to resist both lateral and vertical stresses in many geotechnical projects. The most important characteristics of the geofoam include durability, stability and ability to resist moisture and deterioration. To suit wide range of application, density and stress-strain behavior of EPS geofoam can easily be modified during manufacturing. Cost effectiveness of the geofoam increases when it is used as multipurpose material in geotechnical engineering projects.

Compressible EPS geofoam inclusion placed behind a rigid retaining wall has been suggested to attenuate the dynamic earth forces by allowing controlled yielding of backfill soil [38-45]. The idea of using EPS geofoam as compressible inclusion is not new. Researchers have shown that static lateral loads on retaining walls can be reduced by placing a layer of EPS geofoam between the wall and the backfill soil without increasing the wall stiffness [46-53]. During an earthquake event, compressible EPS geofoam layer allows for the lateral expansion of backfill soil (controlled yielding) by taking up the major portion of the seismic lateral thrust while the remaining thrust is transferred safely to the rigid retaining structure. Lateral expansion of backfill soil also helps in the mobilization of full shear strength of the soil which brings the surrounding soil to active failure state. This technique can be applied to both new and existing structures.

Inglis et al. [54] in a case study reported the first use of seismic buffer in Vancouver, Canada. Vertical EPS panels that are 450 mm to 610 mm thick were placed behind three rigid basement walls to reduce dynamic lateral earth pressures during an earthquake (see Figure 5.1). Pseudo-static analysis [55], Pseudo-dynamic analysis [56-58] and dynamic analysis [59] were performed to compute the seismic earth pressures on the walls. Results from these analyses show that presence of about 1 m thick EPS geofoam inclusion between the rigid retaining wall and the backfill can reduce the lateral seismic earth pressure by about 50% in comparison to rigid retaining wall with no geofoam buffer.

According to Inglis et al. [54] a good buffer material should: (a) be strong and rigid enough to withstand static soil forces with small deformations and creep but at the same time should also be able to resist the possible dynamic forces without causing failure; (b) be inert and should not deteriorate due to water, chemical attack, aging, etc.; (c) be economical in comparison to the cost of the structure.

Several researchers investigated the role of EPS geofoam in attenuating the seismic earth pressure on retaining walls. A summary of some of these studies is given below.

5.3.1 Experimental Studies

Bathurst et al. [42] presented a proof of concept for the application of geofoam as seismic buffer behind rigid retaining walls using 1-g shaking table. Tests were conducted on small-scale physical models of retaining walls with EPS geofoam inclusion of different density placed against the retaining walls. Test results showed that low stiffness (density = 1.3 kg/m^3) geofoam achieved 40% reduction (at a peak base acceleration of 0.8g) while high stiffest (density = 1.6 kg/m^3) geofoam achieved about 15% reduction in earthquake load compared to the control wall (with no EPS geofoam).

Hazarika et al. [60,40] conducted reduced-scale shaking table tests on a 0.7 m high retaining wall models having varying buffer thickness (t/H = 0.02, 0.05 & 0.08; where t = thickness of EPS geofoam and H = wall height). The buffer used in this study was a sponge type material having density of 22 kg/m^3.Tests were performed under a 3.3 Hz frequency sinusoidal base acceleration record (having peak accelerations of 0.2, 0.44, 0.6 and 0.8g) applied in the horizontal direction. Results showed that provision of EPS geofoam layer between the wall and backfill soil could reduce the peak lateral load on the wall by about 30-60 %.

Dasaka et al. [44] performed 1-D shaking table tests on reduced-scale physical models of gravity retaining wall subjected to both surcharge and seismic loading. Surcharge pressures of 10, 30 & 50 kPa were applied on top of the backfill and for each pressure increment, a 3 Hz sinusoidal stepped-amplitude horizontal base acceleration with a peak acceleration amplitude of 0.7g was applied to the model. It was found that provision of ESP geofoam (density 10 kg/m^3) behind gravity retaining walls could reduce the maximum seismic lateral thrust on the wall by about more than 28%. In a similar study, Dave et al. [61] studied the effect of boundary conditions at the wall base (with and without hinge). Retaining walls with a hinge showed a hydrostatic seismic pressure distribution while fixed walls showed a curvilinear seismic pressure distribution. It was found that EPS geofoam of density 10 kg/m^3 reduced the total lateral thrust by about 23% and 28%, for retaining walls with and without hinge boundary conditions, respectively.

Ertugrul et al. [45,62,63] investigated the effect of geofoam as a seismic buffer behind flexible cantilever walls using 1-g shaking table tests. Comparison of tests results showed that geofoam with the lowest stiffness (density = 15 kg/m^3) could reduce up to 50% of the dynamic thrust acting

on the wall. It was also found that the point of application of the dynamic thrust could vary from 0.4H to 0.6H depending on the type of geofoam used, the flexibility ratio of the wall and the characteristics of the excitation record.

Although physical testing is helpful in the verification or validation of numerical models, it has limitations with respect to the model scale and the associated cost of large physical models. On the other hand, centrifuge testing provides a valuable mean for testing small-scale models without significant boundary effect issues. Athanasopoulos-Zekkos et al. [43] performed centrifuge tests on 4 m high rigid retaining wall models with and without EPS inclusion. Tests were conducted under a range of sinusoidal motions. Comparison of test results of models with and without geofoam inclusion confirmed reduction of seismic earth pressure due to controlled yielding of backfill soil associated with compression of the geofoam inclusion. For EPS geofoam buffer with a relative thickness, t/H = 0.1, the isolation efficiency was found to vary between 10 and 50 % under an input excitation of 2Hz with peak acceleration of 0.2g. A summary of shaking table test results is presented in Table 5.1.

5.3.2 Numerical Studies

Inglis et al. [54] performed finite difference analysis of a 10 m high wall with EPS seismic buffer. Wall models were tested under a simulated earthquake loading as well as a constant amplitude harmonic sinusoidal loading (1.57 Hz frequency). Results showed that provision of EPS seismic buffer reduced peak lateral stress on the wall by around 50 %.

Pelekis et al. [64] conducted finite element study to investigate the potential application of geofoam as seismic buffer. Reinforced concrete cantilever retaining walls (H = 3.3, 4.8 & 7 m) were subjected to an actual earthquake record with predominant frequencies of 2 and 3 Hz with base acceleration ranging between 0.1g to 0.5 g. It was found that depending on the thickness and stiffness of EPS geofoam a significant reduction in seismic earth pressure can be achieved. On the other hand, intensity of motion (peak acceleration) showed negligible effect on the seismic earth pressure reduction.

Armstrong, Alfaro [65] conducted a numerical study on the benefits of using EPS geofoam behind rigid retaining wall under seismic loading. A 10 m high wall with different EPS geofoam relative thicknesses (t/H = 0.025, 0.05, 0.075 & 0.1; where t = thickness of EPS geofoam and H = wall height) and two backfill soils with friction angles of 30^o and 35^o were considered. Models were tested under an input excitation of 1.5 Hz for 2 seconds, with a peak acceleration of 1.9g. Results

showed that provision of EPS seismic buffer only reduced 25% of the passive seismic thrust while a minimal reduction was observed on active seismic thrust.

Zarnani et al. [66-68] simulated shaking table tests conducted on reduce scale wall models with EPS geofoam inclusion. Results showed that the analysis qualitatively captured the total earth force-time response and in most casaes showed a good agreement with experimental results. Zarnani, Bathurst [69] conducetd a parametric study using validated numerical model to study the effect of wall height; thickness, stiffness and type of EPS geofoam and excitation record on the performance of EPS geofoam as seismic buffer. It was found that geofoam stiffness $K = E/b$; (where E = modulus of elasticity and b = geofoam thickness) plays a vital role in the design of composite systems. Moreover, for mitigation of seismic induced dynamic loads, $K \leq 50$ MN/m^3 was found to be practical for the design of these composite systems.

Athanasopoulos et al. [70] studied the response of retainig walls with EPS geofoam subjected to harmonic base excitations using finite element analysis. It was found that EPS density, thickness, wall height, wall flexibilty, intensity and frequencey of base motion strongly affect the efficiency of EPS geofoam as seismic buffer. In a similar study, Zekkos et al. [71] showed that for non-yielding walls, in general, isolation efficiency increses with the increase in inclusion thickness. On the other hand, for yielding retaining walls, isolation efficiency increses with the increase in inclusion thickness up to a limiting value that can not be exceeded with further increase in inclusion thickness.

Wang et al. [72] numerically simulated the results of shaking table tests conducted by Bathurst et al. [42] on a wall model with EPS geofoam. A reasonable agreement was found between the numerical and measured data.

Wang, Bathurst [73] used finite element to numerically simulate a reduced scale retaining wall tested using shaking table. Numerical results were found to be in reasonable agreement with the experimental results. It was also found that lower density geofoam being the most compressible material could absorb greater portion of energy during earthquake as compared to EPS geofoam higher density. A summary of numerical studies is presented in Table 5.2.

5.4 Scope and Objective

The present study focuses on the use of EPS geofoam in reducing the seismic lateral earth pressure behind rigid non-yielding retaining walls. A 2D dynamic numerical model is developed using finite element software PLAXIS [74]. The results of the FE analysis were validated against the

experimental results reported by Bathurst et al. [42]. Parametric analyses are then performed to investigate the effect of relative thickness, stiffness of EPS geofoam and strength parameters of backfill soil on the seismic lateral earth pressure acting on the wall.

5.5 Description of the Physical Model

Bathurst et al. [42] carried out 1-g shaking table tests on small scale rigid non-yielding retaining wall models with EPS geofoam seismic buffer at the Royal Military College of Canada (RMC). Models were built and tested in a strong rectangular container (2.5 m × 1.4 m × 1.3 m) firmly attached to the shaking table platform (2.7 m × 2.7 m in plan area) as shown in Figure 5.2. A 6 mm thick aluminium rigid wall was placed on linear bearings at the front of the rectangular container, which could be moved to place 0.15 m thick EPS geofoam between the wall and backfill soil. The back wall of the container was rigidly braced.

Backfill soil (dry synthetic olivine sand) was placed and compacted in 200 mm thick lifts. Conventional direct shear tests conducted on sand samples (100 mm × 100 mm) of relative density, D_r, of 86% indicated friction and dilatancy angles of 46° and 15°, respectively. Blocks of Type I EPS geofoam as per ASTM classification [75] having density 16 kg/m^3 were placed between the wall and backfill. Properties of the soil and the geofoam are given in Table 5.3.

A total of 9 load cells (4 horizontal & 5 vertical) were installed to record the components of vertical and lateral earth forces on the rigid wall. Four displacement potentiometers were passed through EPS buffer and installed on the front face of the wall to measure the dynamic compressive strain of the geofoam. An additional potentiometer was attached directly to the shaking table to record the displacement-time history of the model. Four accelerometers were also placed during the placement of the backfill soil at specific locations to record the acceleration response during the tests. An additional accelerometer was attached to the base of the shaking table to measure the acceleration-time history.

A 5 Hz frequency variable-amplitude sinusoidal base acceleration record (with peak accelerations 0.8g) as shown in Figure 5.3(a), was applied as horizontal base excitation in all tests. The acceleration amplitude was increased in increments of 0.05g and each increment was kept for 5 seconds. A 2-second accelerogram window at amplitude step is shown in Figure 5.3(b). This simple stepped-amplitude sinusoidal base acceleration record is more aggressive than an actual earthquake record with same predominant frequency and amplitude [76,77]. A stepped record also simplifies the interpretation of seismic wall response.

According to the scaling rules proposed by Iai [78], a 5 Hz frequency (i.e. 0.2 s period) corresponds to 2 Hz frequency (i.e. 0.5 s period) at 1/6 prototype model scale. Moreover, frequencies ranging from 2-3 Hz are representative of typical predominant frequencies of medium to high frequency earthquakes [76]and fall within the expected earthquake parameters for North American seismic design

5.6 Numerical Analysis and Model Validation

The numerical simulations were performed using a finite element (FE) based commercial software PLAXIS 2D v 20.03.00.60 [74]. Two-dimensional (2D) plane strain models were developed to simulate the dynamic response of rigid retaining wall for following cases: (a) without EPS geofoam (b) with EPS geofoam. The height and width of numerical models and thickness of EPS geofoam were selected to match the dimensions used in the physical tests. Several mesh sizes, time increments, and maximum steps were tested to determine a suitable mesh, time increment, and max steps to maintain a balance between accuracy and computing cost. The FE mesh, geometry and boundary conditions is shown in Figure 5.4. The retaining wall and the back of the box were modelled as plate elements. The backfill soil was modelled using 15-node triangular plane strain elements.

Proper boundary conditions were defined to simulate shaking table test results. The displacements along the vertical boundaries were fixed in the x-direction (smooth rigid) during the initial phase (initial stress state) and released in the x-direction during the dynamic phase. However, displacements along the bottom boundary were fixed in both the x & y-directions (rough rigid) during the initial phase and released in the x-direction during dynamic phase. Interfaces between the wall-backfill, wall-EPS and EPS-backfill were also specified. The backfill soil was modelled using the Hardening Soil (HS) model with Rayleigh damping. The HS model is an elasto-plastic second-order hyperbolic isotropic-hardening model developed by Schanz et al. [79]. The EPS geofoam was modelled as linear elastic material. The material properties of backfill soil and EPS geofoam are given in Table 5.3.

The steps taken in creating the plane strain model can be summarized as follows: (1) Generation of box, retaining wall, backfill soil and EPS geofoam in one initial step; (2) the application of stepped amplitude sinusoidal input excitation at the base with a peak acceleration of 0.8g at the base and the two vertical boundaries of the models.

The results of both the numerical analysis and experimental data for two condition (with and without EPS geofoam) are presented in Figure 5.5. It can be seen that as the time increases from 0 to 86 sec, acceleration amplitude also increases from 0 to 0.8g, which significantly increases the horizontal force on the wall. It is noted that, for clarity, only the peak horizontal wall force is plotted against time. Comparison of the measured and calculated data shows a good qualitative and quantitative agreement. The underprediction at the beginning of the tests (first 15 sec) is mainly attributed to the locked-in stresses developed during the compaction process in the physical test, which could not be simulated in the model. Other than these stresses, numerical results show a reasonable trend for both cases with a slight overprediction for the case where no geofoam. Figure 5.6 represents the results of the FFT analysis conducted using the acceleration time histories obtained from the numerical model. It is clearly shown that the dominant frequency in the backfill soil is the same as that of the frequency of the input signal. i.e. 5 Hz.

5.7 The Effect of Geofoam and Backfill Properties on the Dynamic Lateral Earth Pressure Acting on the Wall

A parametric study was conducted to examine the effect of geofoam density, relative thickness and backfill friction angle (ϕ) on the reduction of dynamic lateral earth force acting on the wall. A 1.0 m high retaining wall model was developed using 15-noded plane strain triangular elements. Retaining wall was modelled as plate element. The backfill soils was modelled using Hardening Soil (HS) model with Rayleigh damping. Four different backfill materials with friction angle (ϕ) values ranging from 30^o to 45^o were considered in the parametric study. The EPS geofoam was modelled as linear elastic material. Four different geofoam densities representing EPS15, EPS22, EPS29 and EPS39 with three different EPS thickness "*t*" to wall height "*H*" ratios, also known as relative thickness (t/H = 0, 0.1, 0.2, & 0.3) were considered. The experimental uniaxial compression curves of the four geofoam materials are shown in Figure 5.7. For geofoam densities of15 (EPS15), 22 (EPS22), 29 (EPS29) and 39 (EPS39) kg/m^3, the reported compressive strength values at 1% strain are 45, 70, 94 and 192 kPa, respectively. Therefore, given the expected range of lateral earth pressure (2-19 kPa), geofoam material was assumed to behave as linear elastic under static and dynamic applied lateral earth pressures. Material properties of both the soil and the geofoam are summarized in Table 5.4. The boundary conditions, input excitation and dynamic time used in all the simulations are the same as those used in the validated model shown in Figure

5.3. In total, 52 simulations were run, 4 without EPS geofoam and 48 with EPS geofoam to study the role of EPS geofoam in reducing seismic earth pressure behind rigid non-yielding retaining wall. The results of the parametric study are presented in the following section.

5.8 Results and Discussion

The results of the parametric study are presented by comparing the computed peak wall force-time response before and after adding geofoam of different thicknesses and density. The peak incremental dynamic wall force or lateral thrust, ΔT, was computed by integrating the peak dynamic horizontal earth pressure distribution along the wall height at a particular time step. The computed peak wall force-time responses are presented in Figure 5.8(a) through 5.8(h) for backfill material with ϕ =30° & 35° and in Figure 5.9(a) through 5.9(h) for backfill material with ϕ =40° & 45°. Four EPS densities, namely, 15, 22, 29 and 39 kg/m^3 and three relative geofoam thicknesses (t/H = 0.1, 0.2, & 0.3) are considered.

5.8.1 Benchmark case (no geofoam):

In Figure 5.8(a) through 5.8(h) and Figure 5.9(a) through 5.9(h), No EPS line shows the value of peak horizontal force acting on the wall due to various backfill materials. The peak force at time t = 0, corresponds to static condition and the peak wall force at time t ≠ 0, corresponds to dynamic condition. For all four backfill soils, it can be seen that as the time increases from 0 to 86 sec, acceleration amplitude also increases from 0 to 0.8g which causes a significant increase in the horizontal force acting on the wall. It was also found that increase in friction angle (ϕ) values from 30° to 45°, static lateral thrust decrease from 3.92 to 2.29 kN/m and seismic lateral thrust increases from 15.7 to 17.25 kN/m.

5.8.2 Effect of geofoam density

It is evident from Figure 5.8(a) through 5.8(h) and Figure 5.9(a) through 5.9(h) that for a given backfill material and EPS thickness, change in EPS density (stiffness) causes reduction in seismic peak wall force on the wall. For example, for a backfill soil with a friction angle ϕ=40° and t/H=0.3, the peak seismic wall forces increased from 10.62 kN/m to 12.70 kN/m as the density of EPS geofoam was varied from 15 to 39 kg/m^3. This is due to the fact that softer geofoam has the ability to absorb more energy under the same applied dynamic lateral thrust, which in turn allows

more movement and consequently less pressure on the wall. Therefore, low density geofoam blocks are more effective than high density geofoam.

5.8.3 Effect of geofoam thickness

Inspection of Figure 5.8(a) through 5.8(h) and Figure 5.9(a) through 5.9(h) reveals that for a given backfill and EPS density, the change in the relative thickness of EPS geofoam (*t/H*) causes reduction in seismic peak wall force on the wall. For example, for a backfill soil with a friction angle ϕ=40° and geofoam density 15kg/m^3 (EPS15), the peak seismic wall forces decreased from 14.30 kN/m to 10.62 kN/m as the relative thickness of EPS geofoam (*t/H*) was varied from 0.1 to 0.3. This is consistent with the fact that thick geofoam blocks compress more as compared to thin geofoam of same density, which results in more compression and more energy is absorbed under the same applied force

5.8.4 Effect of friction angle of the backfill soil

Frictional properties of the backfill soil can affect the magnitude of both static and seismic earth pressure. It was observed that for a given geofoam thickness and density, as the friction angle (ϕ) of the backfill soil changes from 30° to 45°, the static lateral thrust decreased from 3.92 to 2.29 kN/m and the seismic lateral thrust increased from 15.7 to 17.25 kN/m as depicted in Figure 5.8(a) through 5.8(h) and Figure 5.9(a) through 5.9(h). For example, for EPS15 having *t/H* of 0.2, the peak seismic wall forces increased from 11.43 kN/m to 12.03 kN/m as the friction angle (ϕ) of backfill soil was varied from 30° to 45°. It means that under dynamic loading conditions, EPS geofoam works better when used with a backfill soil having higher frictional properties.

5.8.5 Isolation Efficiency (I_E)

The performance of EPS geofoam behind rigid retaining walls under seismic conditions can also be evaluated by computing the Isolation Efficiency (I_E), which is "the ratio of the difference between the peak lateral seismic thrust for benchmark (no geofoam) case (T_o) and the case where geofoam is installed (T_{EPS}) to the peak lateral seismic thrust for the benchmark case (T_o)" as expressed below:

$$I_E = \frac{T_o - T_{EPS}}{T_o} \times 100$$

Figure 5.10(a) through 5.10(d) show the influence of backfill frictional properties, geofoam densities and relative thicknesses on the isolation efficiency (I_E). Isolation efficiency is directly related to the relative thickness of the geofoam, friction angle of backfill soil and inversely related to geofoam density. It was observed that for thinner geofoams (t/H=0.1) of different densities, higher isolation efficiency was observed in soils with low friction angles 30° to 35°. However, for thicker geofoams (t/H=0.3) of different densities, higher isolation efficiency was observed in soils with high friction angles 40° to 45°.

5.9 Practical Implication

Results of present numerical study are summarized in the form of guidance charts (see Figure 5.10) for the selection of minimum thickness and density of geofoam to achieve a desired isolation efficiency (I_E) for a given backfill material. A design example is presented in this section to explain how the design charts presented in Figure 5.10 can be utilized by geotechnical engineers.

Design Example:

Given Data:

H = 1.0 m

$\phi = 40^o$

$I_E = 30$ %

Find geofoam EPS15 thickness = t =?

Solution:

For $I_E = 30$ %

Using Figure 5.10(c):

$t/H = 0.19$

$t = 0.19 \times H$

$t = 0.19 \times 1 = 0.19$ m = 19 cm

The required EPS15 thickness (t) to satisfy a 30% reduction = 19 cm

5.10 Conclusions

In the present study, a 2D FE model is developed to study the effect of geofoam on the seismic earth pressure acting on rigid retaining walls. Numerical model was first validated using results of shaking table tests. A parametric study was then conducted to investigate the effectiveness of EPS geofoam density, relative thickness of the EPS geofoam with respect to the wall height and

frictional angle of backfill soil on reduction of seismic earth pressure. Based on the results of numerical analyses following conclusions can been drawn:

1. An optimal design of retaining structure requires, lesser loads to be transferred to the retaining structure under applied loading. Provision of EPS geofoam placed between the wall and backfill soil provides controlled yielding of soil (i.e. mobilization of major portion of soil strength) under dynamic loading which leads to reduction in seismic thrust on the wall. An advantage of this technique is that it could be applied to both new and existing structures.
2. The behavior of backfill soil and EPS geofoam are reasonably well predicted by using Hardening Soil (HS) material model for backfill soil and linear elastic model for EPS inclusion.
3. The performance of EPS geofoam as seismic buffer is a function of density of EPS geofoam, relative thickness and frictional properties of backfill soil. It was found that low density geofoam provides better performance as compared to high density geofoam. On the other hand, for a same density geofoam, thicker geofoam is found to absorb more pressure than thinner geofoam. It was also found that using geofoam as seismic buffer is more effective in soils with high frictional properties as compared to soil with low frictional angles.
4. The limitation of the present study is that the parametric study was not extended to relative thickness $0.1< t/H< 0.3$ because there exist a limiting value of t/H depending upon the relative thickness of EPS geofoam and stiffness of backfill soil.

Notation

The following symbols are used in this paper:

D_r = Relative density of soil

t = Thickness of geofoam

H = Wall height

σ_E = Elastic limit

ϕ, = Friction angle of soil

I_E = Isolation efficiency

T_o = Total seismic lateral thrust for without geofoam case

T_{EPS} = Total seismic lateral thrust for with geofoam case

T = Total seismic thrust lateral acting on the wall

5.11 References

[1] Horvath JS (1992) New developments in geosynthetics; 'lite' products come of age. Standardization News 20 (9):50-53.

[2] Horvath JS (1995) Geofoam Geosynthetic, Horvath Engineering, P.C. Scarsdale, New York, USA, 217 p.

[3] Horvath JS (1991) The case of an additional function. IGS News 7 (3):17-18.

[4] Aaboe R (2000) Evidence of EPS long term performance and durability as a lightweight fill. Vegteknisk avdeling.

[5] Frydenlund T (1991) Expanded polystyrene: A lighter way across soft ground. vol 1502. ICON Group International.

[6] Elragi AF (2000) Selected engineering properties and applications of EPS geofoam. ProQuest Dissertations and Theses.

[7] Jutkofsky W, Sung J, Negussey D (2000) Stabilization of embankment slope with geofoam. Transportation Research Record: Journal of the Transportation Research Board (1736):94-102.

[8] Sheeley M (2000) Slope stabilization utilizing geofoam. Master's thesis, Syracuse University, New York.

[9] Srirajan S (2001) Recycled content and creep performance of EPS geofoam in slope stabilization. Doctoral dissertation. Syracuse University, New York.

[10] Negussey D (2002) Slope stabilization with geofoam. Report to FHWA and the EPS Industry. Geofoam research center, Syracuse University, New York.

[11] Stark TD, Arellano D, Horvath JS, Leshchinsky D (2004) Geofoam applications in the design and construction of highway embankments. NCHRP web document 65:24-11.

[12] Duskov M (1991) Use of expanded polystyrene (EPS) in flexible pavements on poor subgrades. In: Proceedings of the International Conference on Geotechnical Engineering for Coastal Development, pp 783-788.

[13] Duskov M (1997) Measurements on a flexible pavement structure with an EPS geofoam sub-base. Geotextiles and Geomembranes 15 (1):5-27. doi:http://dx.doi.org/10.1016/S0266-1144(97)00004-6.

[14] Riad HL, Ricci AL, Osborn PW, Horvath JS (2003) Expanded polystyrene (EPS) geofoam for road embankments and other lightweight fills in urban environments. In: Soil and Rock

America, 12th Pan-American Conference on Soil Mechanics and Geotechnical Engineering and 39th US Rock Mechanics Symposium.

[15] Refsdal G (1985) Plastic foam in road embankments: future trends for EPS use. Internal report, Norwegian Road Research Laboratory, Oslo, Norway.

[16] Aaboe R (1987) 13 years of experience with expanded polystyrene as a lightweight fill material in road embankments. Norwegian Road Research Laboratory publication (61):21-27.

[17] Zou Y, Leo C, Small J (2000) Behaviour of EPS geofoam as flexible pavement subgrade material in model tests. Geosynthetics International 7 (1):1-22.

[18] Negussey D, Stuedlein A, Bartlett S, Farnsworth C (2001) Performance of a geofoam embankment at 100 South, I-15 reconstruction project, Salt Lake City, Utah. In: Proceedings on 3rd International Conference on EPS Geofoam.

[19] Farnsworth C, Bartlett SF, Negussey D, Stuedlein A (2008) Rapid construction and settlement behavior of embankment systems on soft foundation soils. Journal of Geotechnical and Geo-Environmental Engineering 134 (3):289-301.

[20] Frydenlund T, Aaboe R (1996) Expanded polystyrene-the light solution. In: Proceedings of Proceedings of International Symposium on EPS Construction Method (EPS-Tokyo'96), Tokyo, Japan, pp. 31-46.

[21] Williams D, Snowdon R (1990) A 47 Great Yarmouth Western Bypass: performance during the first three years (No. 11).

[22] Skuggedal H, Aaboe R (1991) Temporary overpass bridge founded on expanded polystyrene. In: Proceedings of the 1st European Conference on Soil Mechanics and Foundation Engineering, pp 559-561.

[23] McDonald P, Brown P (1993) Ultra lightweight polystyrene for bridge approach fill. In: Proceedings of the 11th Southeast Asian Geotechnical Conference, Singapore, pp 664-668.

[24] Bang S (1995) Experimental and analytical study of expanded polystyrene blocks in highway application. In: Proceedings of International Seminar on the Application of EPS for Embankment Construction, Korea Institute of Construction Technology (KICT), Seoul, Korea, pp 105-133.

[25] Abu-Hejleh N, Zornberg JG, Elias V, Watcharamonthein J (2003) Design assessment of the founders/meadows GRS abutment structure. In: Proceedings of 82nd Annual TRB Meeting.

[26] Meguid M, Ahmed M, Hussein M, Omeman Z (2017) Earth pressure distribution on a rigid box covered with u-shaped geofoam wrap. International Journal of Geosynthetics and Ground Engineering 3 (2):11.

[27] Meguid M, Hussein M (2017) A Numerical Procedure for the Assessment of Contact Pressures on Buried Structures Overlain by EPS Geofoam Inclusion. International Journal of Geosynthetics and Ground Engineering 3 (1):2

[28] Meguid M, Hussein M, Ahmed M, Omeman Z, Whalen J (2017) Investigation of soil-geosynthetic-structure interaction associated with induced trench installation. Geotextiles and Geomembranes 45 (4):320-330.

[29] Zarnani S, Bathurst R (2007) Experimental investigation of EPS geofoam seismic buffers using shaking table tests. Geosynthetics International 14 (3):165-177.

[30] Horvath JS (1997) The compressible inclusion function of EPS geofoam. Geotextiles and Geomembranes 15 (1):77-120.

[31] Bathurst RJ, Keshavarz A, Zarnani S, Take WA (2007) A simple displacement model for response analysis of EPS geofoam seismic buffers. Soil Dynamics and Earthquake Engineering 27 (4):344-353.

[32] Ossa A, Romo M (2011) Dynamic characterization of EPS geofoam. Geotextiles and Geomembranes 29 (1):40-50.

[33] Partos A, Kazaniwsky P (1987) Geoboard reduces lateral earth pressures. In: Proceedings of Geosynthetics' 87 Conference, New Orleans, USA, pp 628-639.

[34] Horvath JS (2010) Lateral pressure reduction on earth-retaining structures using geofoams: Correcting some misunderstandings. In: Earth Retention Conference. pp 862-869.

[35] Koseki J, Bathurst RJ, Guler E, Kuwano J, Maugeri M (2006) Seismic stability of reinforced soil walls. Paper presented at the 8th International Conference on Geosynthetics, Yokohama, Japan, 18-22 Sep. 2006.

[36] AASHTO (2010) American Association of State Highway and Transportation Officials. LRFD bridge design specifications, 5th edition. Washington, DC.

[37] NBCC (2010) National Building Code of Canada. National Research Council of Canada, Ottawa, ON.

[38] Inglis D, Macleod G, Naesgaard E, Zergoun M (1996) Basement wall with seismic earth pressures and novel expanded polystyrene foam buffer layer. Paper presented at the 10th Annual Symposium on Earth Retention System, Vancouver, Canada.

[39] Gaskin AP (2000) Geofoam buffers for rigid walls: An investigation into the use of expanded polystyrene for seismic buffers. Master's Thesis, Queen's University, Kingston, Canada.

[40] Hazarika H, Okuzono S, Matsuo Y (2003) Compressible geo-inclusion as a seismic earth pressure reduction technique. Paper presented at the 38th Japan National Conference on Geotechnical Engineering.

[41] Athanasopoulos GA, Nikolopoulou CP, Xenaki VC, Stathopoulou VD (2007) Reducing the seismic earth pressure on retaining walls by EPS geofoam buffers – Numerical parametric study. Paper presented at the Geosynthetics Conference, Washington DC, USA.

[42] Bathurst RJ, Zarnani S, Gaskin A (2007) Shaking table testing of geofoam seismic buffers. Soil Dynamics and Earthquake Engineering 27 (4):pp. 324-332. doi:http://dx.doi.org/10.1016/j.soildyn.2006.08.003.

[43] Athanasopoulos-Zekkos A, Lamote K, Athanasopoulos G (2011) Seismic isolation of earth retaining walls using EPS compressible inclusions – Results from centrifuge testing. Paper presented at the 4th International Conference on Geofoam Blocks in Construction Applications, Lillestrøm, Norway.

[44] Dasaka SM, Dave TN, Gade VK, Chauhan VB (2014) Seismic earth pressure reduction on gravity retaining walls using eps geofoam. Paper presented at the 8th International Conference on Physical Modelling in Geotechnical Engineering, Perth, Australia.

[45] Ertugrul OL, Trandafir AC (2014) Seismic earth pressures on flexible cantilever retaining walls with deformable inclusions. Journal of Rock Mechanics and Geotechnical Engineering 6 (5):pp. 417-427. doi:http://dx.doi.org/10.1016/j.jrmge.2014.07.004.

[46] Partos A, Kazaniwsky P (1987) Geoboard reduces lateral earth pressures. In: Proceedings of Geosynthetics. pp 628-639.

[47] McGown A, Andrawes KZ, Murray RT (1988) Controlled yielding of the lateral boundaries of soil retaining structures. In: Symposium on Geosynthetics for Soil Improvement at the ASCE Convention. vol Geotechnical Special.

[48] Karpurapu R, Bathurst R (1992) Numerical investigation of controlled yielding of soil-retaining wall structures. Geotextiles and Geomembranes 11 (2):115-131.

[49] Horvath JS (2004) Geofoam compressible inclusions: the new frontier in earth retaining structures. In: Geotechnical Engineering for Transportation Projects. pp 1925-1934.

[50] Lutenegger AJ, Ciufetti M (2009) Full-scale pilot study to reduce lateral stresses in retaining structures using geofoam. Final report, project No RSCH010-983 Vermont DOT, University of Massachusetts, Amherst, MA.

[51] Ertugrul OL, Trandafir AC (2011) Reduction of lateral earth forces acting on rigid nonyielding retaining walls by EPS geofoam inclusions. Journal of Materials in Civil Engineering 23 (12):1711-1718.

[52] Athanasopoulos-Zekkos A, Lamote K, Athanasopoulos G (2012) Use of EPS geofoam compressible inclusions for reducing the earthquake effects on yielding earth retaining structures. Soil Dynamics and Earthquake Engineering 41:59-71.

[53] McGown A, Murray R, Andrawes K (1987) Influence of wall yielding on lateral stresses in unreinforced and reinforced fills.

[54] Inglis D, Macleod G, Naesgaard E, Zergoun M (1996) Basement wall with seismic earth pressures and novel expanded polystyrene foam buffer layer. In: Proceedings of the 10th Annual Symposium of the Vancouver Geotechnical Society, Vancouver, BC.

[55] Hoek E (1985) SARMA – A computer program for non-vertical slice method of slope stability analysis.

[56] Byrne PM, Jitno H, Salgado F (1992) Earthquake induced displacements of soil-structures systems. In: Proceedings of 10th World Conference on Earthquake Engineering. pp 1407-1412.

[57] Jitno H, Byrne PM (1994) A procedure for predicting seismic deformation of earth structures. In: Vertical and Horizontal Deformations of Foundations and Embankments, 1994. ASCE, pp 711-725.

[58] Byrne PM, Janzen W (1981) Soil stress: A computer program for nonlinear analysis of stresses and deformations in soils. Department of Civil Engineering, University of British Columbia.

[59] Cundall P, Board M (1988) A microcomputer program for modelling large-strain plasticity problems. In: Proceedings of the Sixth International Conference on Numerical Methods in Geomechanics, 11-15 April 1988, Innsbruck, Austria. Volumes 1-3 1988.

[60] Hazarika H, Okuzono S, Matsuo Y (2003) Seismic stability enhancement of rigid nonyielding structures. Paper presented at the 13th International Offshore and Polar Engineering Conference, Honolulu, Hawaii, USA.

[61] Dave TN, Dasaka SM (2015) Effect of boundary conditions on earth pressure reduction using eps geofoam. Paper presented at the 15th Asian Regional Conference on Soil Mechanics and Geotechnical Engineering, Fukuoka, Japan.

[62] Ertugrul OL, Trandafir AC (2012) A physical modeling study on the dynamic response of flexible retaining walls with deformable EPS inclusion. Paper presented at the 15th World Conference on Earthquake Engineering, Lisbon, Portugal.

[63] Ertugrul OL, Trandafir AC, Ozkan MY (2017) Reduction of dynamic earth loads on flexible cantilever retaining walls by deformable geofoam panels. Soil Dynamics and Earthquake Engineering 92 (20):pp. 462-471. doi:https://doi.org/10.1016/j.soildyn.2016.10.011

[64] Pelekis P, Xenaki V, Athanasopoulos G (2000) Use of EPS geofoam for seismic isolation of earth retaining structures: Results of a FEM study. In: Proceedings of the 2nd European Geosynthetics Conference, Bologna, Italy. pp 15-18.

[65] Armstrong R, Alfaro M (2003) Reduction of seismic-induced pressures on rigid retaining structures using compressible inclusions: A numerical study. In: Proceedings of the 56th Canadian Geotechnical Conference, Winnipeg, Man. pp 500-505.

[66] Zarnani S, Bathurst RJ (2008) Numerical modeling of EPS seismic buffer shaking table tests. Geotextiles and Geomembranes 26 (5):pp. 371-383. doi:http://dx.doi.org/10.1016/j.geotexmem.2008.02.004.

[67] Zarnani S, Bathurst RJ (2005) Numerical Investigation of geofoam seismic buffers using FLAC. Paper presented at the North American Geosynthetics Society (NAGS)/GR119 Conference, Las Vegas, NV, USA.

[68] Zarnani S, Bathurst R (2010) Numerical parametric study of geofoam seismic buffers with different constitutive models. In: Proceedings of the 9th International Geosynthetics Conference, 2010. pp 1665-1668.

[69] Zarnani S, Bathurst RJ (2009) Numerical parametric study of expanded polystyrene (EPS) geofoam seismic buffers. Canadian Geotechnical Journal 46 (3):pp. 318-338. doi:10.1139/T08-128.

[70] Athanasopoulos G, Nikolopoulou C, Xenaki V, Stathopoulou V (2007) Reducing the seismic earth pressures on retaining walls by EPS geofoam buffers-Numerical parametric analyses. In: Proc. Geosynthetics.

[71] Zekkos AA, Lamote K, Athanasopoulos GA (2012) Use of EPS geofoam compressible inclusions for reducing the earthquake effects on yielding earth retaining structures. Soil Dynamics and Earthquake Engineering 41:pp. 59-71. doi:http://dx.doi.org/ 10.1016/ j.soildyn.2012.05.004.

[72] Wang YM, Li H, Zhang H (2012) Numerical simulation for dynamic response of eps geofoam seismic buffers. Advanced Materials Research 378:pp. 256-261.

[73] Wang D, Bathurst RJ (2012) Numerical analysis of earthquake load mitigation on rigid retaining walls using EPS geofoam. Open Civil Engineering Journal 6:21-25.

[74] Brinkgreve R, Kumarswamy S, Swolfs W, Waterman D, Chesaru A, Bonnier P (2020) PLAXIS 2D Version 20.03.00.60. Netherlands

[75] C578 A Standard Specification for Rigid, Cellular Polystyrene Thermal Insulation. American Society for Testing and Materials.

[76] Bathurst RJ, Hatami K (1998) Seismic response analysis of a geosynthetic-reinforced soil retaining wall. Geosynthetics International 5 (1-2): pp. 127-166. doi:doi:10.1680/ gein.5.0117.

[77] Matsuo O, Yokoyama K, Saito Y (1998) Shaking table tests and analyses of geosynthetic-reinforced soil retaining walls. Geosynthetics International 5 (1-2):97-126.

[78] Iai S (1989) Similitude for shaking table tests on soil-structure-fluid model in 1g gravitational field. Soils and Foundations 29 (1):105-118.

[79] Schanz T (1999) Formulation and verification of the Hardening-Soil model. RBJ Brinkgreve, Beyond 2000 in Computational Geotechnics:281-290.

Table 5.1 Summary of shaking table test results

Property	Bathurst et al. [42]	Hazarika et al. [60,40]	Dasaka et al. [44]	Ertugrul et al. [45,63,64]
Wall height *H* (mm)	1000	700	700	700
Relative thickness, *t/H*	0.15	0.08	0.125	0.14
Wall type	Rigid	Rigid	Rigid	Flexible
Inclusion material	EPS geofoam	Sponge	EPS geofoam	EPS geofoam
Acceleration, a (g)	0.7	0.8	0.4	0.7
Reduction (%)	40	30-60	27	50

Table 5.2 Summary of numerical studies

Reference	Approach / Software	Assumptions / Models	Reduction (%)
Inglis et al. [54]	FDM / FLAC	**Soil:** Mohr Coulomb **EPS geofoam:** Double yield constituency model	50
Pelekis et al. [65]	FEM / FLUSH PLUS	**Soil & EPS geofoam:** Viscoelastic materials with strain-dependent values of shear modulus and damping ratio	>50
Armstrong et al. [66]	FDM / FLAC	**Soil:** Mohr Coulomb **EPS geofoam:** Hyperbolic model	25
Zarnani et al. [67-69]	FDM / FLAC	**Soil:** Mohr Coulomb **EPS geofoam:** Linear elastic-plastic	50
Athanasopoulos et al. [71]	FEM / PLAXIS	**Soil:** Non-linear **EPS geofoam:** Non-linear	50
Zekkos et al. [72]	FEM / PLAXIS	**Soil:** Elasto-plastic **EPS geofoam:** Linear elastic	50
Wang et al. [73]	FDM / FLAC	**Soil:** Mohr Coulomb **EPS geofoam:** Linear elastic	50
Wang, Bathurst [74]	FEM / ABAQUS	**Soil:** Mohr Coulomb **EPS geofoam:** Linear elastic-plastic	50

Table 5.3 Material properties of soil & EPS geofoam (Validated model [42])

Property	**Backfill Soil**	**EPS Geofoam**
Unit weight, γ (kN/m^3)	15.7	0.15
Young's Modulus, E (kN/m^2)	15,200	4700
Poisson's ratio, υ	0.33	0.09
Cohesion c' (kN/m^2)	0	-
Peak friction angle ϕ_p (degrees)	51	-
Residual friction angle ϕ_r (degrees)	46	-
Dilatancy angle Ψ' (degrees)	15	-
Specific gravity	2.88	-
c_c (coefficient of curvature)	1.27	-
c_u (coefficient of uniformity)	2.5	-
Percent finer than #200 sieve (%)	<3	-

Table 5.4 Material properties of soil and EPS geofoam (Present study)

Property	**Backfill Soil**	**EPS15**	**EPS22**	**EPS29**	**EPS39**
Material model	Hardening Soil	Linear Elastic	Linear Elastic	Linear Elastic	Linear Elastic
Unit weight, γ (kN/m^3)	15.7	0.15	0.22	0.29	0.39
Young's Modulus, E (kN/m^2)	15,330	4,200	6,910	10,000	178,000
Poisson's ratio, υ	0.33	0.11	0.12	0.13	0.15
Cohesion c' (kN/m^2)	0	-	-	-	-
Friction angle ϕ' (degrees)	30^o - 45^o	-	-	-	-
Dilatancy angle Ψ' (degrees)	15	-	-	-	-
K_o determination	0.292 – 0.50	-	-	-	-

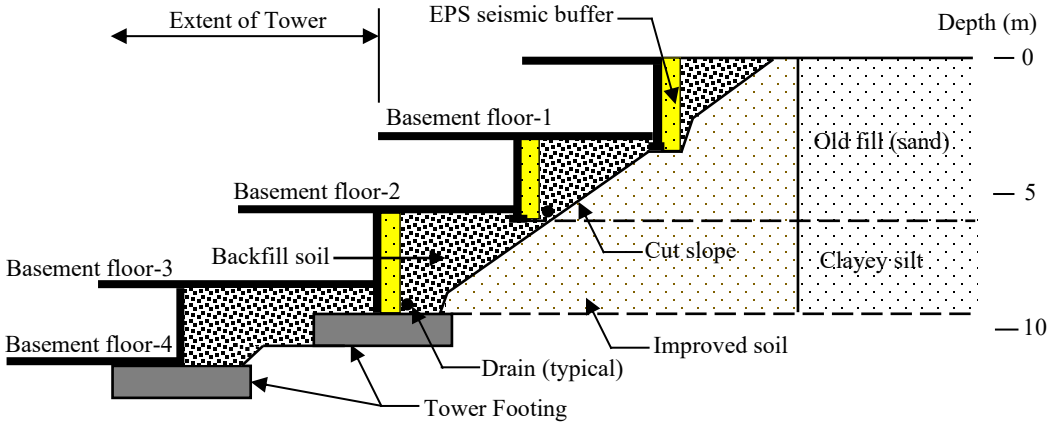

Figure 5.1 EPS seismic buffer behind basement walls in Vancouver Canada (after Inglis et al. [54])

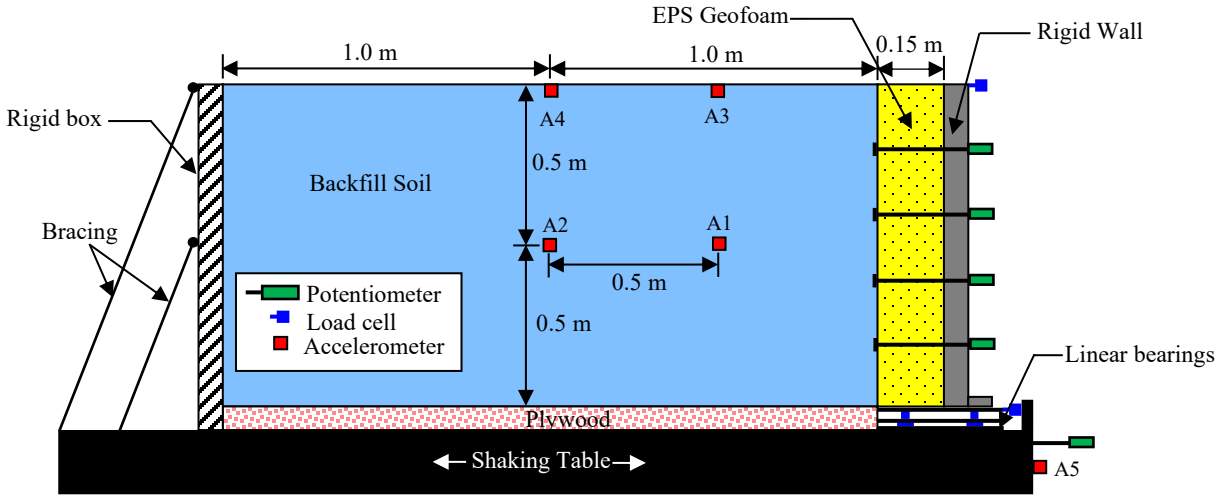

Figure 5.2 Physical shaking table test setup (after Bathurst et al. [42])

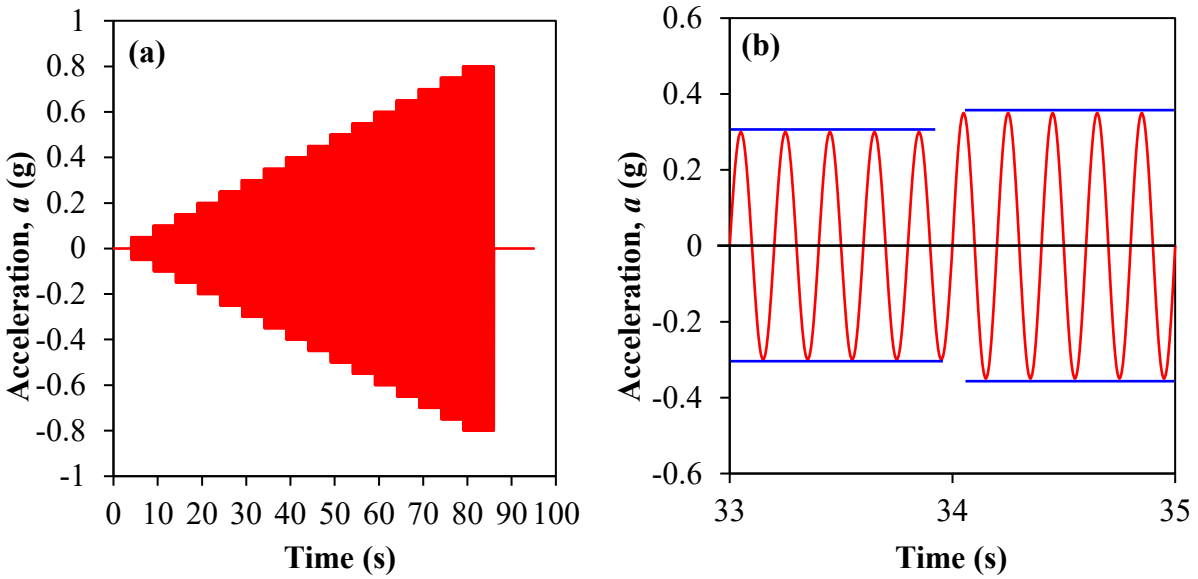

Figure 5.3 (a) Input horizontal base accelerogram; (b) 2-second accelerogram window at amplitude step (after Bathurst et al. [42])

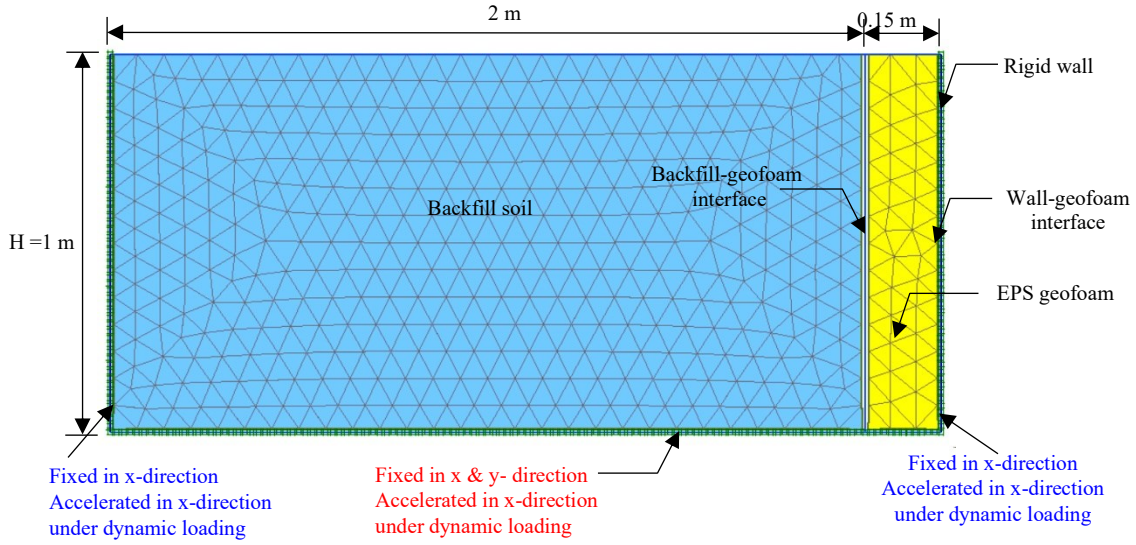

Figure 5.4 Plaxis FE mesh of the rigid non-yielding retaining wall with geofoam buffer

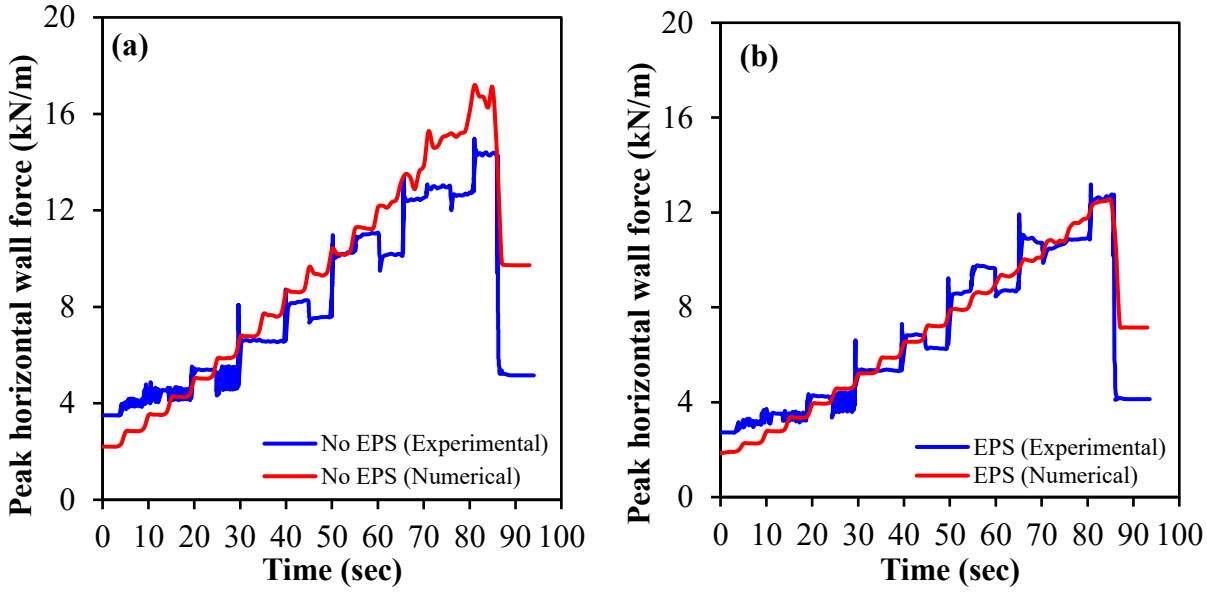

Figure 5.5 Validated PLAXIS Models (a) **w**ithout EPS geofoam (b) with EPS geofoam

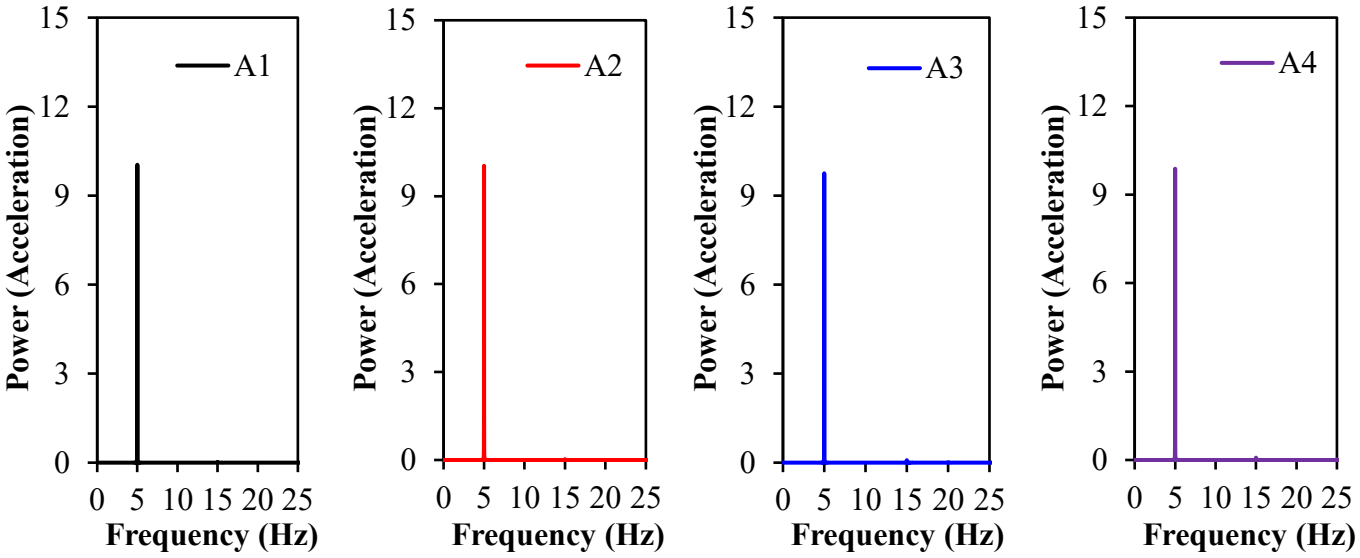

Figure 5.6 FFT plots for acceleration at location A1, A2, A3 and A4 (Numerical)

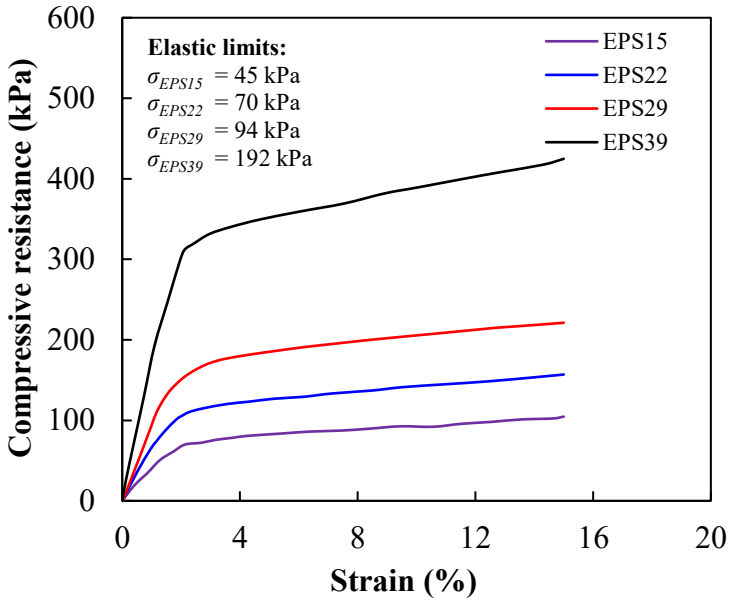

Figure 5.7 Stress-strain relationships of EPS15, EPS22, EPS29 & EPS39

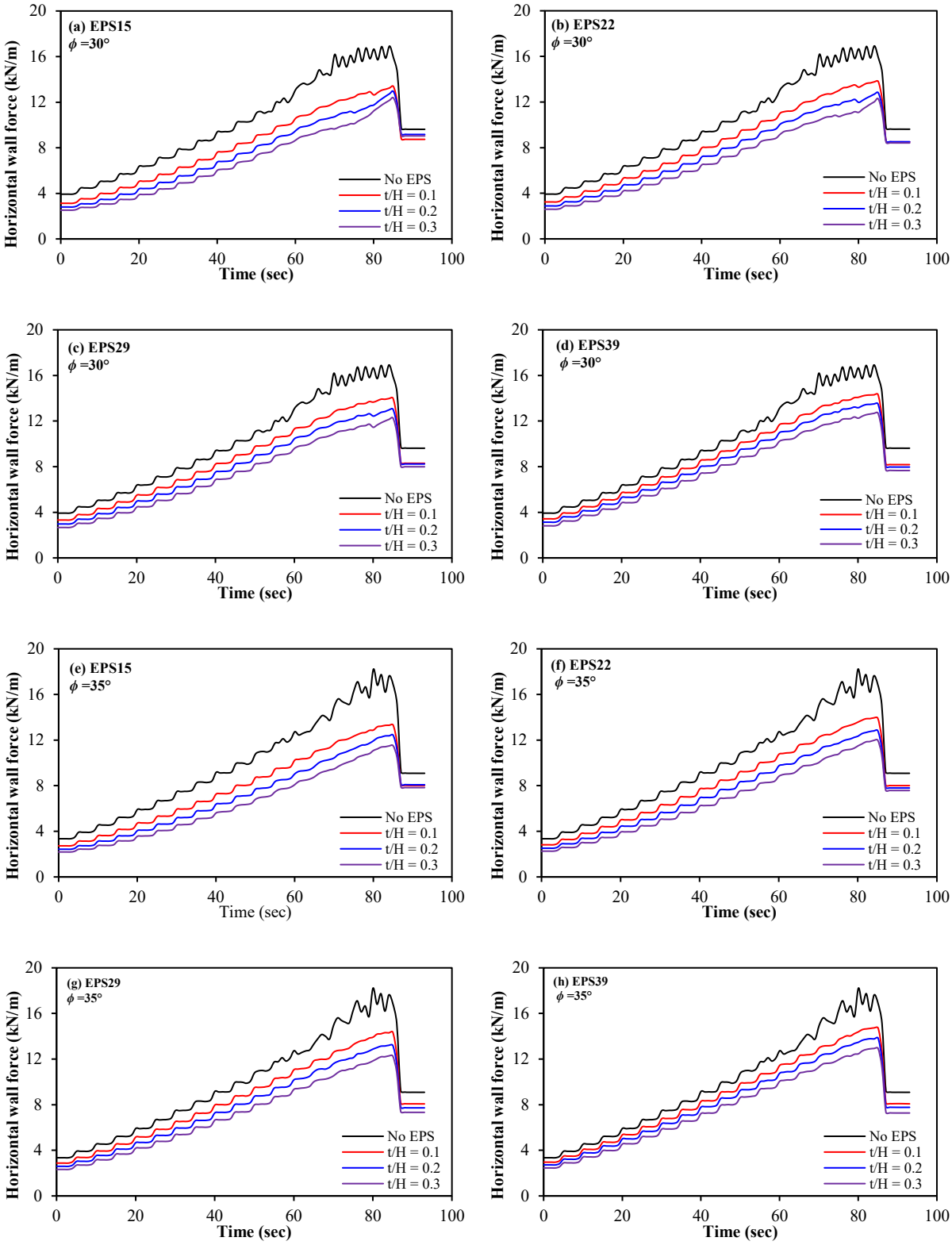

Figure 5.8 Horizontal wall force for different geofoam densities, thicknesses, and backfill material (ϕ =30° & 35°)

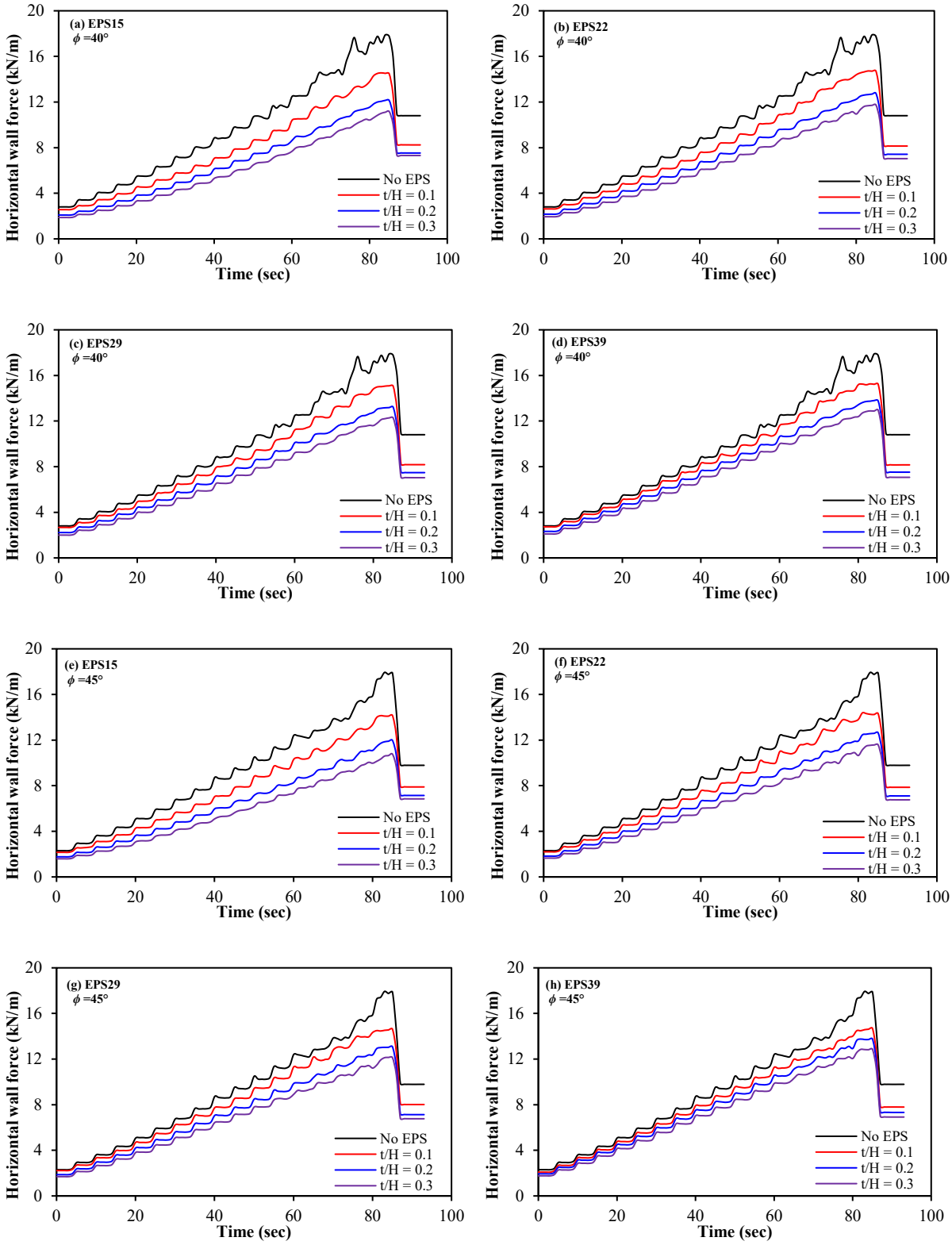

Figure 5.9 Horizontal wall force for different geofoam densities, thicknesses, and backfill material (ϕ =40° & 45°)

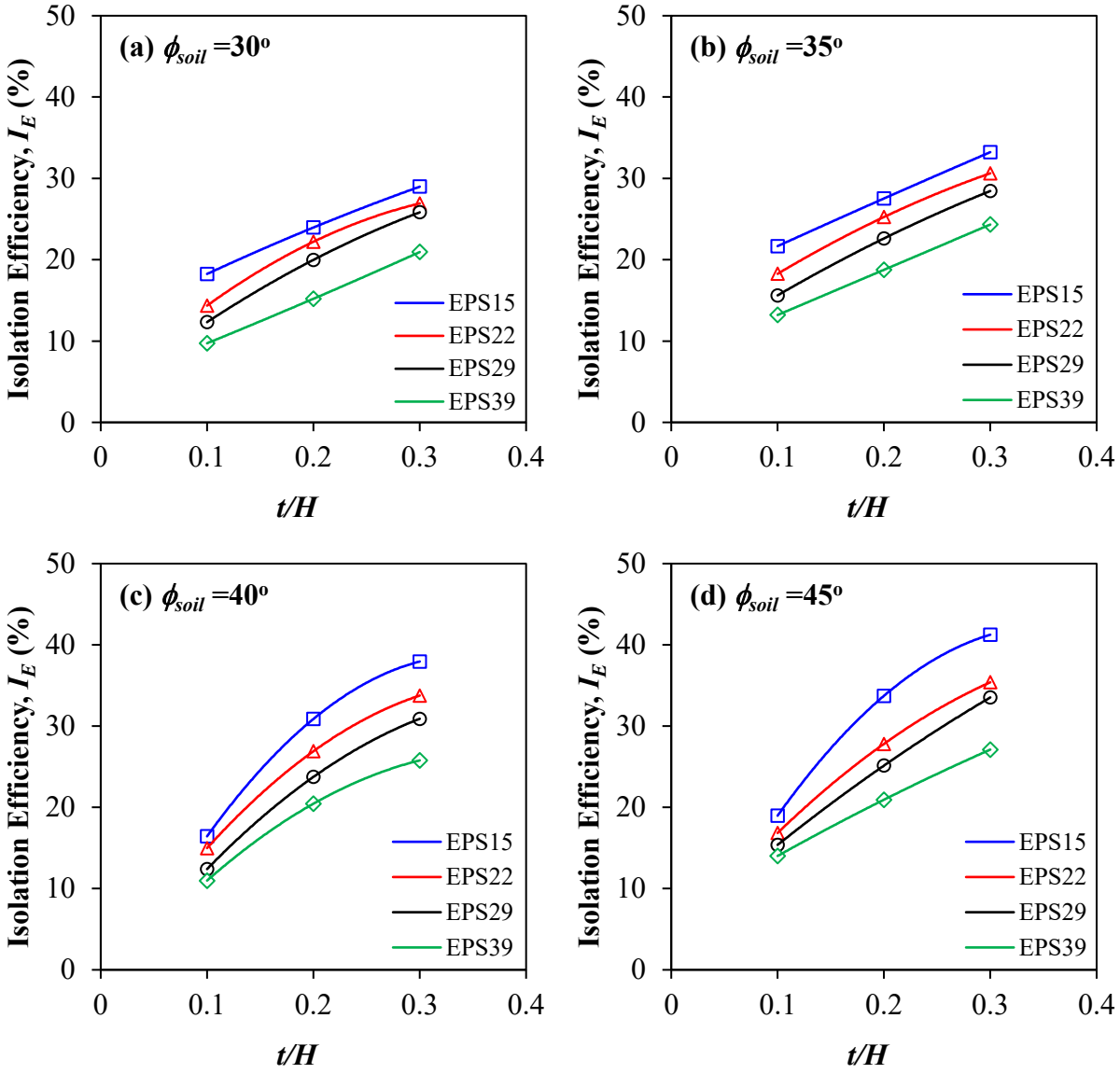

Figure 5.10 Isolation efficiency I_E vs t/H for EPS22, EPS29 & EPS39: (a) ϕ=30°, (b) ϕ=35°, (c) ϕ=40°, (d) ϕ =45°

6

Conclusions and Recommendations

6.1 Overview

The present research aimed at: (i) evaluating the shear strength of geofoam monoblock of different densities and the interface strength of geofoam interacting with different materials; (ii) to numerically investigate the role of using EPS geofoam panels in reducing lateral earth pressure on rigid non-yielding retaining walls under both static and dynamic loading conditions.

6.2 Conclusions

The following are the global conclusions drawn from the present research:

1. In chapter 2, a series of direct shear tests was performed to determine the shear strength of EPS monoblocks. In addition, interface shear tests were also conducted to determine the shear strength at EPS-PVC and EPS-sand interfaces. Tests were conducted using three different geofoam densities, namely, EPS15, EPS22 and EPS39. All direct shear tests were conducted under a normal stress range of 18 to 54 kPa. Results showed that:
   - No actual failure plane develop in the monoblocks and only shear deformations were recorded within the tested blocks. The shear strength of EPS monoblock was found to be mainly dependent on the material cohesion. Material cohesion showed significant increase with the increase in EPS density. However, internal friction angle, showed a slight decrease with the increase in EPS density.
   - EPS-PVC interface showed an increase in adhesion and a slight decrease in interface friction angle with the increase in geofoam density. However, for EPS-sand interface, increase in geofoam density resulted in a decrease in adhesion value and an increase in interface friction angle.
   - Thickness of EPS geofoam was found to have a significant effect on the vertical compression for both monoblocks and interface tests. Monoblocks samples experienced

more compression due to greater thickness as compared to geofoam samples used in interface tests.

2. In chapter 3, a series of direct shear tests was performed to investigate the shear behavior of EPS geofoam with different construction materials e.g. concrete, wood and steel. Three geofoam samples of different densities namely, EPS15, EPS22 and EPS39 were used. The following conclusions can be drawn from this experimental study:
   - The density of EPS geofoam and applied normal stress both showed significant effects on the interface resistance.
   - EPS blocks in contact with concrete, wood and steel showed an increase in adhesion values with the increase in geofoam density. However, interface friction angle was found to increase for the case of concrete as compared to other materials.
   - Vertical compression of EPS geofoam was found to be directly related to the applied normal stress and inversely related to the geofoam density.
3. In chapter 4, a plane strain finite element model was developed to investigate the effect of EPS geofoam inclusion on the earth pressure acting on rigid non-yielding retaining walls. A numerical model was first validated against the results of physical tests. A parametric study was then carried out to investigate the role of EPS geofoam density, relative thickness and backfill frictional properties on the static lateral earth pressure on the wall. Three different geofoam samples having three different thicknesses interacting with four different backfill soils were used in this study. The following conclusions can be drawn from this numerical study:
   - The presence of EPS geofoam panels placed behind rigid retaining walls could help in reducing lateral earth pressure due to controlled yielding of the backfill soil.
   - For a rigid retaining wall under static loading conditions, the response of the backfill soil and EPS geofoam were reasonably predicted using Mohr-Coulomb elastoplastic material and linear elastic models, respectively.
   - Isolation efficiency of EPS geofoam was found to be dependent on the relative thickness, density of the EPS geofoam and the frictional properties of the backfill soils. It is also found that low density geofoam can provide better performance compared to higher density material.

4. In chapter 5, a plane strain finite element model was developed to study the role of EPS geofoam panels placed between a rigid wall and backfill under dynamic loading conditions. Numerical model was first validated using shaking table test results. A parametric study was then conducted to investigate the effects of EPS geofoam density, relative thickness and backfill frictional properties on the seismic earth pressure acting on the rigid retaining wall. Four different geofoam samples having three different thicknesses interacting with four different backfill materials were used in this study. The following conclusions can be drawn:
   - For a rigid retaining wall under dynamic loading conditions, the response of the backfill soil and EPS geofoam were reasonably predicted using Hardening Soil (HS) and linear elastic models, respectively.
   - Isolation efficiency of EPS geofoam was found to be dependent on relative thickness, density of the EPS geofoam and the frictional properties of the backfill soils

6.3 Claims of Originality

1. Evaluating the shear properties of different geofoam materials and measuring the interface shear properties of geofoam interacting with other construction materials.
2. A numerical model was validated and used to study the effectiveness of EPS geofoam in reducing static earth pressures on rigid retaining walls.
3. A dynamic numerical model was validated and used to study the role of EPS geofoam on the reduction of seismic earth pressures on rigid retaining walls.
4. New normalized charts were developed based on the obtained results, which can be used to guide design of composite structures involving EPS geofoam.

6.4 Recommendations for Future Work

Building on the results reported in this thesis, the research can be expanded in the future to include

- Studying the effect of EPS geofoam density, thickness and backfill properties in reducing earth pressure on gravity and flexible walls.
- Develop simplified design approach that could be adopted by engineers in different seismic zones in Canada and elsewhere in the world.

Appendix (A)

A.1 Direct Shear Test Setup

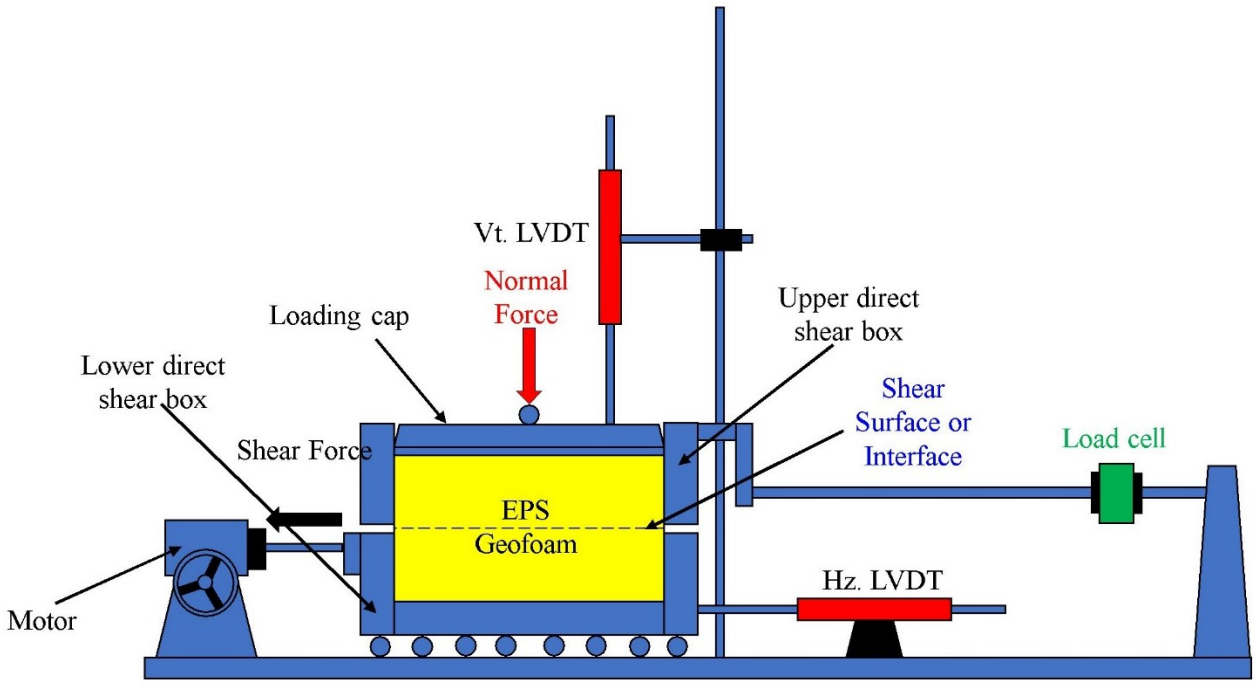

Figure A.1 Schematic diagram of direct shear test setup

A.2 Finite Element Constitutive Models

A brief summary of finite element constitutive models used in this research are presented in detail as follows:

A.2.1 Linear Elastic Model

This model is based on Hooke's law of isotropic elasticity. It is a simple model and requires only two input parameters Young's modulus, E and Poisson's ratio, v to define the linear elastic behavior. A typical stress strain curve of a linear elastic material is shown in Figure A.2. An ideal elastic material does not undergo permanent deformation and returns to its original shape when the loads are removed. Also, there is no dependence on the rate of loading or straining.

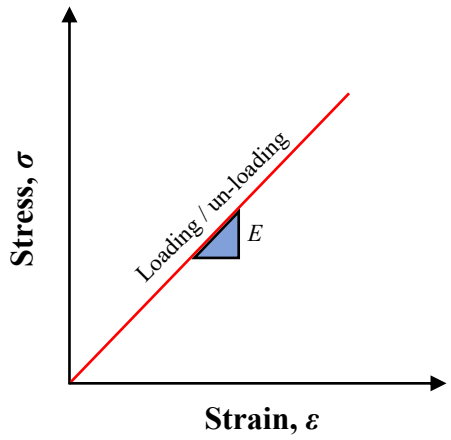

Figure A.2 Stress strain curve of an elastic material

A.2.2 Mohr-Coulomb Model

The Mohr-Coulomb soil model is a linearly elastic and perfectly plastic model as shown in Figure A.3. The linear elastic portion of the Mohr-Coulomb model is based on Hooke's law of isotropic elasticity and the perfectly plastic portion is based on the Mohr-Coulomb failure criterion. This model requires five input parameters i.e. Young's modulus, E and Poisson's ratio, v for soil elasticity; friction angle, ϕ and cohesion, c for soil plasticity and ψ as an angle of dilatancy.

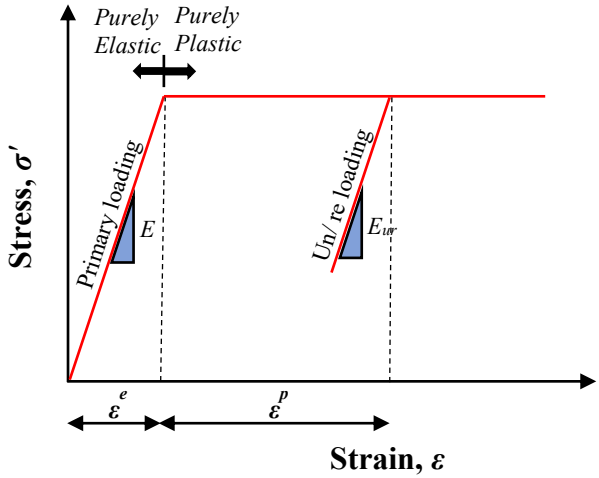

Figure A.3 Stress strain curve of a perfect elasto plastic material

According to principle of elasto-plasticity, total strain, $\boldsymbol{\varepsilon}$, is divided into elastic, $\boldsymbol{\varepsilon^e}$, and plastic, $\boldsymbol{\varepsilon^p}$, strains.

$$\varepsilon = \varepsilon^e + \varepsilon^p$$

Similarly, strain rate is also divvied into elastic and plastic components.

$$\dot{\varepsilon} = \dot{\varepsilon}^e + \dot{\varepsilon}^p$$

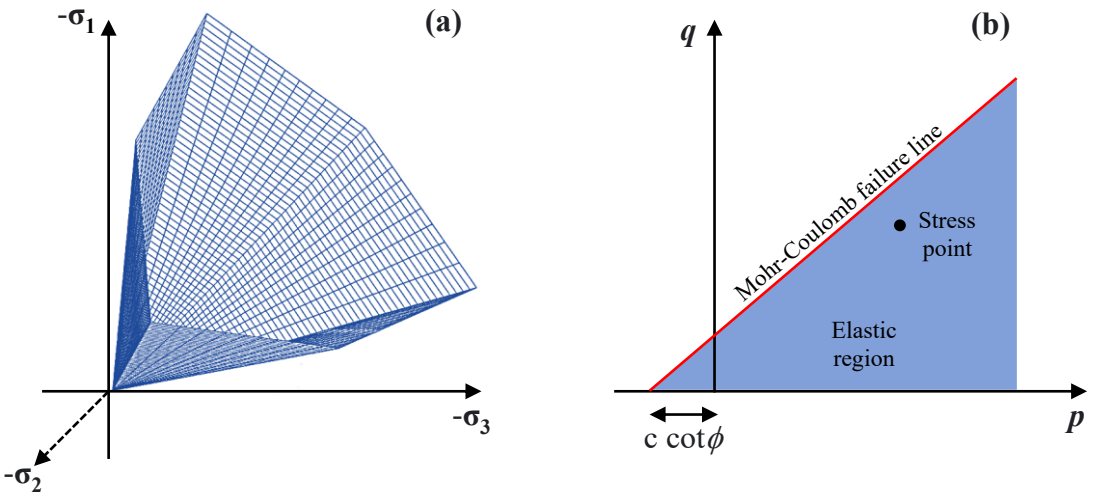

Figure A.4 The Mohr-Coulomb model yield surface in (a) principal stress space (c = 0); (b) p-q plane

The Mohr Coulomb model has a fixed yield surface as shown in Figure A.4. The material behavior is elastic within the region below the yield surface. However, as the stress approaches to yield surface (boundary of elastic region), the material behavior becomes plastic. The yield function, f, defined by Mohr-Coulomb (1773) using soil shear stress, τ, normal stress, σ, friction angle, ϕ and cohesion, c as

$$f = |\tau| - \sigma \tan\phi' - c'$$

Plastic yielding occurs when the yield function is equal to zero ($f = 0$).

A.2.3 Hardening Soil (HS) Model

Hardening Soil (HS) model is an advanced model (see Figure A.5) as compared to Mohr Coulomb model and is used to simulate behavior of both soft and stiff soils. Nonlinear, inelastic and stress dependent behavior of soil could be captured using Hardening Soil model. HS model also considers the variation of elastic stiffness with stress which is taken as a constant value in Mohr-Coulomb model.

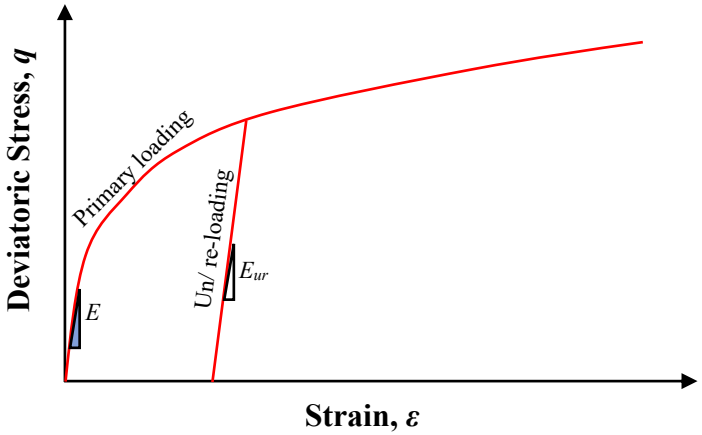

Figure A.5 Stress strain curve of an elastic material

As compared to the yield surface of Mohr-Coulomb model, the yield surface of hardening soil model is not fixed but can expand due to plastic straining as shown in Figure A.6. There are two main types of hardening contained by HS model, namely shear hardening and compression hardening. Shear hardening models irreversible strains due to primary deviatoric loading while compression hardening models irreversible plastic strains due to primary compression in oedometer loading and isotropic loading. HS model requires five parameters i.e. friction angle, ϕ and cohesion, c, E_{50}^{ref}, E_{oed}^{ref}, E_{50}^{ref} to model soil behavior.

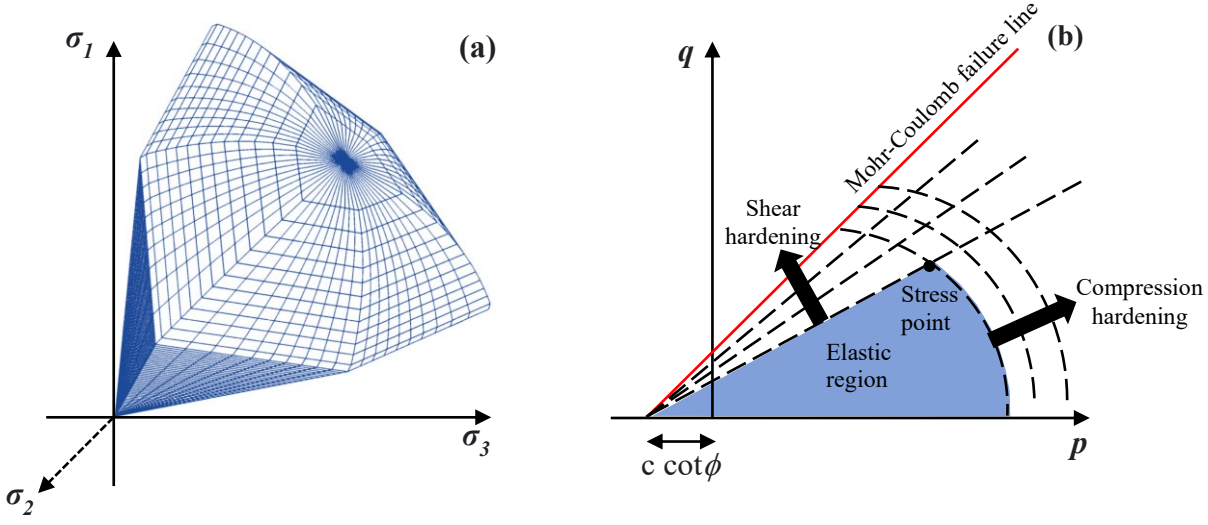

Figure A.6 The Hardening Soil model yield surface in (a) principal stress space (c = 0); (b) p-q plane